L_2, L_3 SUBSHELL FLUORESCENCE YIELDS AND COSTER-KRONIG TRANSITION PROBABILITIES IN THE MIDDLE Z REGION

A THESIS

Presented to

The Faculty of the Division of Graduate

Studies and Research

By

Saradamandiram Mohan

In Partial Fulfillment

of the Requirements for the Degree

Doctor of Philosophy

in the School of Nuclear Engineering

Georgia Institute of Technology

September, 1972

In presenting the dissertation as a partial fulfillment of the requirements for an advanced degree from the Georgia Institute of Technology, I agree that the Library of the Institute shall make it available for inspection and circulation in accordance with its regulations governing materials of this type. I agree that permission to copy from, or to publish from, this dissertation may be granted by the professor under whose direction it was written, or, in his absence, by the Dean of the Graduate Division when such copying or publication is solely for scholarly purposes and does not involve potential financial gain. It is understood that any copying from, or publication of, this dissertation which involves potential financial gain will not be allowed without written permission.

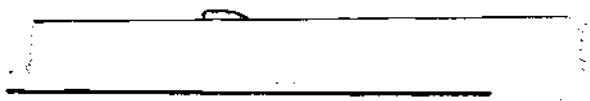

7/25/68

L_2, L_3 SUBSHELL FLUORESCENCE YIELDS AND COSTER-KRONIG TRANSITION PROBABILITIES IN THE MIDDLE Z REGION

Approved:

R. W. Fink

G. G. Eichholz

D. S. Harmer

Date approved by Chairman: 14 SEPTEMBER 197

ACKNOWLEDGMENTS

I wish to express my deepest gratitude to my thesis advisor, Professor R. W. Fink for suggesting the thesis, for financial support and unstinting encouragement, guidance and inspiration. To Professor G. G. Eichholz is extended my sincere appreciation for his guidance and encouragement.

I thank Drs. D. S. Harmer, E. J. Patronis and T. F. Moran for serving on the thesis committee.

I am most grateful for the invaluable assistance extended by Professor P. V. Rao, Dr. H. U. Freund, Dr. W. D. Schmidt-ott and Dr. J. C. McGeorge, who collaborated with me on parts of this study.

Part of this work was done at the Emory University and I am grateful to the Physics Department of Emory University for the use of the equipment, especially to Dr. P. V. Rao, Dr. R. E. Wood and J. M. Palms.

I wish to thank my colleague, D. W. Nix, for his kindness and friendship, and also W. M. Chew and F. Tolea.

Finally, I thank Mrs. Claudine Taylor for typing and editing this manuscript.

TABLE OF CONTENTS

TABLE OF CONTENTS (Continued)

LIST OF TABLES

LIST OF TABLES (Continued)

LIST OF ILLUSTRATIONS

SUMMARY

The L_2 and L_3 subshell x-ray fluorescent yields and Coster-Kronig transition probabilities were measured at Z = 70, 73, 76, 78 and 81 using carrier-free radioisotopes and high resolution semiconductor detectors by L x-ray - K x-ray coincidences. The results agree with recent theoretical predictions for the radiative yields ω_2 and ω_3; however, some discrepancy persists between theory and experiment for the Coster-Kronig yield f_{23}.

CHAPTER I

INTRODUCTION

Since the discovery of x-ray in the late Nineteenth Century and the development of the Bohr atom model with quantized electronic orbits, the study of characteristic x-rays has been utilized to develop the understanding of atomic structure. It is usual to distinguish the means by which inner shell transitions occur in atoms as being radiative, or nonradiative. The availability of high resolution, cooled semi-conductor x-ray and electron detectors and fast electronics has given a major impetus to the study of these inner shell transitions and their yields. The theoretical calculation of these radiative and nonradiative transitions is also becoming increasingly refined. In this study, it is proposed to measure the L shell radiative (fluorescent) yields and non-radiative (Coster Kronig) yield (1, 2).

1.1 Motivation for the Study of X-ray Fluorescence Yields and Coster-Kronig Transition Probabilities

A knowledge of fluorescence and Coster-Kronig yields is necessary in interpreting many problems which involve atomic electrons in nuclear processes. The multipolarity of internally converted x-rays and the available transition energy in electron capture decay (QEC) is often determined by measuring x-ray and electron intensities and a knowledge of fluorescence yields is needed for their interpretation. Atomic collision cross sections in which inner shells are ionized are measured through the detection of characteristic x-rays. Recently, identification

of fission fragments and their yields have been made by study of their characteristic x-ray spectra, and in such cases, a knowledge of the change in fluorescence yields as a result of multiple ionization is needed.

Nonradiative transitions probabilities are more sensitive to the nature of atomic wavefunctions than many other measurable atomic quantities. A systematic study of radiation-less transitions can therefore be used as a test of current methods of generating atomic wavefunctions.

X-ray fluorescence methods have been applied practically in a wide variety of cases including non-destructive testing, medical research trace element analysis, analysis of geological samples, etc. Because x-ray detectors can detect even single photons, it is possible to develop x-ray fluorescence analysis into an extremely sensitive analytical tool. This has found application in such diverse fields as air-pollution measurements, analysis of moon rocks brought back by the Apollo expedition, determination of mercury contamination in fish, and determining the authenticity of paintings, antiques, etc. In all these applications, a knowledge of the fluorescent yield is required.

Auger electron spectroscopy and low energy electron diffraction are used in surface physics studies for the detection of minute quantities of contaminants. Values of fluorescence and Auger yields are needed here.

Finally, the importance of x-ray fluorescence yields in the calculation of photon transport processes needs to be mentioned. After a gamma photon traverses many radiation lengths, the remaining energy loss and consequent absorbed dose is due to secondary fluorescence radiation. Thus accurate knowledge of fluorescence

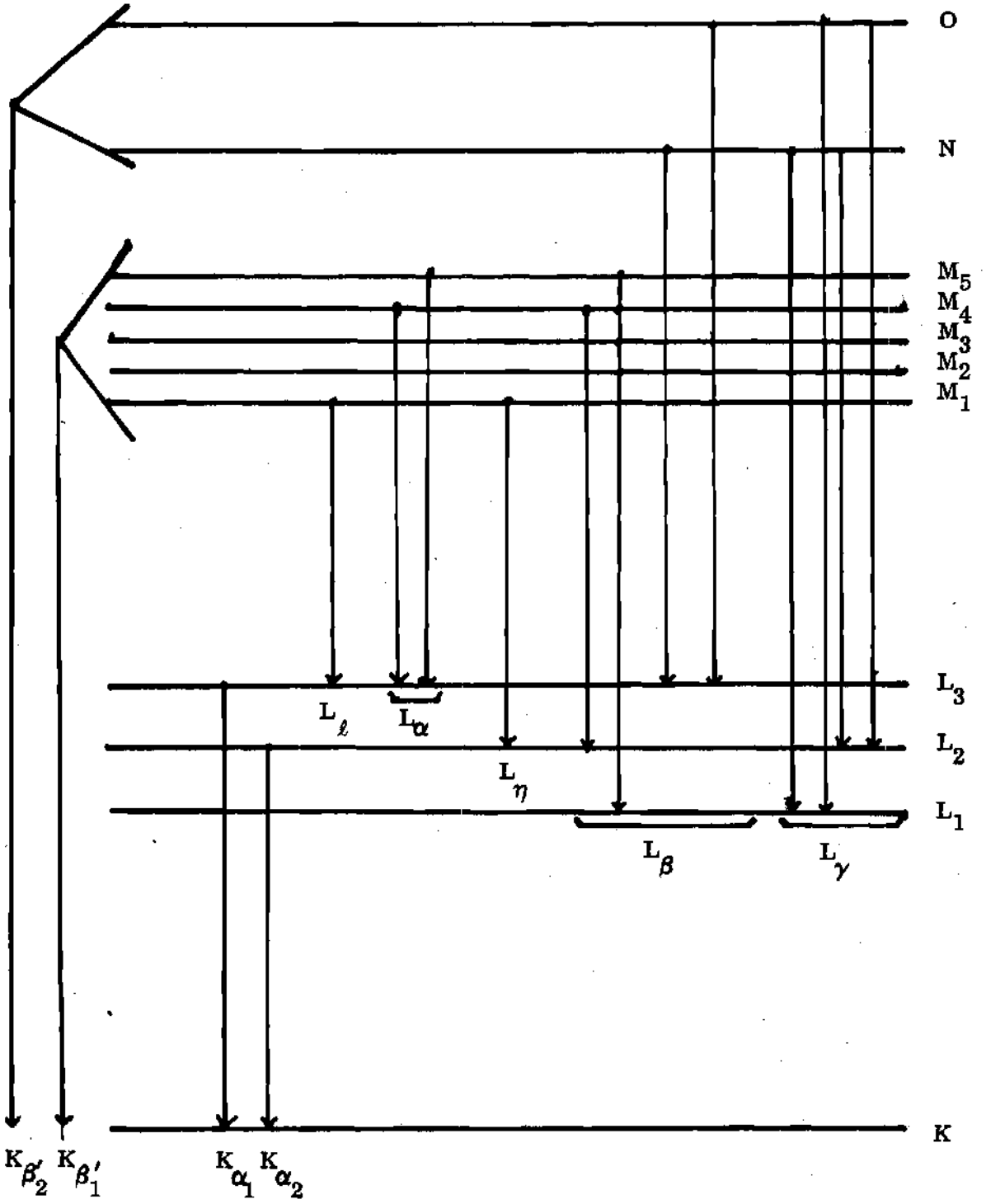

Figure 1. Major K and L Shell Radiative Transitions.

Table 1. Major K and L Shell Radiative Transitions

X-Ray or X-Ray Group	Transition
K_{α_1}	$K - L_3$
K_{α_2}	$K - L_2$
$K_{\beta'_1}$	$K - M$
$K_{\beta'_2}$	$K - N, O$
L_1	$L_3 - M_1$
L_α	$L_3 - M_4, M_5$
L_η	$L_2 - M_1$
L_β	$L_2 - M_4$
	$L_3 - N, O$
	$L_1 - M$
L_γ	$L_1 - N_2, N_3$
	$L_1 - O_2, O_3$
	$L_2 - N, O$

radiation yields is needed in dose build-up calculations. Another example is the design of stacked or graded shields, which are made such that each layer is particularly effective in stopping the fluorescent radiation produced in the preceding one. Many of the computer codes used in the design of such shields incorporate the best values of such quantities.

1.2 Definitions

Vacancies are created in an inner shell or subshell of an atom in a variety of ways, including fluorescent excitation, charged particle bombardment, and radioactive processes such as electron capture, internal conversion, α-decay, etc. When such a vacancy is created (in subshell i of a major shell x, say) the atom is left in an excited state and can de-excite by two main modes: (Fig. 1).

A) Radiative transitions: An electron from an outer shell y_j fills the vacancy, energy and angular momentum being conserved by emission of an x-ray.

Between two pure single electron states, the allowed radiative transition is electric dipole (E1). Magnetic dipole (M1) transitions as well as higher multi-poles are forbidden, but lines due to such transitions are noticed at higher Z, owing to relativistic effects.

Discussion of the selection rules governing radioactive decay have been given by many authors, among them Compton and Allison (11) or Condon and Shortley (12).

B) Nonradiative transitions: An electron from a higher shell y_j fills the vacancy, with conservation laws being satisfied by ejection of an electron from an outer shell, leaving the atom doubly ionized in its outer shells. This is called an

Auger transition (1) and the standard notation is $X_i Y_j - Y_\ell$. An example of an L-Auger process will be $L_1 - M_4 N_5$ (see Fig. 1).

If the electron filling the vacancy comes from the higher subshell of the same major shell, the process is called a "Coster-Kronig transition" $X - X Z_k$, for example $L_1 - L_3 M_5$. Thus the Coster-Kronig (CK) transition (2) represents a vacancy shift within a major shell. The nonradiative Coster-Kronig effect differs from the Auger effect only in that the original vacancy is filled from an orbital of the same principal quantum number n, whereas in the Auger effect it is filled from a shell of principal quantum number $n'(n' > n)$.

Possible coupling schemes and final states in nonradiative processes have been examined by Burhop (14), Bergström and Nordling (15) and Mehlhorn (16), among others.

The relative rates of these competitive modes are measured by the following yields:

1. Fluorescence yield, ω_i^x, is the probability that a vacancy in the shell x_i fills radiatively from any of the outer shells.
2. Auger yield, a_i^x, is similarly the probability that it can be filled by an Auger process.
3. Coster-Kronig yield, f_{ij}^x, is the probability for a vacancy shift to occur from subshell i to subshell j within the main shell x_1 (with simultaneous ejection of an electron from an outer shell).

Thus, in the L shell there are three subshells and nine yields

ω_1	ω_2	ω_3	fluorescence yields
a_1	a_2	a_3	Auger yields
f_{12}	f_{13}	f_{23}	Coster-Kronig yields

These are related by the equation

$$\omega_i + a_i + \sum_{j>i} f_{ij} = 1 \tag{1}$$

Hence there are only six independent quantities. Equation (1) can be written separately for each subshell as

$$\begin{aligned} \omega_3 + a_3 &= 1 \\ \omega_2 + a_2 + f_{23} &= 1 \\ \omega_1 + a_1 + f_{12} + f_{23} &= 1 \end{aligned} \tag{1a}$$

However, it has been proposed that the small radiative somponent in the Coster-Kronig transitions which involves only the orbitals of the same principal quantum number n should be included in the Coster-Kronig yield as its radiative component ω_{ij}. According to this proposal the Coster-Kronig yield f_{ij} is

$$f_{ij}^{x} = a_{ij}^{x} + \omega_{ij}^{x} \tag{1b}$$

and

$$\omega_i + a_i = \sum_{j>1} (a_{ij} + \omega_{ij}) = 1 \tag{1c}$$

Additional quantities which have been useful from an experimental viewpoint are the ν_i's, which were also formerly called the fluorescent yields. The quantity ν_i is the total number of all L x-rays observed per vacancy in an L_i subshell. (In the actual fluorescence yield, ω_i, it is required that the L x-ray transitions go to only the L_i shell). The ν_i therefore include the result of the Coster-Kronig transitions and hence $\nu_3 = \omega_3$, $\nu_2 = \omega_2 + f_{23}\omega_3$ and $\nu_1 = \omega_1 + f_{13}\omega_3 + (f_{12} + f_{23})\omega_2$.

Then we can define an average L yield by $\bar{\omega}_L = \sum_{i=1}^{k} \omega_i V_i$ (3)

Another average yield ω_{KL} has also been used, defined as the average L shell fluorescence yield following a K-x-ray emission.

1.3 Historical Survey of L Yields

Auger (1) was the first to measure a mean Auger electron yield $\bar{a}_L$. He obtained a mean L-shell fluorescence yield $\bar{\omega}_L = 1 - \bar{a}_L$, defined as the probability that a vacancy in the L shell is filled by an L x-ray transition. This was done by using a cloud chamber filled with gases and photographing the Auger electron tracks. Lay (3) in 1935 undertook a systematic measurement of $\bar{\omega}_L$ values by fluorescent excitation of gaseous targets or foils and measuring the intensity of the emitted radiation by means of photographic plates. Elements of $40 < Z < 92$ were investigated. Fluorescent yields for the L_3-subshell for the elements between tantalum and bismuth were measured by Küstner and Arends (4) and by Stephenson (5) for lead, thorium and uranium. These authors used essentially the same method: a determination of the amount of secondary radiation

emitted from a target irradiated with x-rays at a wavelength lying between the absorption limits of L_2 and L_3 levels. Küstner and Arends (4) also attempted to measure the fluorescent yields of L_2 and L_3 levels by means of critical absorbers. Küstner et al. did not correct for the then unknown CK transitions.

Stahel (6) in 1935 measured the L yields from the decay of RaD, but he based the vacancy formation rates on the earlier work of Lay (3). Kinsey (7) reinvestigated this result and also measured the L yields from the decay of ThC where the internal conversion coefficients were better known. The detector was a (xenon + argon) - alcohol gas counter operated both as a proportional counter and as a G-M counter. α - x coincidences were also observed.

The mean fluorescent yields $\bar{\omega}_L$ were derived by dividing the theoretical radiation widths by the experimental values of total widths; i.e. $\bar{\omega}_L = \Gamma_L/\Gamma_{total}$.

Hohmuth (8) obtained ω_{KL}, a mean fluorescent yield composed of the L_2 and L_3 subshell yields and observed by means of K - L coincidences as well as $\bar{\omega}_L$ for the elements rubidium, niodium, silver, holmium and mercury using Sr^{85}, Mo^{93}, Cd^{109}, Er^{165}, and Tl^{204} and with γ - L coincidences for tellurium and lanthanum using I^{125} and Ce^{139}. Proportional counters and scintillation detectors were utilized. Hohmuth and Winter (9) measured ω_{KL} for Z = 47, 54, and 59 using Cd^{109}, Cs^{131} and Ce^{141}, respectively. Jopson et al. (10) undertook an extensive investigation of 23 heavy elements of $57 < Z \ 83$ using Co^{57} x-rays for fluorescent excitation and NaI(Tl) scintillation detectors. The work of Goldberg (11) in measuring the L yields in $73 < Z < 92$ using electron bombardment must also be mentioned.

All the foregoing experiments suffered from the poor resolution of the detectors. Hohmuth's results were influenced by poor knowledge of efficiencies in proportional counters and the results of Jopson were inaccurate due to x-ray self absorption in target foils. It was only after the advent of high resolution semiconductor detectors that significant accuracies could be claimed in the measurements of L yields. An evaluation of the accuracy of these, as well as the newer experiments, will be made in a later chapter.

CHAPTER II

EXPERIMENTAL L YIELDS

2.1 Basic Requirements

The complete description of the decay of an excited state with an L vacancy by radiative and non-radiative transitions requires us to measure at least six of the nine possible L subshell yields (equation 1). The basic requirements to obtain such detailed information are

(A) Controlled production of primary single L vacancies.

(B) High resolution study of the photon or electron emission spectra arising from the decay of these primary vacancies, with the resolution being adequate to distinguish the major groups from each subshell.

2.1.1 Vacancy Creation Processes

The primary vacancy distribution in the three L subshells is highly dependent on the nature of the process of vacancy creation. The main such processes are

(1) Fluorescent excitation.

(2) Charged particle (electron or heavy ion) bombardment.

(3) Radioactive decay processes such as (i) L orbital electron capture , (ii) K capture (followed by (4) below , or (iii) L-internal γ-ray conversion. The γ-rays can arise from the decay of a nucleus following β decay, etc. Also, radioactive decay processes can create vacancies in the K shell which can

then lead to L vacancies as in (4) below.

(4) Filling of a K vacancy from the L shell producing K_{α_1} and K_{α_2} x-rays or Auger electrons.

Which primary vacancy distribution is used in the study of the L yields depends upon the experimental technique employed, as by requirement (B) above. These techniques can broadly be divided into singles methods and coincidence methods.

2.1.2 Singles Spectrum Method

In the singles method, the total number of L x-rays arising from an event (e.g. a radioactive transition or fluorescence excitation) is measured and a mean fluorescence L yield $\bar{\omega}_L$ is calculated from the relationship

$$C_L = C_o\, p\, \bar{\omega}_L(\epsilon f \Omega) \tag{4}$$

where C_L is the number of L x-rays, C_o is the number of events leading to L vacancies, P is the probability of producing a vacancy per event, ϵ is the detection efficiency, Ω is the solid angle subtended by the detector at the source, and f is a correction factor for the attenuation of L x-rays before reaching the detector.

$\bar{\omega}_L$ will be dependent on the final vacancy distribution ratios V_1, V_2, and V_3. These are related to the primary vacancy distribution ratios N by

$$\begin{aligned} V_1 &= N_1 \\ V_2 &= N_2 + f_{12}N_1 \\ V_3 &= N_3 + f_{23}N_2 + (f_{13} + f_{12}f_{13})N_1 \end{aligned} \tag{5}$$

If the final vacancy distribution is known and detector resolution is adequate, some of the subshell yields also can be estimated. If only ν's are needed, the Coster-Kronig yield f_i need not be known.

2.1.3 Coincidence Methods

The coincidence method consists in selecting a particular distribution of primary vacancies and observing the L x-rays arising therefrom. For instance, we may observe a K_{α_1} x-ray (called the gate) which specifies a primary distribution of $N_1:N_2:N_3:0:0:1$ in coincidence with the L x-rays. The basic equations to be applied in all coincidence methods is

$$C_{L(g)} = C_g\, p\, (N_1\nu_1 + N_2\nu_2 + N_3\nu_3)\, \epsilon\omega f\, \epsilon_c \qquad (6)$$

where $C_{L(g)}$ is the number of L x-rays in coincidence with gate g (this may be K x-rays, γ-rays, conversion electrons, etc.). C_g is the number of gate counts, p is the fractional probability of an L vacancy being excited by each event in the gate, and C_c is the efficiency of the coincidence system or the ratio of recorded coincidence to actual coincidences. The quantities, ϵ, ω, f are as in equation (4) and ν is the total fluorescence yield as defined in Chapter I.

2.2 Methods of Primary Vacancy Creation

The primary vacancy creation is considered in greater detail below.

2.2.1 Direct Fluorescent Excitation

Direct fluorescent excitation consists of creating vacancies by exposing target foils to x-rays or γ-rays. It has been historically an important method for

creating primary vacancies for the measurement of L fluorescence yields (i.e. Lay (3), Kūstner (4), and Jopson (10)). The method has been used for both ω_K and $\bar{\omega}_L$ measurements; L-subshell yields have been estimated using the method of critical absorbers.

Jopson et al. (10) measured L fluorescence yields for 23 elements using a K x-ray-L x-ray coincidence method, using a Co^{57} source (122 keV energy) to produce K vacancies in the target foil. The foils have to be very thin in order to minimize self-absorption of L x-rays.

The use of the direct fluorescence method requires that accurate photo-excitation cross sections be available. Bearden (17) has compiled experimental x-ray absorption coefficients for many elements. Guttman and Wagenfeld (18), using hydrogenic wavefunctions and including dipole, dipole-octupole, Compton and quadrupole terms in the calculation, have produced theoretical absorption cross sections, which are in good agreement with experimental values away from absorption edges. Together with older work like that of Deslattes (19) these results give reliable tabulations on total x-ray absorption coefficients.

However, L shell measurements require the subshell vacancy distributions to be known and these have not been available with the necessary accuracy. For this reason, and owing to experimental difficulties, such as self absorption of the L x-rays in the target foil, scattering of the primary radiation into L detector, difficulty of making thin foils, etc., the direct fluorescence excitation method has not been used for L yields measurements recently.

2.2.2 Charged Particle Excitation

Electron beams have been employed to produce primary vacancies. The rate of vacancy creation must be calculated using the theory of atomic collisions.

The beam current is measured accurately by means of a biased Faraday cup. The vacancy distribution rates among the subshells also needs to be theoretically estimated. Electron beams that are sufficiently energetic to ionize inner shells with large enough probabilities will also produce bremsstrahlung x-rays which would make it difficult to observe the subsequent radiation emitted by the atom. For these reasons, the measurement of L fluorescent yields by the electron bombardment method of vacancy creation may not be accurate.

Heavy ions could also be utilized to produce L vacancies and in this case bremsstrahlung is negligible. In case of heavier incident particles, the theoretical estimates of vacancy creation and vacancy ratios are not considered accurate enough to permit L shell fluorescence measurements.

2.2.3 Primary L Shell Excitation by Radioactive Decay

Radioactive decay of nuclei, especially electron capture and internal conversion, may produce primary L subshell vacancies by two mechanisms.

(A) Orbital electron capture: Depending on the nature and energy of the transitions, the subshell vacancy distribution created in orbital electron capture can be calculated. In the majority of cases, K-capture predominates, giving rise to L vacancies by K x-ray, K-LL, and X - L_X Auger electron emission. In case of pure L capture (when K capture is energetically impossible) with allowed and non-unique first forbidden transitions, vacancies appear

predominantly in the L_1 subshell. For decay energies well above the L shell binding energies ($P_{L_2}|P_{L_1}$) ~ 0.15 and P_{L_3} is very small (20). Such a transition provides an adequate source of L_1 vacancies (e.g. in W^{181}). Tables of $P_L|P_K$ and $P_{L_2}|P_{L_1}$ capture ratios as a function of Z and decay energy Q_{Ec} are available (21). Here P_K, P_{L_1}, P_{L_2} etc. signifies capture probability to the K, L_1, L_2, etc. shells.

(B) L shell internal conversion: L vacancies are produced by internal conversion as well with theoretical internal conversion coefficients α_{Li} (whose values indicate the number of vacancies formed in the subshell i); as a function of transition energy and atomic number Z in case of pure multipolarity, are available. In many cases K conversion also occurs and L vacancies are created by K x-ray or K-Auger emission. An accurate knowledge of the K conversion coefficient α K is also needed in such cases. In some even α emitters low energy E2 transitions are predominantly converted in the L_2, L_3 subshells and in such cases L_2, L_3 subshell yields are measured by α-L x-ray coincidences.

2.2.4 L Shell Vacancies Following the Filling of K Shell Vacancies

In many of the radioactive decay cases, the L vacancies appear as the second stage of a cascade which begins with the creation of a K vacancy. The two phenomena which result in L vacancies are K x-ray and K Auger electron emission.

In the radiative case, a K vacancy is filled by an electron from the L_2 or L_3 shell, resulting in the emission of a K_{α_2} or K_{α_1} x-ray, respectively. K-L_1 transitions are forbidden by the electric dipole selection rule $\Delta \ell = \pm 1$. However,

a very small number of L_1 vacancies may be created by K-L_1 transition of the M1 type. The "primary subshell ratio" is equal to the intensity ratio of the x-rays $K_{\alpha_2}/K_{\alpha_1}$ and this ratio is well known (48). Non-radiative transitions filling the K vacancies from the L shell are of two types: K-LL where an electron from the L shell filled the K vacancy, the excess energy being carried away by ejecting an L electron and (ii) K-LX where the excess energy is carried off by an ejected electron from a shell X higher than L

The L subshell vacancy distribution following the filling of a K vacancy can be calculated from a knowledge of the K x-ray and K Auger emission rates. It should be noted that in the case of non-radiative transitions, the atom is doubly ionized. Let $M_{K_{Li}}$ be the average number of primary Li vacancies created in the filling of a K shell vacancy by an electron from an Li subshell.

$$n_{KL_1} = (1-\omega_K)\left[\frac{2I(K\text{-}L_1L_1)+I(K\text{-}L_1L_2)+I(K\text{-}L_1L_3)+I(K\text{-}L_1X)}{I_{KLL}+I_{KLX}+I_{KXY}}\right] \quad (7a)$$

$$n_{KL_2} = \frac{\omega_K I_{K_{\alpha_2}}}{I_K} + (1-\omega_K)\left[\frac{2I(K\text{-}L_2L_2)+I(K\text{-}L_1L_2)+I(K\text{-}L_2L_3)+I(K\text{-}L_2X)}{I_{KLL}+I_{KLX}+I_{KXY}}\right] \quad (7b)$$

$$n_{KL_3} = \frac{\omega_K I_{K_{\alpha_1}}}{I_K} + (1-\omega_K)\left[\frac{2IKL_3L_3+IKL_1L_3+IKL_2L_3+IKL_3X}{I_{KLL}+I_{KLX}+I_{KXY}}\right] \quad (7c)$$

where I_{KLL}, I_{KXY} etc. are the Auger electron intensities, I_K is total K x-ray intensity and $\Sigma\, n_{KL_i} = 1$.

2.3 Basic Equations

Because the semiconductors can resolve the main L x-ray groups the basic equations which contain them are appropriate for the use of semiconductor detectors, whether used in coincidence or singles mode. The detector can resolve the L x-ray spectrum into groups L_ℓ, L_α, L_β, L_γ (Figure 1). The counting rates are corrected for the photopeak detection efficiency and fractional solid angle subtended by the active volume of detector at the source, source self-absorption, attenuation of L x-rays between source and detector and any possible summation effects, etc.

The "radiative branching ratios" S_1, S_2, S_3 are defined as the ratios of intensities of resolved L x-ray groups arising from the radiative filling of L_1, L_2 and L_3 levels, respectively. For the L_1 subshell we write

$$S_1 = \frac{I(L_1 \rightarrow N) + I(L_1 \rightarrow O) + \ldots}{I(L_1 \rightarrow M)} \qquad (8a)$$

$$= \frac{\text{Intensity of } L_\gamma \text{ x-rays originating from } L_1 \text{ vacancies}}{\text{Intensity of } L_\beta \text{ x-rays originating from } L_1 \text{ vacancies}}$$

where $I(L_1 \rightarrow X)$ is the intensity of the radiative transitions by X shell electrons filling L_1 vacancies. Similarly

$$S_2 = \frac{I(L_2 \rightarrow N) + I(L_2 \rightarrow O) + \ldots}{I(L_2 \rightarrow M)} \qquad (8b)$$

$$= \frac{\text{Intensity of } L_\gamma \text{ x-rays originating from } L_2 \text{ vacancies}}{\text{Intensity of } (L_\eta + L_\beta) \text{ x-rays from L vacancies}}$$

and

$$S_3 = \frac{I(L_3 \rightarrow N) + I(L_3 \rightarrow O) \ldots}{I(L_3 \rightarrow M)} \tag{8c}$$

$$= \frac{\text{Intensity of } L_\beta \text{ x-rays originating from } L_3 \text{ vacancies}}{\text{Intensity of } L_\ell + L_\alpha \text{ x-rays from } L_3 \text{ vacancies}}$$

Let N be the primary vacancy distribution and $\sum_i N_i = 1$. Let p be the probability of exciting an L vacancy in an event (electron capture, internal conversion) and C_o be the number of events. I_{L_ℓ}, I_{L_α}, I_{L_η}, I_{L_β}, and I_{L_γ} are the subscripts intensities respectively of the L_ℓ, L_α, L_η, L_β and L_γ x-ray groups. The V's are the modified vacancy distributions. We have

$$I_{L_{\ell,\alpha}} = \frac{C_o p V_3 \omega_3}{1 + S_3} = \frac{C_o p \omega_3}{I + S_3} [N_1(f_{13} + f_{12}f_{23}) + N_2 f_{23} + N_3] \tag{9a}$$

$$I_{L_{\eta,\beta,\gamma}} - S_3 I_{L_{\ell,\alpha}} = C_o p[V_1\omega_1 + V_2\omega_2] = C_o p[N_1(\omega_1 + f_{12}\omega_2) + N_2\omega_2] \tag{9b}$$

$$I_{L_{\eta,\beta}} - S_3 I_{L_{\ell,\alpha}} = C_o p \frac{V_1\omega_1}{1+S_1} + \frac{V_2\omega_2}{1+S_2} = C_o p \frac{N_1\omega_1}{1+S_1} + \frac{(N_2+N_1f_{12})\omega_2}{1+S_2} \tag{9c}$$

and

$$I_{L_\gamma} = C_o p \frac{V_1 S_1 \omega_1}{1+S_1} + \frac{V_2 S_2 \omega_2}{1+S_2} = C_o p \frac{N_1 S_1 \omega_1}{1+S_1} + \frac{(N_1 f_{12} + N_2) S_2 \omega_2}{1+S_2} \tag{9d}$$

where

$$I_{L_{\ell,\alpha}} = I_{L_{\ell}} + I_{L_{\alpha}}$$

$$I_{L_{\eta,\beta}} = I_{L_{\eta}} + I_{L_{\beta}} \qquad (10)$$

$$I_{L_{\eta,\beta,\gamma}} = I_{L_{\eta}} + I_{L_{\beta}} + I_{L_{\gamma}}$$

The quantity p in equation (9) can be obtained from a detailed knowledge of the events under consideration. If the events are pure L capture decays, p is P_L, the L capture probability. If the event is an internal conversion process, $p = \alpha_L/\alpha_{total}$, the rate of the L shell to total internal conversion coefficient. If the event is the filling of a K vacancy, $p = n_{KL}$ and so on. If (as in a singles spectrum study), all these processes are involved simultaneously, p is a function of all these above quantities.

In the singles method, if the resolution of the L x-ray detectors is sufficient, the L_γ peak can be resolved into L_{γ_1} (corresponding to L_1 shell) and L_{γ_2} (corresponding to L_2 subshell) and equation (9d) can be split up into

a) $$I_{L_{\gamma_1}} = C_o p\, \omega_1 V_1 \frac{S_1}{1+S_1}$$

$$\omega_1 = I_{L_{\gamma_1}} \left[C_o p V_1 \left(\frac{S_1}{1+S_1}\right)\right]^{-1} \qquad (11)$$

b) $$I_{L_{\gamma_2}} = C_o p\, \omega_2 V_2 \frac{S_2}{1+S_2}$$

Thus we have a means of evaluating ω_1, if we obtain the other quantities such as V_1 and S_1 from other experiments or theory.

2.4 The Coincidence Method

The coincidence method is used to select only certain kinds of events among all the C_o events present, thus choosing a specific primary distribution of L vacancies. The technique is very useful for the following reasons: It removes the need to rely on calculated vacancy distributions (except for estimates of minor corrections), thus relative independence from nuclear decay schemes, conversion coefficients, capture probabilities, etc. is achieved. The coincidence spectra, which are simpler than the direct (or singles) spectra, can be analyzed with greater accuracy.

Four types of coincidence experiments have been used to measure L yields:

(1) L x-ray - K x-ray coincidences

(2) L x-ray - γ-ray coincidences

(3) L x-ray - conversion electron coincidences

(4) L x-ray - α particle coincidences

The equations applicable to any coincidence experiment are as follows:

Let g stand for the gate, K x-ray, conversion electron, γ-ray etc. Then C_g is the number of total gate counts. $C_{L(g)}$ is the number of L x-rays in coincidence with g as before.

Then

$$C_{L_{\ell,\alpha}(g)} = C_g\, p\, \frac{V_3 \omega_3}{1+S_3} \qquad (12a)$$

$$C_{L_{\eta,\beta,\gamma(g)}} - S_3 C_{L_{\ell,\alpha(g)}} = C_g p[V_1\omega_1 + V_2\omega_2] \tag{12b}$$

$$C_{L_{\eta,\beta(g)}} - S_3 C_{L_{\ell,\alpha(g)}} = C_g p \frac{V_1\omega_1 S_1}{1+S_1} + \frac{V_2\omega_2 S_2}{1+S_2} \tag{12c}$$

$$C_{L_{\gamma(g)}} = C_g p \frac{V_1\omega_1 S_1}{1+S_1} + \frac{V_2\omega_2 S_2}{1+S_2} \tag{12d}$$

The V's here are the specific vacancy distribution selected by the coincidence requirement.

2.4.1 $L(K_\alpha)$ Coincidences

When a K vacancy is filled from the L_2 subshell, a K_{α_2} x-ray is emitted and similarly when it is filled from the L_3 subshell, a K_{α_1} x-ray is emitted. Thus, the K_{α_2} and K_{α_1} x-rays signal the formation of pure L_2 and L_3 subshell vacancies.

For K_{α_1}

$$N_1 = 0,\ N_2 = 0,\ N_3 = 1,\ p = 1$$

and

$$C_L(K_{\alpha_1}) = C_{K_{\alpha_1}} \omega_3 (\epsilon \quad f\epsilon_c).; \tag{13}$$

$$S_3 = \frac{C_{L_\beta}(K_{\alpha_1})}{C_{L_{\ell,\alpha}}(K_{\alpha_1})} \tag{14}$$

Similarly with K_{α_2}

$$N_1 = 0,\ N_2 = 1,\ N_3 = 0,\ p = 1$$

and

$$C_L(K_{\alpha_2}) = C_{K_{\alpha_2}}\, \nu_2 (\epsilon \Omega f \epsilon_c) = C_{K_{\alpha_2}} (\omega_2 + f_{23}\omega_3)(\epsilon \Omega f \epsilon_c) \tag{15}$$

$$\frac{C_{L_{\ell,\alpha}}(K_{\alpha_2})}{C_{L_{\ell,\alpha}}(K_{\alpha_1})} = \frac{C_{K_{\alpha_2}}}{C_{K_{\alpha_1}}} \cdot f_{23} \tag{16}$$

$$S_2 = \{ C_{L_\gamma}(K_{\alpha_2})/C_{L_\beta}(K_{\alpha_2}) - S_3\, C_{L_\alpha}(K_{\alpha_2}) \} \tag{17}$$

Thus, by separately gating on K_{α_2} and K_{α_1} x-rays, all the L_2L_3 subshell values as well as the radiative branching ratios S_2 and S_3 are obtained.

The experiment could be performed by either fluorescent excitation of foils (10, 22 and 23) or by using radioisotopes. In the foil excitation method, a measurement of f_{23} (Coster-Kronig yield) is prevented by the fact that many L_3 vacancies are directly created.

However, this difficulty can be eliminated if one uses carrier-free radioisotopes. Source self-excitation of L_3 vacancies is negligible in such a case. A large number of $L(K_\alpha)$ coincidence experiments have been made (26-28).

2.4.2 Gamma L X-ray Coincidences

L x-ray-gamma-ray coincidences are possible when two nuclear transitions are in cascade connected by an intermediate state that is not long lived. Here the

L vacancies created in the internal conversion of one transition are in coincidence with the gammas from the other transition. Another case could be when orbital electron capture leads to an excited state that emits a prompt gamma ray. Ideally a pure L capture would lead to an excited state that would decay by a prompt gamma to the ground state. Such a case in W^{181} was used as a source of L_1 vacancies to estimate L_1 yields (28).

The primary L vacancies produced in all the transitions in cascade with the gating gamma ray could be due to one or more of the processes such as electron capture, internal conversion, K - x-ray emission, K - Auger emission etc. Accurate knowledge of these contributions is needed. When there are several gammas, great care is needed to exclude Compton contribution etc. from the higher energy γ-rays.

2.4.3 Conversion Electron - L X-ray Coincidences

In an internally converted gamma transition, the number of conversion electrons emitted gives the number of vacancies in the corresponding shells. If L conversion electrons are used, these directly signal the creation of L vacancies. Ideally this nuclear transition should not be preceded or followed by nuclear events in which L vacancies are produced. When such vacancies are produced, however, (as in the formation of K vacancies by K - conversion which in turn gives rise to L vacancies) the contribution to L vacancies can usually be estimated.

Very high resolution is needed to separate individual L subshell electrons and this in most cases is not available. In such cases, the vacancy distribution has to be estimated from conversion coefficient tables.

Thus

$$N_1:N_2:N_3 = \frac{\alpha_{L_1}}{\alpha_L}:\frac{\alpha_{L_2}}{\alpha_L}:\frac{\alpha_{L_3}}{\alpha_L}$$

where α_L denotes the internal L shell conversion coefficient. If K conversion electrons are used instead of L conversion electrons

$$N_i = \frac{\alpha_K}{\alpha_{total}} \quad n_{K_{L_i}} \tag{18}$$

In the low Z region, K vacancies are mostly filled by Auger transitions leading to double vacancy states and then K conversion electron - L x-ray coincidences can be used to study them.

2.4.4 α- L Coincidences

If the decay of an α-excited nuclear level occurs to the ground state and this takes place by L, M--shell converted γ transitions without any K conversion, then L subshell yields may be measured by α- L x-ray coincidences. The above requirements restrict application to high Z nuclides with low-lying levels. Of these, even-even nuclides give low energy E2 ground state transitions ($N_1:N_2:N_3 = 0:1:1$) and odd-A nuclides give E1, M1 transitions ($N_1:N_2:N_3 \sim 0.9:0.1:0$). Thus the results from E2 transitions give information on L_2 and L_3 subshells and the results from the E1 transitions give information on the L quantities. Hence both odd-A and even-A nuclides must be used to obtain the subshell quantities for a given element. The method is generally used in conjunction with L(γ) coincidences.

The method has been applied by Byrne (29), Halley (30) and Ferreira (31)

to determine the fluorescence yields for Ra, Th, V, Pu and Cm. Following Byrne, we define

$$I_L(\alpha)/C_\alpha = F \tag{19a}$$

$$\frac{(N_3+N_2 f_{23})\,\omega_3}{N_2\,\omega_2} = F_3' \tag{19b}$$

$$N_3/N_2 = C_3' \tag{19c}$$

and

$$\omega_2 = \frac{F(1+C'_3\nu)}{(\alpha L/\ell+\alpha t)(1+F'_3)} \tag{20a}$$

$$f_{23} = \frac{\omega_2}{\omega_3} F_3' - C_3' \tag{20b}$$

It is necessary to assume ω_3, which is a serious limitation of this method.

CHAPTER III

THEORETICAL APPROACHES TO THE CALCULATION OF L YIELDS

Since one of the aims of L subshell fluorescence yields measurements is to enable one to check the validity of atomic structure calculations, it is necessary to discuss these calculations in some detail.

The basic approach of these calculations is to assume that an atom can be represented by a simple atomic model, assume various wave functions and solve the Schroedinger equation for the atom and obtain the radiative and non-radiative transition probabilities for the various shells which can then be compared with the experimental transition probabilities.

A wide variety of wavefunctions are used in these calculations, two general approaches being (i) the hydrogenic wavefunctions with screening and (ii) central-field approximations with self-consistent-field techniques.

In the first case, the electron whose transition probability we wish to consider is assumed to be a single electron orbiting a nucleus, as in the hydrogen atom. The presence of the other electrons in the atom modifies this nuclear potential or "screens" it. In the second case, the electron moves in a field contributed to by the nucleus and all the other electrons. We shall give here an indication of these methods and discuss later on calculations using these approaches.

3.1 Hydrogen Atom

The simplest atomic case is that of hydrogen, with one electron orbiting a nucleus of unit charge Z. The time dependent Schrodinger equation for this case is

$$H\Psi = \left(\frac{h^2}{2M}\right)^2 - \frac{Ze^2}{4\pi\epsilon_o r}\Psi = E\Psi \qquad (21)$$

where Ψ is the wavefunction of the electron and $\mathcal{H}$ is the Hamiltonian and M the reduced mass of the electron. In atomic units, ($e = m_e = h = 1$), this equation becomes

$$(\tfrac{1}{2}\Delta^2 - Z/r)\Psi = E\Psi \qquad (22)$$

Separating the variables, the angular part of the equation has the standard spherical harmonics as solutions, and the radial equation becomes

$$\frac{d^2P(r)}{dr^2} + 2\left[E + \frac{Z}{r} - \frac{1(1+1)}{2r^2}\right]P(r) = 0 \qquad (23)$$

where $P(r) = rR(r)$.

The solutions for the radial part are called the "hydrogenic" class of wavefunctions and are widely used in atomic structure calculations.

3.2 Central Field Approximation and Self Consistent Field Techniques

3.2.1 Central Fields Approximation

When we have more than one electron, the exact solution of the Schrödinger

equation is impossible and one has to proceed with approximations.

First of all, one assumes that each electron (non-interacting with the others) moves in a spherically symmetric potential formed by the nucleus and the other (Z-1) electrons. This potential is called the central field and the central field theory must be modified by considering spin-orbit coupling and Coulomb interaction between electron pairs. The coupling can be of the LS, JJ or intermediate types, depending on the strength of the spin-orbit interaction. (Coupling schemes are important in considerations of hydrogenic wavefunctions as well.)

Let us consider the Hamiltonian by

$$\mathcal{H} = \mathcal{H}_o + \mathcal{H}_c + \mathcal{H}_{s.o} \tag{24}$$

where $\mathcal{H}_o = \left(\frac{h^2}{2\mu}\Delta^2 - \frac{Ze^2}{r_i}\right)$ is the hydrogenic Hamiltonian.

$\mathcal{H}_c = \sum_{i \neq j} e^2/r_{ij}$ is the Coulomb interaction of electron pairs.

$\mathcal{H}_{s.o} = \sum_i \xi(r_i)(\vec{\ell}_i \cdot \vec{s}_i)$ is the spin-orbit interaction.

The different coupling schemes are given by

$\mathcal{H}_c >> \mathcal{H}_{s.o}$: LS coupling

$\mathcal{H}_c << \mathcal{H}_{s.o}$: JJ coupling

$\mathcal{H}_c \sim \mathcal{H}_{s.o}$: Intermediate coupling

A) L.S. coupling: In the L.S-coupling scheme, a vacancy is characterized by the quantum numbers n and ℓ e.g. as a 2S or 2P hole or in other words an L_1, or

$L_{2,3}$ vacancy. Because of the electrostatic interaction of the electrons, the electron configuration is split into terms of different energies characterized by L and S.

B) J.J. coupling: There the spin-orbit interaction dominates and the vacancies are characterized by η, ℓ, j (e.g. $2P_{\frac{1}{2}}$, $2P_{3/2}$, etc.). Extreme JJ coupling takes into account only the spin-orbit interaction, which is a relativistic effect so that in relativistic theory JJ coupling is invariably used.

C) Intermediate coupling: In this case, the number of possible transitions is greater. The notation and results depend upon whether intermediate coupling is approached from a pure LS or pure JJ coupling.

3.2.2 Self Consistent Fields

Following Hartree (32) the Schroedinger equation for a single electron mowing in the spherically symmetrical central field is solved and the solutions for many electrons are combined to build up the charge density of the atoms. The potential arising from this charge density is found making the requirement of self-consistency: in the final potential most agree with the initial one which had been assumed to set up the Schroedinger equation.

Thus, an iterative procedure is used for the calculation: one assumes an initial field carries out calculations and obtains final wavefunctions: These final functions are used as the initial function in the next step and so on, until the initial and final fields agree within some specified accuracy.

The charge field of the nucleus is "screened" by the core electrons from the one electron under consideration and hence the nuclear charge is replaced by

an effective charge $Z^{*}e = (Z - \sigma)_e$ where σ is the so-called screening factor. The results obtained are very much dependent upon this screening and different authors have used different values. Hartree derives the screening constant from the ratio of the mean hydrogenic radius $\bar{r}_H$ to the mean radius derived from a "more realistic" wavefunction $\bar{r}$.

$$\sigma = Z - \frac{\bar{r}}{\bar{r}_H}$$

Another approach has been to choose an effective charge $Z^{*}e$ such that the binding energy obtained for a single hydrogenic atom is the same as that observed for an electron in the corresponding state in the actual atom of charge Z.

3.2.3 Hartree-Fock Method and the Exchange Term

The second postulate of the self consistent field theory (SCF) is that of the spin of the electron, and the third consists of the application of the Pauli exclusion principle to the electron, derived from the fact that the electrons obey Fermi-Dirac statistics. This last requirement can also be derived from the postulate of Pauli, namely: the wavefunction for a many electron system must change sign when the coordinates of the electrons are interchanged.

Then, if U_1, U_2 ... are the spin-orbitals of individual electrons whose space and spin-coordinates are characterized by $U_1(1)$, $U_1(2) \ldots U_1(N)$, then the simplest, antisymmetric, N particle wavefunction can be expressed by the determinant

$$\begin{vmatrix} U_1(1) & U_1(2) & U_1(N) \\ U_2(1) & U_2(2) & U_2(N) \\ U_N(1) & U_N(2) & U_N(N) \end{vmatrix} \tag{25}$$

In the Hartree equation, the one-electron wavefunctions $U_1(x)$, $U_2(x)$ ... are varied in such a way as to make

$$\int U^*(x_1)\, U_2^*(x_2) \ldots H\, U_1(x_1) \ldots U_N(x_N)\, dx_1 dx_2 \ldots dx_N \tag{26}$$

an extremum and by requiring that the function U be normalized. This leads to a minimization of energy. In the Hartree-Fock method (33) instead of the product function, a product determinant is used and thus the quantity

$$\frac{1}{N!} \int \begin{vmatrix} U_1^*(x_1) \ldots U_1^*(x_n) & U_1(x_1) \ldots U_1(x_n) \\ U_n^*(x_1) \ldots U_n^*(x_n) & U_n(x_1) \ldots U_n(x_n) \end{vmatrix} \begin{matrix} dx_1 \\ \vdots \\ dx_n \end{matrix} \tag{27}$$

is made an extremum. Here the integration includes summation over spin. The Hartree-Fock equation can be written in the form

$$\left\{ H_1 U_1(x_1) + \left[\sum_{k=1}^{n} \int U_k^*(x_2) \left(\frac{e^2}{\vec{r}_{12}} \right) U_K(x_2)\, dx_2 \right] U_1(x_1) \right.$$

$$\left. - \left[\sum_{k \neq 1}^{n} \int U_k^*(x_2) \left(\frac{e^2}{\vec{r}_{12}} \right) U_i(x_L) dx_2 \right] U_k(x_1) \right\} = E_1 U_1(x_1) \tag{28}$$

The H_1 is the kinetic energy operator for the electron of coordinate x_1

plus its potential energy in the field of all electrons; $e^2/\vec{r}_{12}$ is the Coulomb energy of interaction of electrons 1 and 2; thus the second term is the Coulomb potential energy acting on the electron at position x_1, of all the electronic charge including that of the i^{th} wavefunction which is under consideration. The third term then corrects for the fact that the electron does not act on itself and this is called the exchange term.

If we consider an electron of spin + 1/2 and assume that all positive (+ 1/2) spin electrons contribute a charge density ρ^+, with all negative (-1/2) spin electrons contributing a charge density ρ^-, the field at the electron under consideration would consist of that due to the whole of ρ^-, but that of ρ^+ would be corrected by removing from the immediate vicinity of the electron whose wavefunction is under consideration, an exchange charge density correction whose total amount is equal to that of a single + 1/2 electron. Thus, the corrected charge density equals (n-1) electron charges and there is a sort of "hole" surrounding the electron in question consisting of a deficiency of charge of the same spin as the electron under consideration. This hole is called the Fermi or exchange hole. The exact form of the hole varies for different orbitals and different wavefunctions U_i.

Slater (34) showed that by forming a weighted mean of exchange charges (averaged and weighted over the various electronic functions at a given region of space) one can set up an average potential field including exchange for all the orbitals. Further, he replaced the average exchange charge by the corresponding charge in a free electron gas whose local density is equal to the density of the actual charge at the point in question. This is called the free electron exchange

approximation. The free electron exchange potential, when $\rho^+ = \rho^-$ is

$$V(\rho)_{exch} = -6[3/(8\pi)|\rho|]^{1/3} \tag{29}$$

where ρ is the actual charge density.

The Slater modification greatly simplifies the application of SCF method as cumbersome exchange integrals need not be evaluated. The field based on Eq. (28) with Slater exchange correction is called the HFS field. The HFS field utilizing the SCF method has been the basis of the majority of atomic structure calculations for the determination of L-fluorescence and Coster-Kronig yields. We shall examine below some of the current efforts.

3.3 Calculation of Transition Probabilities

In order to obtain the theoretical fluorescence and Coster-Kronig yields, one must calculate the radiative and nonradiative transition probabilities. In such calculations, the wavefunctions and potentials are generally obtained from self-consistent field (SCF) calculations mentioned above.

3.3.1 Radiative Transition Probability

From time-dependent perturbation theory, the transition probability per unit time from an initial state i to a final state f is given by

$$W_{if} = \frac{2\pi}{h} \left| \int \Psi_f^* \mathcal{H} \Psi_i \, d\tau \right|^2 \rho(E_f) \tag{30}$$

where Ψ_f, Ψ_i are the final and initial wavefunctions, $\mathcal{H}$ is the interaction

Hamiltonian and $\rho(E_f)$ the density of final states of energy E_f that satisfy conservation of energy. This transition probability includes the radiative and non-radiative components. It is customary to expand the radiative part in multipoles L according to the angular momentum carried off by the quantum.

3.3.2 Non-Radiative Transition Probabilities

In a non-radiative transition (Auger or Coster-Kronig) a radiation less transition fills the inner shell vacancy and an electron is ejected, leaving the atom doubly ionized. The state of such nearly closed shell configurations with two holes can be represented in terms of completely closed shell configurations together with the correlated two electron configurations (13). The initial and final states can therefore be given by two electron configurations related to two-hole states that consist initially of one inner shell vacancy and one hole in the continuum and finally of two inner shell vacancies. Then in equation (30) we replace the matrix element by

$$D = \int\int \Psi_a^*(1)\, \Psi_b^*(2)\, \frac{e^2}{\vec{r}_{12}}\, \Psi_c(1)\, \Psi_d(2)\, d\tau_1\, d\tau_2 \qquad (31)$$

The identification numbers (1) and (2) here pertain to the electrons. Here Ψ_b is a continuum wavefunction, while Ψ_a, Ψ_c, and Ψ_d are bound-state wavefunctions.

For the sake of autosymmetry the exchange matrix corresponding to the indistinguishable exchange operation ($\Psi_d \rightarrow \Psi_a$; $\Psi_c \rightarrow \Psi_b$) must be included. It is

$$E = \int\int \Psi_a^*(2)\, \Psi_b^*(1)\, \frac{e^2}{\vec{r}_{12}}\, \Psi_c(1)\, \Psi_d(2)\, d\tau_1\, d\tau_2 \qquad (32)$$

and the transition probability per unit time is

$$W_{fi} = \frac{2\pi}{h} |D\text{-}E|^2 \rho(E_f) \qquad (33)$$

The total transition rate for the radiationless decay of a given atomic state is the properly weighted sum of the probabilities W_{fi} for all possible radiation transitions.

3.3.2 Theoretical Calculations of Fluorescence Fields

One of the earliest calculations of L fluorescent yields was made by Kinsey (7) who deduced them by dividing theoretical radiation widths by experimental values of total widths. The total widths were measured by studying the shapes of the absorption edges of the three L-shell levels. Richtmeyer et al. (35) measured the width of the three L levels by fitting the constants of a theoretical formula to suit the experimental curve for the shape of absorption edges. On the low energy side the shape of the edge corresponds to that given by the formula; on the higher energy side, the experimental shape is distorted by the uneven distribution of energy of the states of the free electron in the solid material of the target. Bearden and Snyder (36) and Coster and de Lang (37) also obtained experimental widths which were fitted to the low energy side of the Richtmeyer formula.

The radiation and Auger widths for gold (Z=79) were calculated by Ramberg and Richtmeyer (38) by a non-relativistic theory with a Thomas-Fermi field for doubly ionized Tl (Tl^{++}). The ionic radius was adjusted to account for the difference in nuclear charge of gold and thallium. The continuous wavefunctions were calculated from the Kramers asymptotic formula. The predicted total L widths are too

large.

Massey and Burhop (39) made relativistic calculations with better results screened hydrogenic wavefunction, with Slater's screening constant (equation 29). However, some of the weaker lines were neglected and also relative Auger electron intensities are somewhat too large.

Many of the more recent calculations of fluorescence yields start off with the Herman-Skillman radial wavefunction derived from the radial HFS equation. To begin

$$\left(-\frac{d^2}{dr^2} + \frac{\ell(\ell+1)}{r^2} + V(r)\right) P_{nl}(r) = E_{nl}\, P_{nl}(r) \tag{34}$$

where $P_{nl}(r) = rR_{nl}(r)$ and R is the radial wavefunction. The potential $V(r)$ is the sum of the nuclear Coulomb potential and the exchange potential. Tentatively $V_o(r) = V_o(r)$ at all r and

$$V_o(r) = -\frac{2Z}{r} - \frac{2}{r}\int_o^r \sigma(t)\, dt - 2\int_r^\infty (\sigma(t)/t)dt - 6[3/8\pi\rho(r)]^{1/3} \tag{35}$$

where t is summary variable for r. $\rho(r) = \sigma(r)/4\pi r^2$ is the spherically averaged total charge density. The distances are in Bohr units. The screening constant σ is given by

$$\sigma(r) = -\sum_{nl} \omega_{nl}\left[P_{nl}(r)\right]^2 \tag{36}$$

where the occupation number $\omega_{nl} = 2(2\ell + 1)$ for closed shells. The $P_{nl}(r)$ are

normalized wavefunctions.

The first term in (35) is the Coulomb energy. The second is the potential energy in field of a charge located inside a sphere of radius r (inner shielding). The third term arises from the charge outside the sphere of radius r (outer-shielding) and the last term is the exchange correction.

The free electron exchange approximation fails at large distances and the potential is hence modified as

$$\begin{aligned} V(r) &= V_o(r) && r < r_o \\ &= -2(Z-N+1)/r_o && r > r_o \end{aligned} \tag{37}$$

where Z is the nuclear charge and N the number of electrons in the atom or ion.

Relativistic effects and spin orbit coupling are introduced in terms of the perturbation theory. The radial wave equation is now written as

$$[\mathcal{H}_o(r) + \mathcal{H}_m(r) + \mathcal{H}_d(r) + \mathcal{H}_{s\cdot o}(r)]R(r) = ER(r) \tag{38}$$

where $\mathcal{H}_o(r)$ is the non-relativistic Hamiltonian.

$$\mathcal{H}_m(r) = -\frac{\alpha^2}{4}[E^o - V(r)]^2 \tag{39}$$

corrects for the relativistic variation of mass. α is the fine structure constant and E^o is the nonrelativistic energy eigen value.

The term $\mathcal{H}_d(r)$ corrects for the shift in orbitals with relativistic effect. For a Coulomb potential the correction is unity for $\ell = 0$ and zero for $\ell \neq 0$.

Finally, the spin orbit term

$$\mathcal{H}_{s\cdot o}(r) = -\frac{\alpha^2}{4}(-\ell)\left(\frac{1}{r}\right)\frac{dV(r)}{dr} \quad ; \; j = \ell + \tfrac{1}{2}$$

$$= -\frac{\alpha^2}{4}(\ell+1)\left(\frac{1}{r}\right)\frac{dV(r)}{dr} \quad ; \; j = \ell - \tfrac{1}{2} \qquad (40)$$

$$= 0 \qquad \ell = 0.$$

McGuire (40) approximated the quantity $-rV(r)$ by straight line segments where $V(r)$ is the relativistic Herman-Skillman potential. This quantity was used to calculate one electron potentials. These were then applied to radial Schrödinger equations in a central field which are exactly solvable. Radiative and nonradiative transition probabilities were then calculated by this approach.

Scofield (41) made relativistic calculations for the radiative L vacancy decay rates, including the effect of retardation (finite speed of propagation of electromagnetic radiation). The Herman-Skillman relativistic potentials were used and the exchange term was set as

$$V = -\frac{3}{2}\, e^2 (3\rho/\pi)^{1/3}$$

Iterative procedures were used to find the potential arising from the occupation of single particle levels by the specified number of electrons. The radial matrix elements were then found by integrating the products of the initial and final wave functions and the spherical bench functions.

Rosner and Bhalla (42) made use of the same model as Scofield but included the effects of finite nuclear size.

Non-relativistic calculations for the L subshell yields were made by Chen,

Crasemann, et al. (43) using screened hydrogenic wavefunctions. A screened Coulomb wavefunction [the Gordan wavefunction (44)] was used for the continuous wavefunction and the screening constant used in all cases was

$$\sigma = Z - \bar{r}_H / \bar{r} \tag{41}$$

where $\bar{r}$ H is the mean hydrogenic radius and $\bar{r}$ the mean Hartree Fock radius for the neutral atom. The radiontionless transition widths obtained from the calculations were combined with Scofield's radiative rates in order to obtain the fluorescence yields.

Callan (45) used non-relativistic screened wavefunctions, together with the Gordan wavefunctions in a manner analogous to that of Chen, Crasemann et al. (43) to calculate the $L_1L_{2,3}M_{4,5}$ Coster-Kronig transition rates. The screening constants used were those of Lõwdin and Appel (46). Due to the energetics of the transition, this transition ($L_1L_{2,3}M_{4,5}$) is possible only in a certain Z range; these lower and higher cut-off points were found at Z = 50 and Z = 73, respectively.

Talukdar and Chatterji (47) made a relativistic calculation for $L_1L_2M_{4,5}$ Coster-Kronig transitions, using for the direct matrix D the form

$$|D|^2 = \left|\frac{2\pi}{h} \int\int \frac{1^2}{r_{12}} \left[\exp(2\pi\nu f_i |\vec{r}_{12}|/c)\right] X(\rho_1\rho_2 - j_1 j_2) d\tau_1 d\tau_2\right|^2 \tag{42}$$

where ρ_1, ρ_2, j_1, j_2 represent relativistic wavefunctions.

$$\begin{aligned} \rho_1 &= -1(\Psi^*_{1f} \Psi_{1i}) & j_1 &= 1(\Psi^*_{1f} \vec{\alpha} \Psi_{1i}) \\ \rho_2 &= -1(\Psi^*_{2f} \Psi_{2i}) & j_2 &= 1(\Psi^*_{2f} \vec{\alpha} \Psi_{2i}) \end{aligned} \tag{43}$$

One of the more recent calculations by Chen and Crasemann (49) used the analytic independent particle model of Green et al. (50) to calculate L_2 subshell fluorescence yield and L_2-L_3X Coster-Kronig yield. Using the Green's analytic potential (50) instead of the simple Coulomb potential used in the former calculations results in a slight reduction of the discrepancy between theoretical and experimental results for f_{23}.

To summarize the theoretical situation, a large number of calculations exist for the L yields, but all start from very similar premises. The calculations all assume a hydrogenic potential or central field and the difference in the calculations lie in the potentials assumed, coupling rules used and in the numerical methods of calculation. Therefore, it is essential to have experimental results to compare with, and thus a choice between the various calculations can be made.

CHAPTER IV

BASIS OF THE EXPERIMENTAL DETERMINATION OF L YIELDS BY L(K) COINCIDENCES

The measurement of L(K) x-ray - x-ray coincidences is the method that has been utilized for the present set of experiments. The basic equations for the L(K) coincidences have been discussed in Chapter II. It now remains to look at some details, such as detector requirements, and corrections to be applied.

In the study of L-sub shell fluorescent and Coster-Kronig yields, one measures the coincident intensity ratios for resolved groups of L x-rays. The present set of experiments covers the 5-12 keV region for L x-rays. Suitable detectors are those, such as Si(Li) having a high efficiency and a fairly flat efficiency-energy response curve in this region, in order to minimize errors in comparing intensity rates of x-ray groups of different energy.

The "gate" in these experiments is a K_{α_i} x-ray or a γ-ray. To detect these, the detectors should have great resolution and high efficiency in the 40-100 keV region. Cooled Ge(Li) or Ge (intrinsic) detectors satisfy this requirement. The Ge detectors can be used for L x-ray detection as well, but the efficiency curve in this case has a discontinuity at 11.1 keV (Ge K-edge) and great care is needed in the intensity comparisons in that vicinity.

Thus, the high resolution semiconductor detectors available at present are well suited to study L x-ray yields. Their resolution (150-400 eV FWHM at 5.9

keV K_{α} x-ray lines of Mn from Fe^{55} decay) is adequate to resolve the major groups of L x-rays, and efficiencies ($\approx 10^{-3}$) are sufficient to permit coincidences. With care they can be used at energies as low as 3 keV. Below 3 keV proportional counters can be used to measure x-rays, especially if the sources can be internally situated. Diffraction spectrometers (bent crystals) have extremely good resolution and can be used to isolate individual transitions, but their detection efficiencies are generally too small for them to be used in coincidence experiments. A combination of crystal (diffraction) x-ray spectrometer used for isolating individual transitions, with solid state detectors, proportional counters and scintiallation counters for measuring total L x-ray spectrum or L x-ray groups can lead to measurement of L yields which might otherwise be inaccessible. In the present work, cooled Ge(Li) or Si(Li) semiconductor detectors were employed throughout to measure L yields by coincidence techniques. The experiment is done by using cooled Si(Li) detectors to see the L x-rays. This is called a "spectrum" detector. A Ge(Li) detector is used to see the K x-rays and this is referred to as a "gate" detector. Certain K x-ray lines are isolated by means of single channel analysers (i.e. K_{α_2}, K_{α_1}, etc.) and these are referred to as "gating lines" or "gates." A coincidence event or coincidence count occurs when one such "gate" count arrives at the coincidence unit as one L x-ray "spectrum" count.

Since the measurement of L yields involves the measurement of absolute L x-ray intensities in the L(K) coincident spectra, a careful estimation of the L x-ray detection efficiency is essential. The L x-ray detection efficiency is reduced by absorption in the beryllium window, in the "dead" surface layer and in the "dead"

annular ring around the edge of the detectors. Variations in the electric field distribution in the detector and incomplete charge collection in the detector can also impair the efficiency of the detector. These factors, which are different for individual detectors give rise to a certain unpredictability in the efficiency of each detector. For this reason, the absolute efficiency of the L detector was measured in each experiment separately by using calibrated (IAEA) standard sources, reproducing as far as possible the identical geometry and counting rate as in the experiment.

An extensive investigation of the efficiencies of the detectors used in these experiments has been carried out by Hansen, Freund and Fink (51) as well as McGeorge, Schmidt-ott, Nix, Unus, and Fink (52).

The following corrections have to be applied to the results of the L(K) coincidence experiment:

1. Standard corrections: The counting rates have to be corrected for the photopeak detection efficiency and fractional solid angle subtended by the active volume of the detector at the source, source self absorption (exceedingly small with carrier-free radioactive sources), attenuation of the L x-rays between source and detector (by air absorption in the intervening distance, absorption in the Be window of the detector, etc.) and any possible summation effects.
2. Coincidence efficiency: The system used may not register all the coincident events and hence the coincidence efficiency has to be measured in each case. This is generally done by taking a time spectrum, i.e. the coincidence

resolving time is varied and the number of coincident events is registered, and it is verified that the entire prompt coincidence peak is observed in the coincidence period used for the experiment. In general, the coincidence efficiency is very close to unity.

3. Gate composition: (Fig. 2) Due to the fact that the gate detector is of finite resolution, the K_{α_1} and K_{α_2} x-rays are not completely separated from each other. Further, if these are higher energy γ-rays or the source is a β emitter, the K x-rays ride on a fairly large continuum. Thus the typical gating pluse, say K_{α_2}, contains, in addition to true K_{α_2} events, background plus continuum counts and K_{α_1} events due to overlap of K_{α_1} and K_{α_2} x-rays. This overlap is resolved by super-imposing a single line taken in the same detector under the same conditions on the K_{α_1} line and estimating the fraction that falls under the K_{α_2} gate.
4. Chance coincidences: Due to the finite resolving time of the coincidence circuit, a certain number of the coincidence events are due to chance. These can be estimated by a separate chance coincidence run, in which a delay of several microseconds is inserted in one of the branches (K or L) so that no true events are possible and taking an L(K) coincidence run as before. Alternately, the chance rate may be estimated as in (5) below.
5. Nuclear cascading: When nuclear decay involves a cascade of two or more transitions which give rise to K and L vacancies, the coincident spectrum contains in addition to true events and chance coincidences, x-ray coincidences arising out of nuclear cascading, L vacancies created directly by nuclear

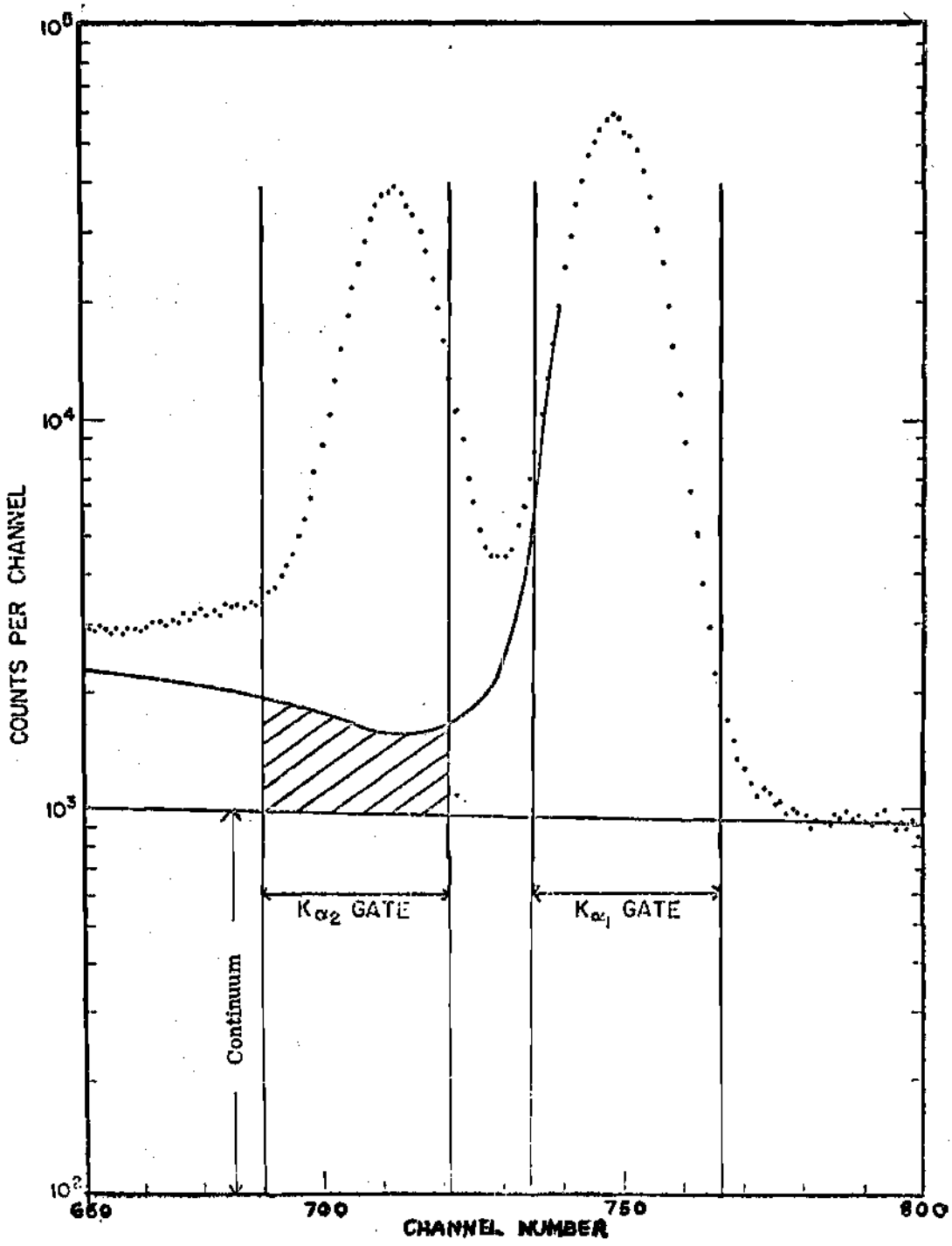

Figure 2. Typical Gate Composition.

events such as internal conversion of L capture. These can be accounted for by setting a gate on the Kβ line and taking L(Kβ) coincidences (27) since Kβ lines arise out of K-M or K-N transitions, any L x-rays found in coincidence with Kβ must be due to chance and a nuclear cascade. Thus L(K β) coincidence spectra (normalized to account for the difference in Kα and Kβ counting rates) can be used to correct for chance and nuclear cascade in L(Kα) coincidences. The equations pertinent to the correction are given by McGeorge and Fink (27).

6. Angular correlation: The suggestion that true x-rays emitted in succession as an atom de-excites should be angularly correlated was made by Moellering and Jensen in 1956 (53) and by Beste in 1968 (54). Such an angular correlation follows the same rules as in nuclear γ angular correlation and the correlation function is described by

$$W(\theta) = 1 + \sum_{\ell} a_{\ell}(\gamma_1)\, a_{\ell}(\gamma_2)\, P_{\ell}(\cos\theta) \qquad (44)$$

where the angular correlation function $W(\theta)$ is defined as the probability of γ_2 (K or L x-ray) being emitted into a unit solid angle at an angle θ with respect to a line γ_1. The quantity $P_{\ell}(\cos\theta)$ are Legendre polynomials of degree ℓ and the coefficients a_{ℓ} are functions of the angular momentum of the states and the multipolarity of the transitions between these states.

For the correlation of a K-L x-ray cascade, the spin of the intermediate level (L_2 or L_3) is $\leq$ 3/2 and terms of higher than second order are zero (55).

Katz and Coryell (56) and Wood (25) have measured the angular correlation

in K-L x-ray coincidences. Katz showed (57) that magnetic quadrupole (M_2) admixtures in E_1 transitions must be taken into account and that the angular correlation function is sensitive to even small mixing ratios. Scofield (41) calculated the relative contributions in x-ray transitions using HFS wavefunctions. Using the results of the above workers, the angular correlation contribution in each experiment can be calculated and the results corrected for this contribution.

CHAPTER V

APPARATUS AND EXPERIMENTAL MEASUREMENTS

The experiments were done by the standard fast-slow coincidence method; i.e., the energy and time information are treated separately so as to reduce the overall resolving time. This has the effect of reducing the chance coincidence rate without in any way affecting the coincidence efficiency. Multiple routing (double or quadruple) facilitates the simultaneous running of many coincidence spectra. A typical circuit (used for $Tm^{170,171}$) is given in Figure 3.

The K x-rays are observed in the Ge(Li) detector A. The amplified detector output is taken through a biased amplifier (TC-250) in order to set the K x-ray gates by means of single-channel analyzers (Ortec Model 406). The total output of the gate detector is taken through a fast amplifier. The L x-ray spectrum from detector B is similarly taken through a fast amplifier and a triple coincidence was achieved in the coincidence units (Ortec Model 418) (i.e. coincidence between the fast output of the L x-ray detector, the fast output of the K x-ray detector and the output of the single-channel analyzers). The output of the coincidence circuit was taken through a mixer (Ortex Model 433) to the multi-channel analyzer (Nuclear Data ND-2200 or ND-180) in the multigroup mode, where it met the suitably amplified pulses from the L x-ray detector. The routing information was carried to the multichannel analyzer from separate outputs of the coincidence unit. Linear delays were inserted in all branches to adjust carefully the timing requirements. The

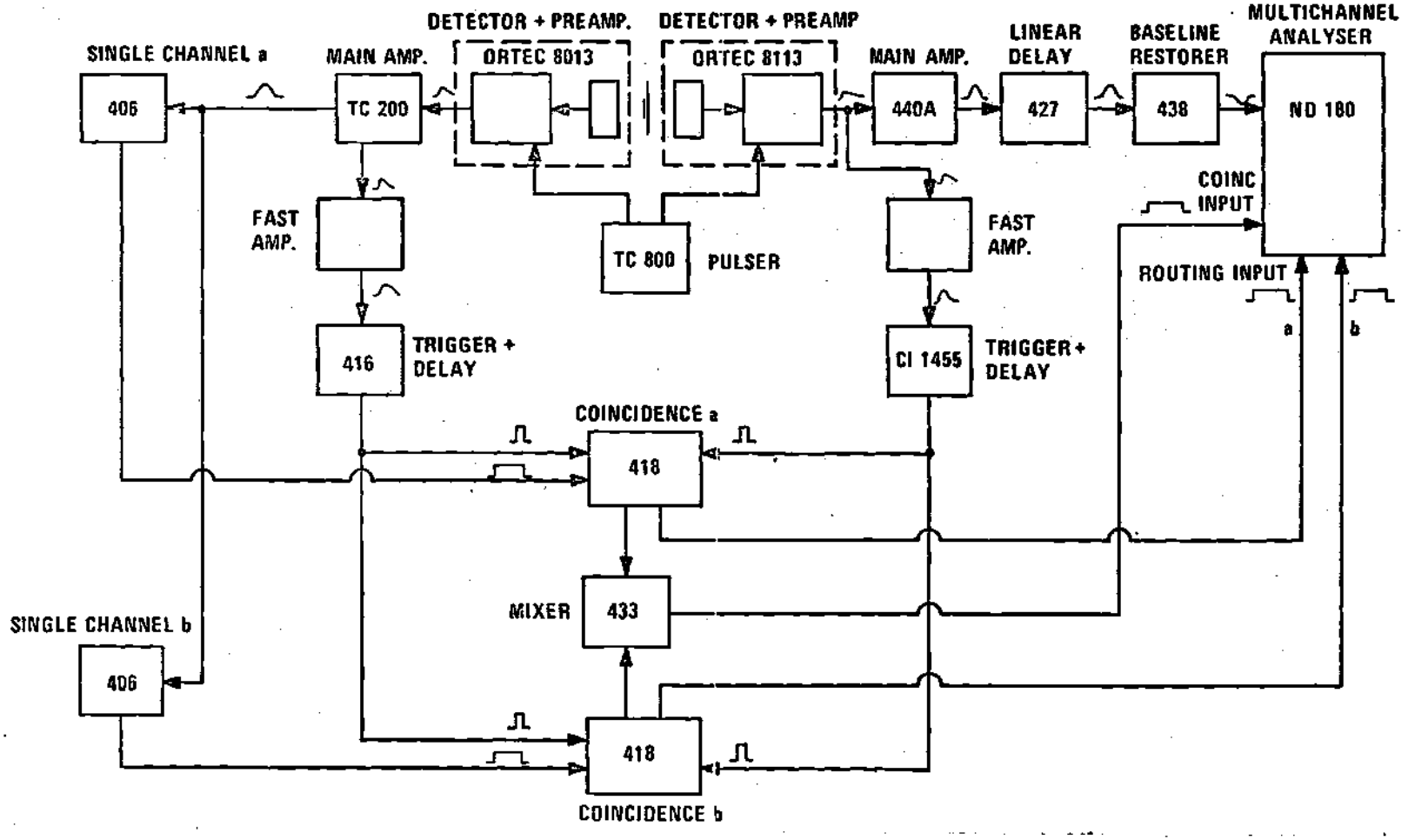

Figure 3. Coincidence Circuit with Multiple Routing.

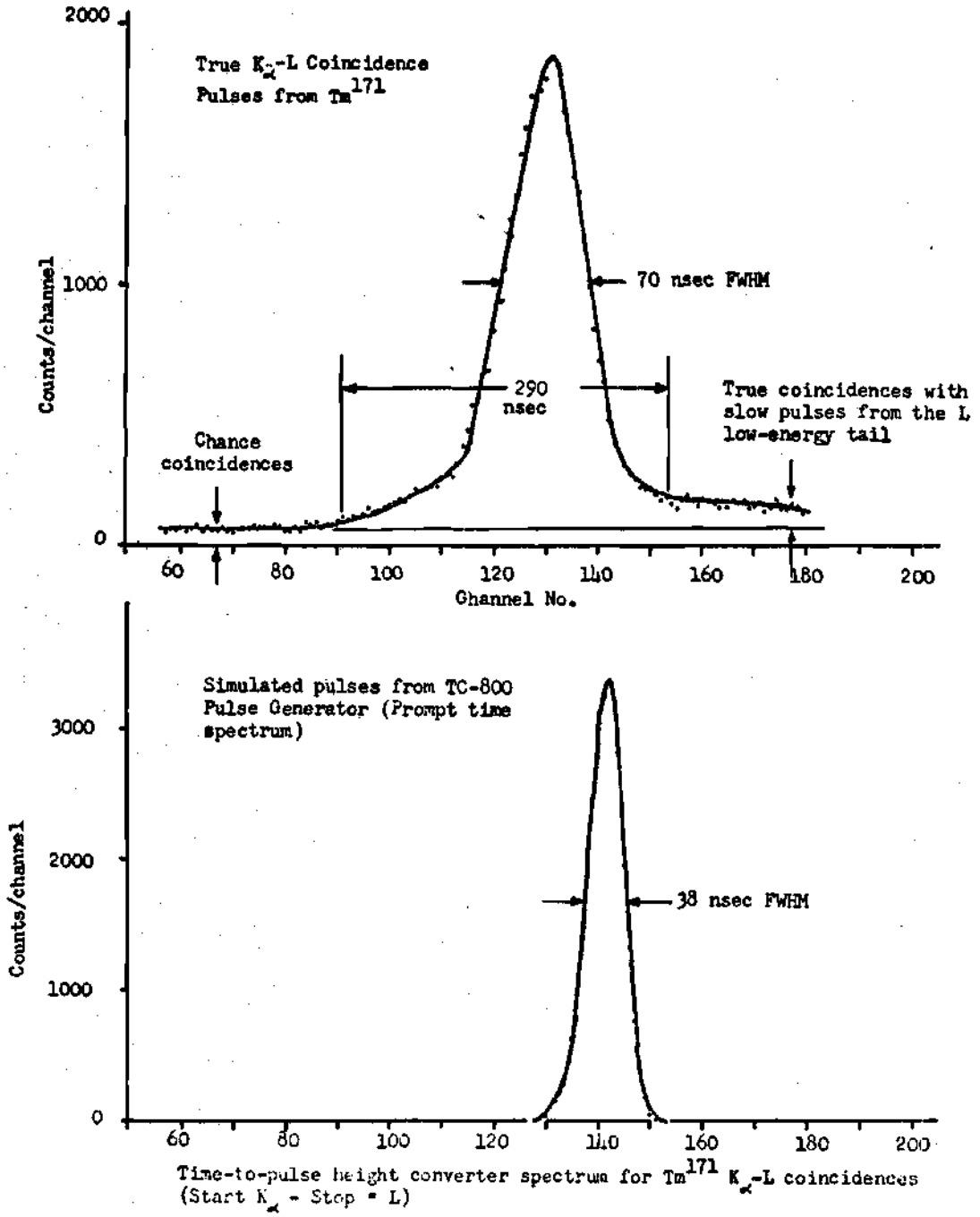

Figure 4. Time Spectra of the Coincidence Experiment.

pulser (Tennelec Model 800) enables the setting of the coincidence leading edge pulses, and thus permits the satisfaction of timing requirements in the true spectrum. The prompt resolution of the true pulses was measured by taking a time-to-pulse height conversion spectrum. This showed that essentially all coincidences were obtained with a resolving time of only 100-200 ns. The resolving time of the Ortec Model 418 units was set at above 1μs, and hence the coincidence spectra were fully enveloped. The coincidence resolving time was taken very large compared to the prompt resolution of the time coincidence pulses, in order to include all the "degraded" pulses which are shower and result in a small "tail" in the time-to-pulse-height converter. This permits the application of the same degradation correction, if any, to both singles and coincidence spectra.

In all cases, coincidence spectra are taken with differing resolving times. The coincidence efficiency was checked in all cases and found to be very close to unity. The chance coincidences were either taken separately by inserting an appropriate delay in one branch or by gating on K_β lines, as discussed in Chapter IV. The following corrections and errors were taken into consideration in all cases (whenever appropriate). Details of these corrections will be given when discussing measurements on individual nuclides.

5.1 Corrections

1. Detector efficiency and geometry.
2. Background under Gaussian peaks.
3. Chance coincidences.
4. Nuclear cascade coincidences.

5. Coincidence efficiency.
6. Gate analysis: separating the true gate counts from contributions due to continuum of other x-ray or γ-ray peaks, Compton humps, escape peaks, etc.
7. Summing effects (at high counting rates).
8. Radioactive decay.
9. Counting statistics and standard deviation.
10. Directional correlation effects.

In addition, errors can result from the following causes and checks must be made.

1. Degraded pulses.
2. Count rate effects such as pulse pile-up and dead times.
3. Shifts of the single-channel window and geometry. The outputs of the single-channels were monitored through printing scalars whenever possible, and the total gate counts are collected in scalars.
4. "Jitter" and shape distortion of pulses were checked occasionally.
5. "Leakage" in gates (i.e. pulses beyond the single channel window).
6. Source effects such as self absorption, backscattering, etc.

In some cases, a time-to-pulse height converter (TAC) served as the main coincidence unit, the coincidence gate (of adjustable revolving time) being opened by the fast gate pulse and stopped by the fast (L) spectrum pulse (Fig. 5). This "fast" information is combined with the "slow" information from the single channel analysers to give output information in the normal manner, i.e. the peak

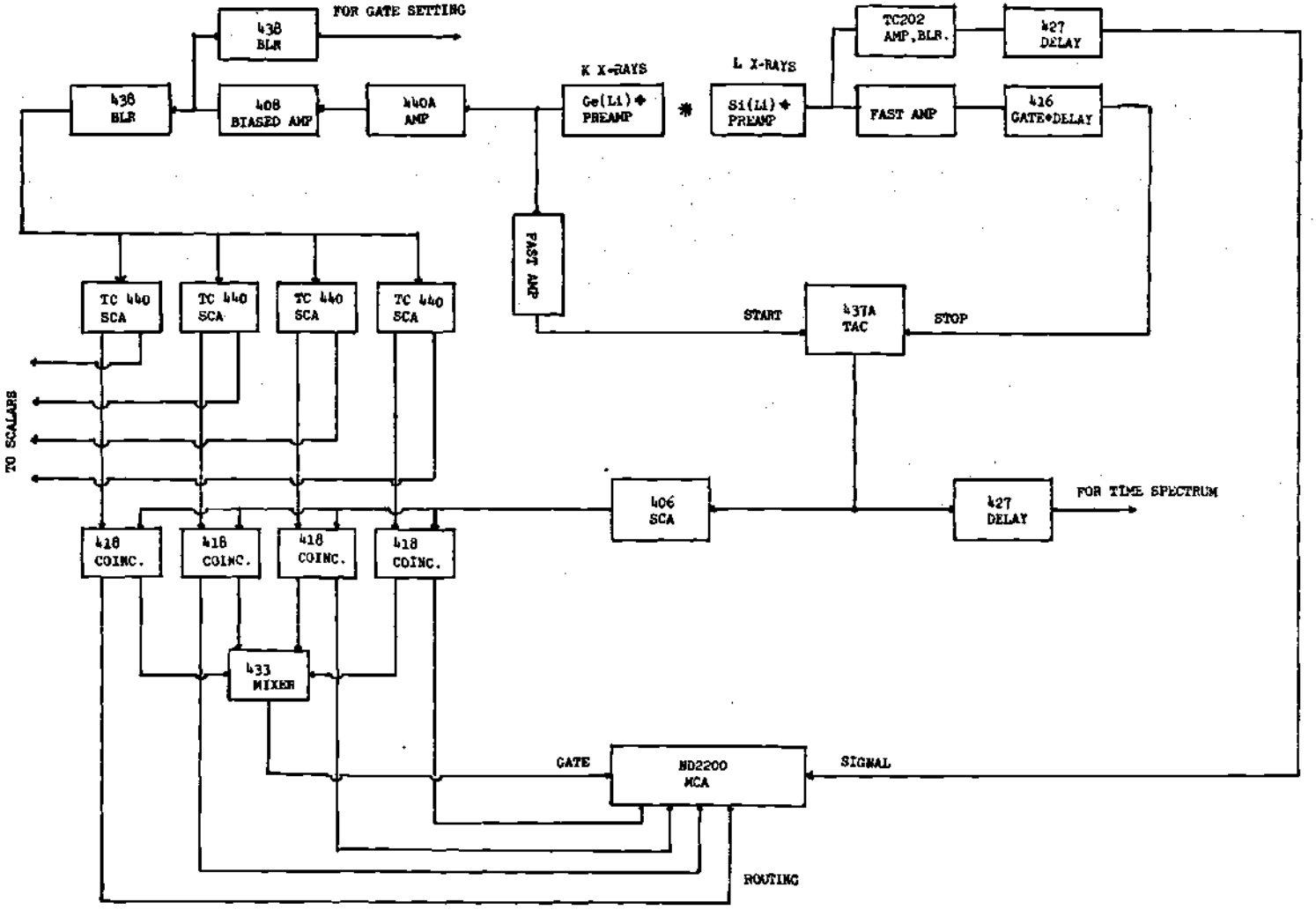

Figure 5. Time-to-Amplitude Converter (TAC) Used as Coincidence Unit.

of the time distribution is selected with a timing single-channel analyzer (Tennelec Model TC 445) and its extended output carries the time information to the coincidence unit. In these units, slow coincidences taken with gate pulses from the gate detector (amplified and biased off pulses) are selected with single channel analysers. The stretched output of the timing SCA Te445 are mixed with output pulses from the coincidence unit 418 (coincidence beta slow K-gates and fast pulses from the TAC) in a summing amplifier (Ortec Model 433) and its output triggers the gate of the multichannel analyzer. The gate information is carried by routing pulses from the coincidence units to the multichannel analyzer. A variable delay in the linear L x-ray branch matches the timing of this signal to the associated gate in the analyzer. The above set up was used in Au^{195}, Hg^{203} and Ir^{192} experiments. In all cases, the singles L- and K- x-ray gates were checked at the beginning and end of each run. Counting rate shifts due to possible slight geometry changes, drift of single-channel windows, "leakage" in gates, etc. could be corrected for in this manner.

5.2 Experimental Details

5.2.1 Subshell Yields in Yb(Z=70) from the Decay of Tm^{170} and Tm^{171}

The L(K) x-ray coincidence technique was used in this experiment to measure L subshell yields for the first time with radioactive sources of L-vacancies. Jopson et al. (22) had measured the L_2 and L_3 subshell fluorescence yields by coincidence methods, using NaI(Tl) detectors and Yb foil targets in which K and L vacancies were produced by 122 keV γ-rays from a Co^{57} source. Two different sources leading to daughter products of the same Z would enable the results to be

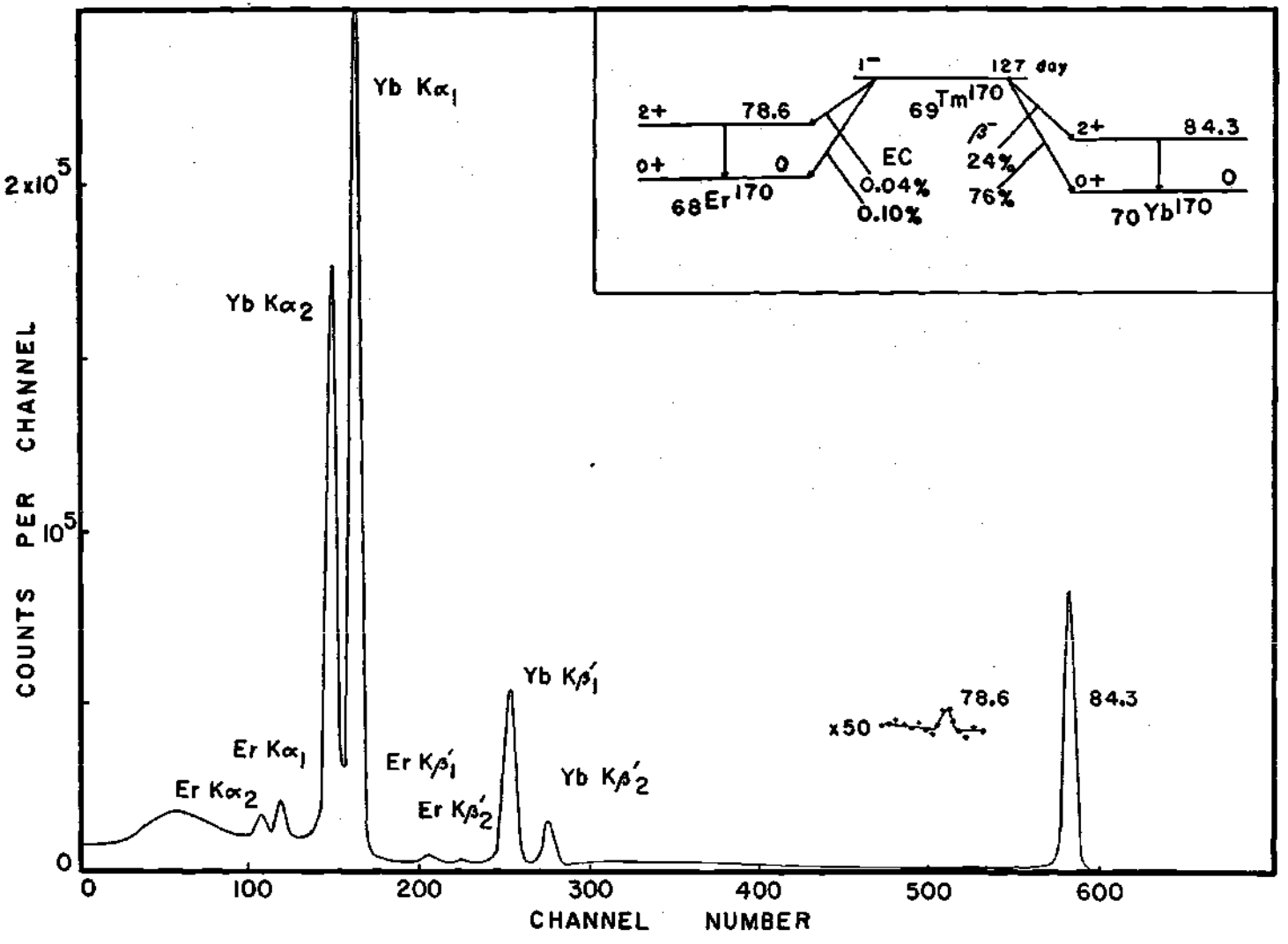

Figure 6. Tm^{170} Decay Scheme and Photo Spectrum Between 50–85 keV.

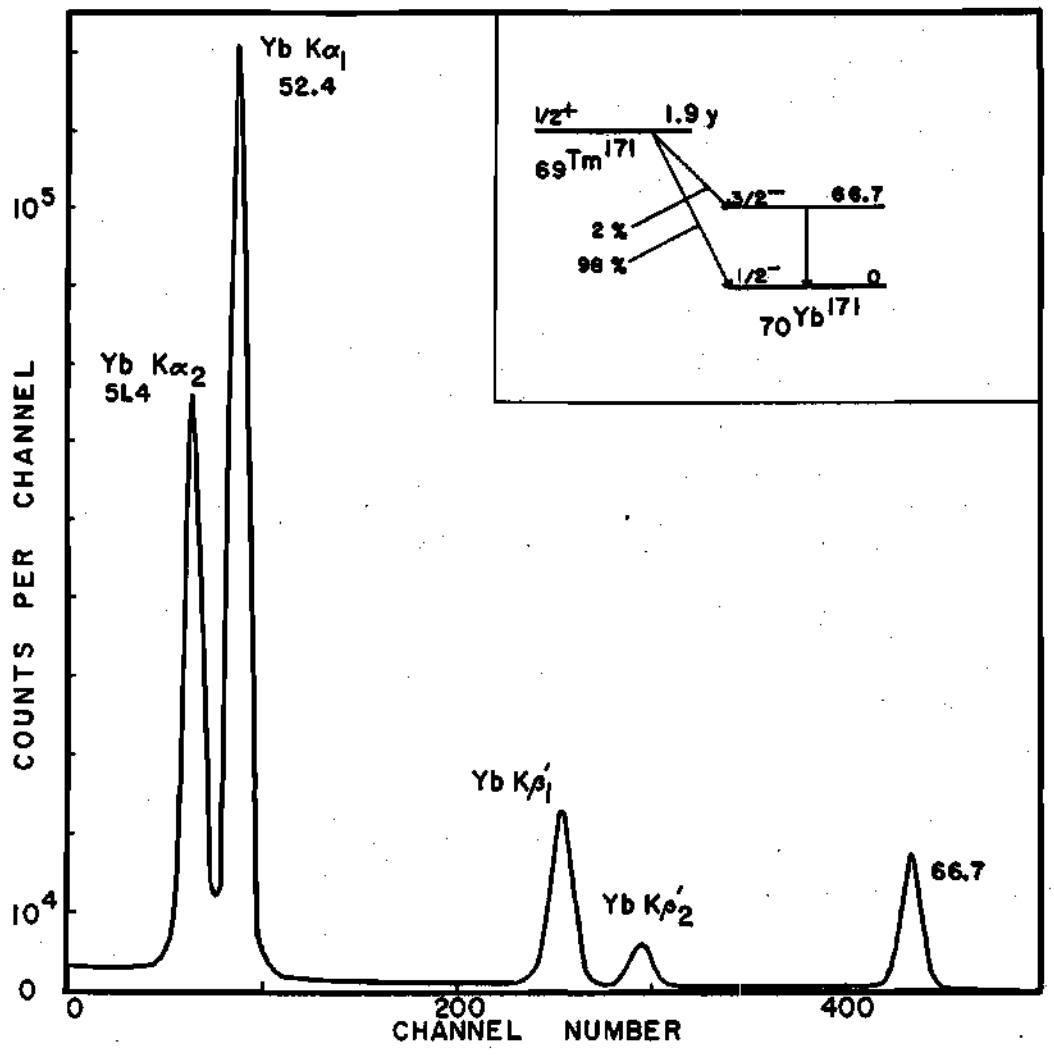

Figure 7. Tm^{171} Decay Scheme and Photon Spectrum Between 50–70 keV.

verified.

The decay schemes of the Tm^{170} and Tm^{171} decays are given in Figs. 6 and 7.

A) Source preparation: Thin, uniform sources of about 2 mm dia. were prepared by evaporating the active salt from dilute HCl solution on to a plexiglas holder. The Tm^{170} source was of high specific activity and was determined to be less than $10\mu g/cm^2$ thickness; the Tm^{171} source was carrier-free. The sources exhibited an activity of approximately $10\mu Ci$ each.

B) Singles spectral studies; Contamination checks: The singles K and γ spectra of the Tm^{170} and Tm^{171} sources are shown in Figures 6 and 7. The spectra were taken with a Si(Li) detector of 290 eV FWHM resolution at 6.4 keV. Er and Yb K x-rays are seen to be separated in Figure 6 (decay of Tm^{170}). Spectra taken with a 16 cc coaxial Ge(Li) detector showed the presence of γ-rays with energies of 66.7 and 443 keV. These are attributed to trace contamination of Tm^{168} and Tm^{171} in the Tm^{170} source. The Tm^{168} contributes Er K x-rays from its electron capture decay, and Tm^{171} contributes Yb K x-rays from the conversion of the 66.4 keV transition in Yb^{171}. The contributions were calculated from known values of the intensity ratios of Er K x-rays to 443 keV γ-rays in Tm^{168} decay (58) and from the ratio of Yb K x-rays to the 66.7 keV γ in Tm^{171} decay in the present experiment (Appendix A). The results indicated that 5.01% of the Yb K x-rays arose from the contribution from a Tm^{171} contamination and this factor was taken into consideration in the gate analysis and chance coincidence studies. The contamination by Tm^{168} was

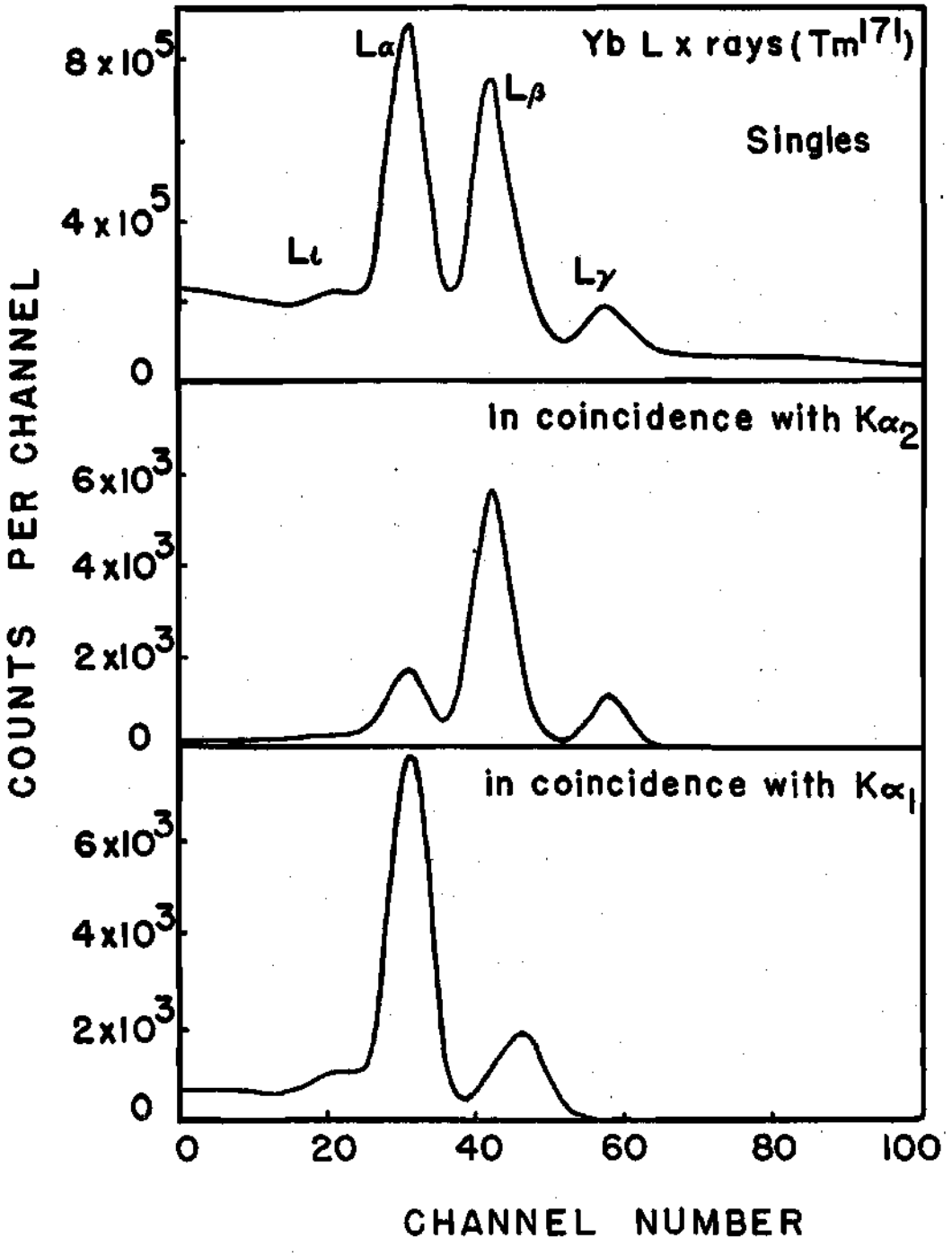

Figure 8. Singles and Coincidence L x-ray Spectra in Tm^{171} Decay.

too small to be significant. A trace of Bi^{207} was identified, but this again had no influence on the present experiment. No Tm K x-rays were noticed, indicating that the source thickness was small enough for source self excitation to be negligible.

In the decay of Tm^{171}, no significant amount of contaminants could be found. Contamination by Tm^{170} was estimated to contribute less than 0.37 to the total Yb K x-ray intensity in the Tm^{171} decay.

C) Coincidence studies: Two Ge(Li) detectors (8 mm dia. x 5 mm depth; 0.005" thick Be window; 400 eV FWHM at 6.4 keV) were used at 180^{o} for the coincidence studies.

A close geometry (source-to-window distance $\leq$ 3 mm) was made with β- x-ray coincidences, and proved that production of β-excited K x-rays was negligible ($< 0.8\%$).

Two complete sets of runs were made in both cases, with coincidence resolving times of 600 ms and 1200 ms respectively, with double routing (simultaneous runs of $L(K\alpha_1)$ and $L(K\alpha_2)$ coincidences). The coincidence efficiency was found to be unity, as verified by the independence of the results on coincidence resolving times, and by a time-to-pulse-height converter spectrum, which showed that complete enveloping of the prompt coincidence peak could be achieved in only 290 ns, whereas the resolving times were twice and four times as long in the actual runs. A separate set of chance coincidence runs was made in both cases, introducing a 5 μ sec. delay in the gating channel. The bremsstrahlung contribution was found to be small. Table 2 gives

Table 2. Gate Composition in Tm^{170}, Tm^{171} Measurements

Fraction Falling Under Gated Peak of (%)	Gated Peaks			
	Tm^{170}		Tm^{171}	
	K_{α_2}	K_{α_1}	K_{α_2}	K_{α_1}
High energy continuum (background)	9.60%	6.01%	4.25%	3.0%
Overlap from K_{α_1}	5.11%	-	5.25%	-
True Peak (%)	86.71	93.99%	90.5%	97.0%

Table 3. True and Chance Contributions in Tm^{170}, Tm^{171} Coincidences Composition of Coincidence Spectra.

	Tm^{170}		Tm^{171}	
	$L(K_{\alpha_1})$ coincidence	$L(K_{\alpha_2})$ coincidence	$L(K_{\alpha_1})$ coincidence	$L(K_{\alpha_2})$ coincidence
Chance Coincidences	6.68%	7.30%	7.75%	7.00%
True Coincidences	93.32%	92.70%	92.25%	93%

the gate composition in both cases, and Table 3 gives the count rates in the true and chance runs.

5.2.2 Measurements on Tungsten-181

The decay scheme of W^{181} is given in Figure 9. The source was prepared from high specific activity solution (2.62 Ci/g of W in 0.1 NHF) with droplet evaporation onto 1.5 mg/cm^2 mylar. Two sources were prepared, of 5 and 10μ Ci, respectively, with diameters of about 2 mm.

The L x-ray spectra were observed with a Si(Li) detector of 2.5 mm depletion depth fitted with a 0.002" Be window and having a resolution of 260 eV FWHH at 6.4 keV. The Ta K x-rays were detected by a Ge(Li) detector (470 eV FWHH at 6.4 keV) and the 153 keV γs were seen by a 4 cm^3 Ge(Li) detector. No significant source contamination of any kind was observed.

The coincidences were made in the TAC arrangement described before, (Figure 5) with double routing and a resolving time of 80 ns with a coincidence efficiency of 0.96. The gate composition is given in Table 4. The data were taken at the different geometries.

5.2.3 Platinum L Yields from Au^{195} Decay

The electron capture decay of Au^{195} into $_{78}Pt^{195}$ was utilized to measure the L subshell yields of platinum. The decay scheme of the 183-day Au^{195} decay is given in Figure 11. The sources were made by droplet evaporation on thin mylar and a source of approximately 5 μCi was used in the coincidence runs.

The gates were set on $K\alpha_1$, $K\alpha_2$, $K\beta_1$ and the continuum above the K spectra. The four-fold coincidence setup using the triple coincidences made in the Ortec 418

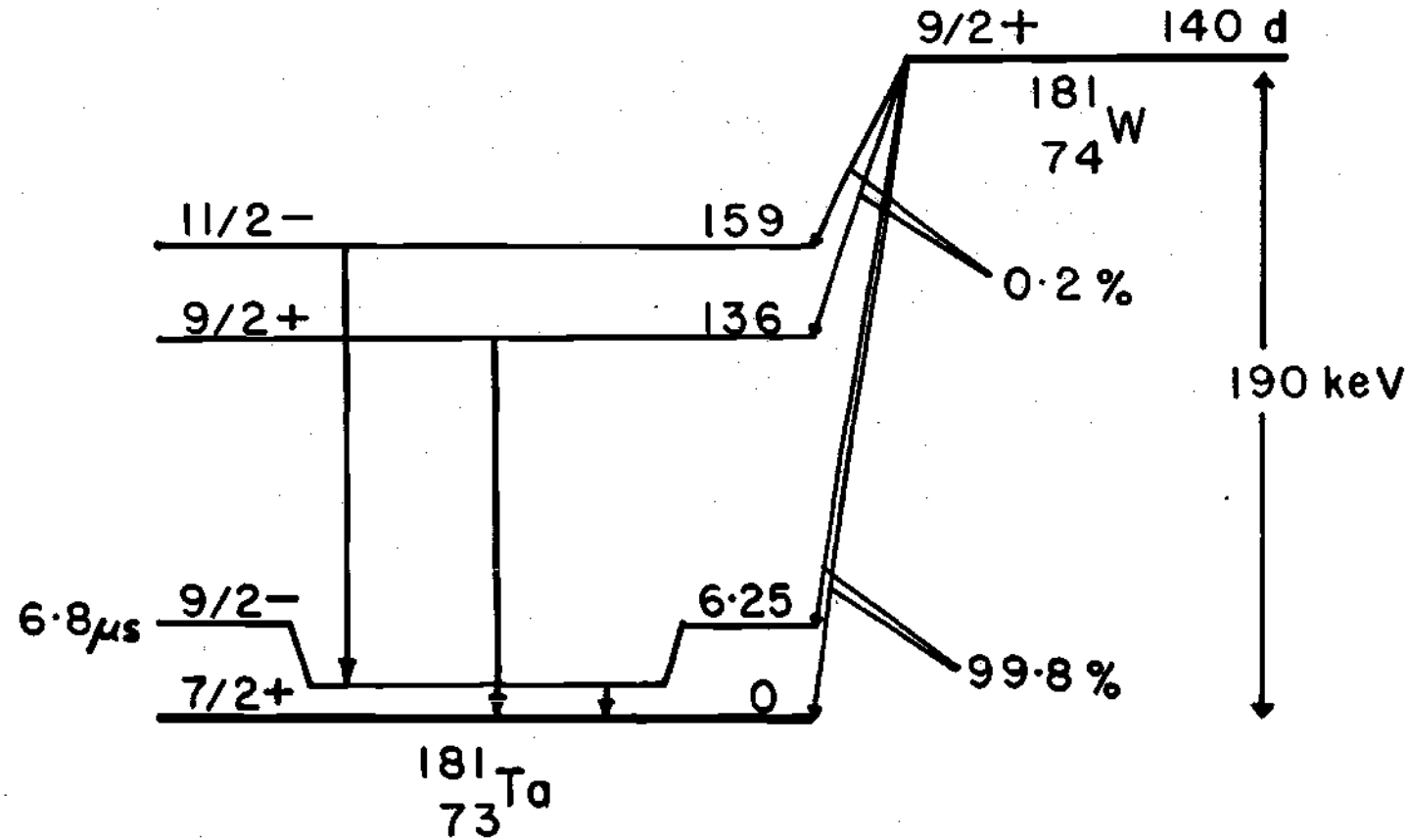

Figure 9. Decay Scheme of W^{181}.

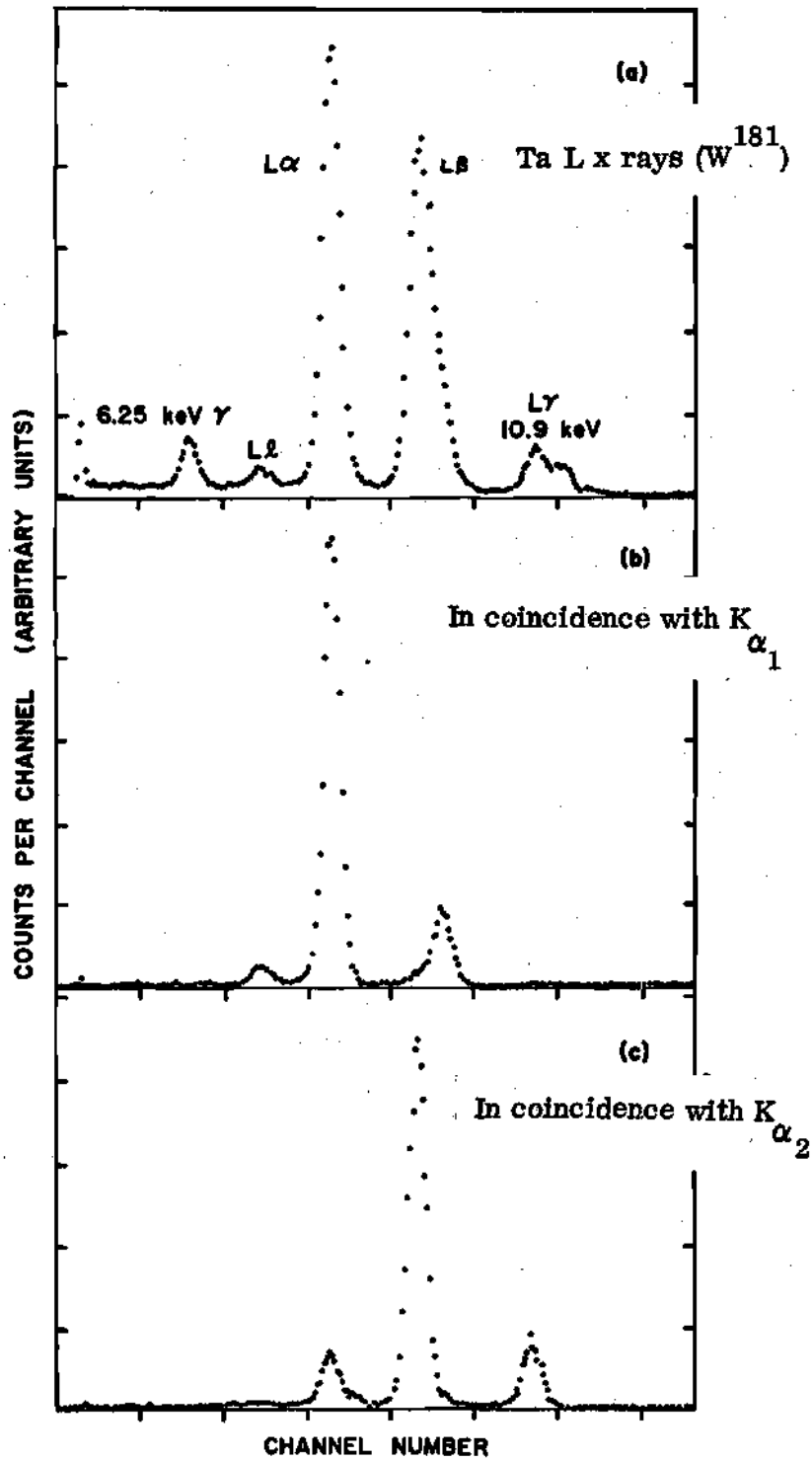

Figure 10. Single and Coincidence L Spectra in W^{181} Decay.

Table 4. Gate Composition in W^{181} Measurements.

Fraction Falling Under Gated Peak of (%)	K_{α_1} Gate	K_{α_2} Gate
Continuum from higher energy	1.35%	2.06%
Overlap from K_{α_1}	-	5.01%
True Peak	98.65%	92.93%

Table 5. True and Chance Contributions in W^{181} Measurements Composition of Coincidence Spectra.

	$L(K_{\alpha_1})$ Coincidences	$L(K_{\alpha_2})$ Coincidences	L(γ 153 keV) Coincidences
Chance Coincidences	2.95%	2.62%	negligible
Coincidence with Higher Energy Continuum	negligible	negligible	negligible
True Coincidences	97.05%	97.38%	100%

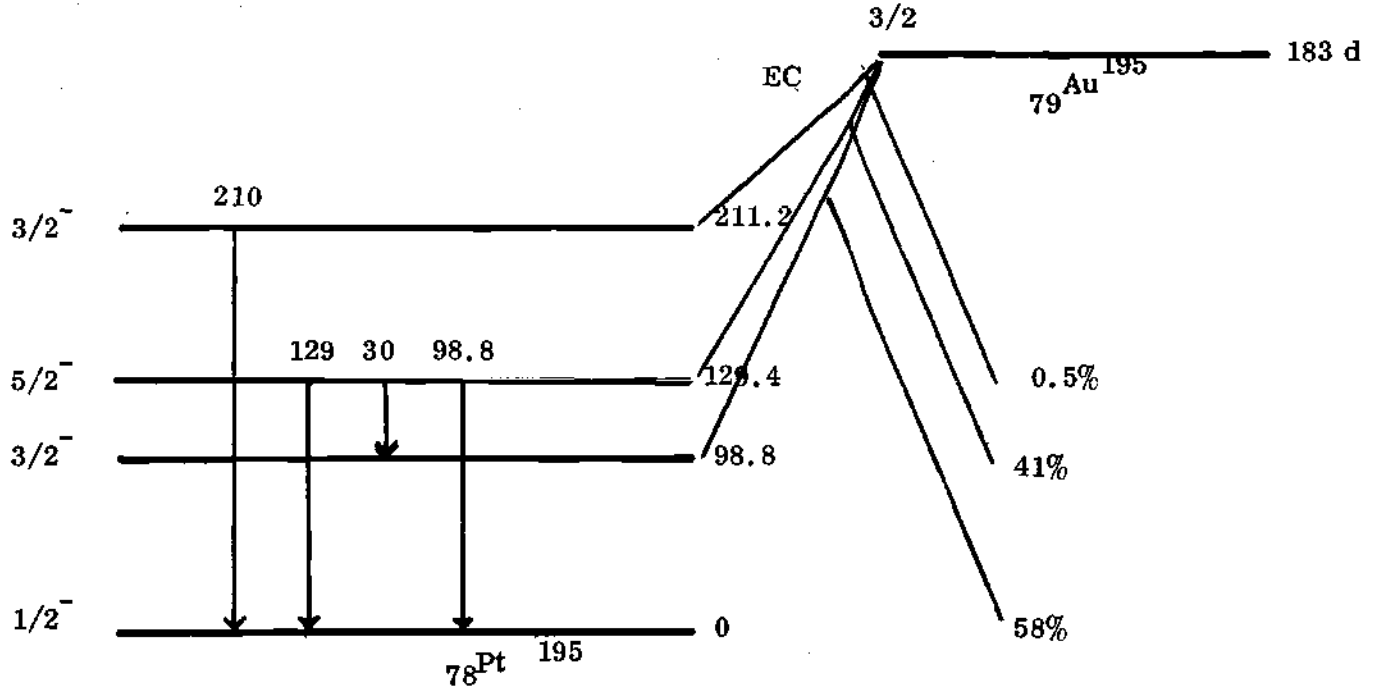

Figure 11. Decay Scheme of Au^{195}.

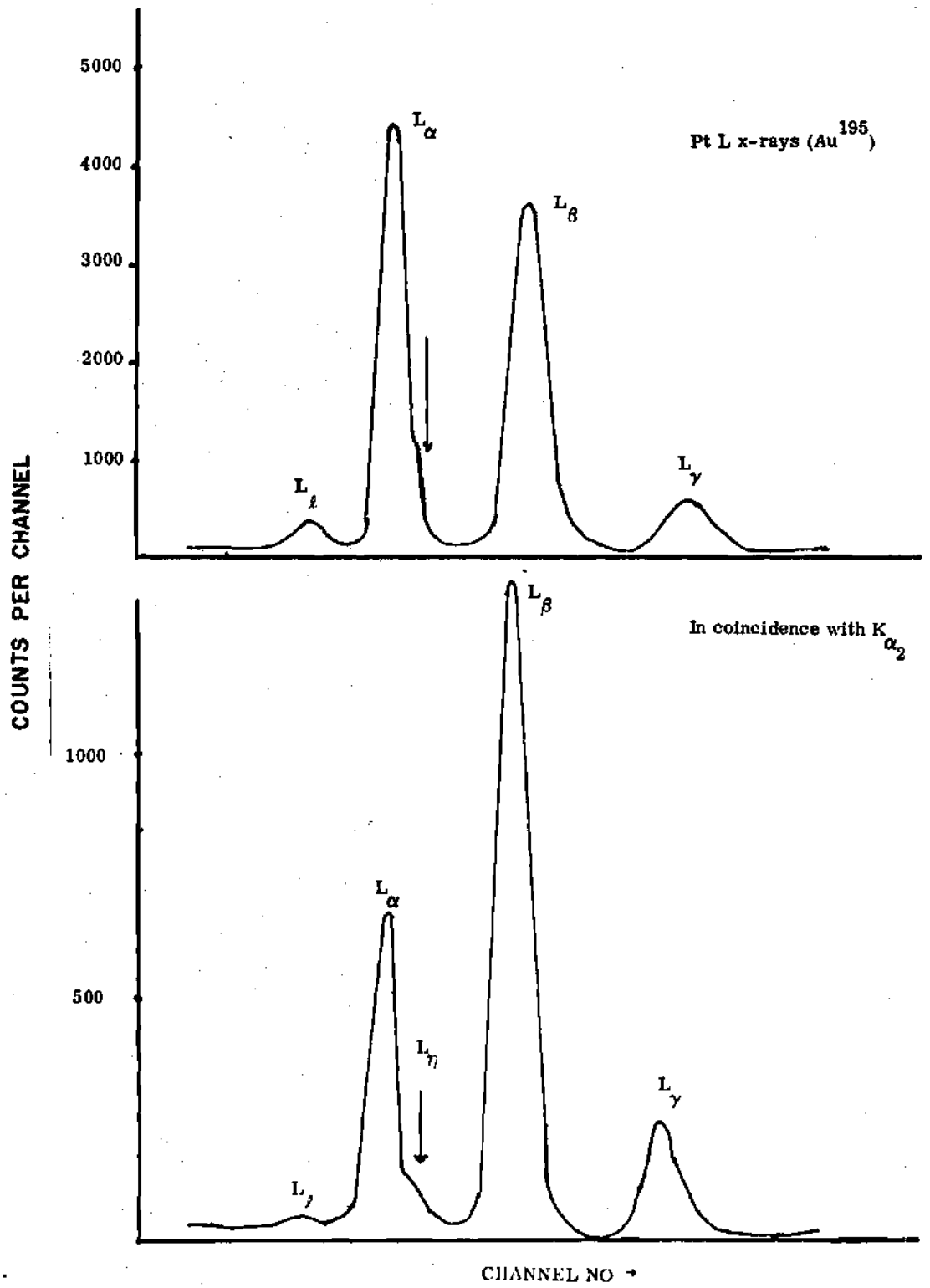

Figure 12. Coincidence L Spectra in Au^{195} Decay.

Table 6. Gate Composition in Au^{195} Measurements.

Fraction Falling Under Gated Peak of (%)	K_{α_1} Gate	K_{α_2} Gate
Higher Energy Continuum	0.91%	1.28%
Overlap from K_{α_1}	-	3.30%
True Peak	99.09%	95.42%

Table 7. True and Chance Contributions in Au^{195} Measurements. Composition of Coincidence Spectra.

	$L(K_{\alpha_1})$ Coincidences	$L(K_{\alpha_2})$ Coincidences
Chance and Nuclear Cascade Coincidences	28.7%	25.4%
Coincidences with the Higher Energy Continuum	4.05%	5.75%
True Coincidences	67.25%	68.85%

coincidence boxes was used. The Si(Li) detector used for the L x-ray detection had resolution adequate to resolve the $L\eta$ transition from the $L\beta$ and $L\alpha$ lines (Fig. 12), and hence the L_2M_1 transition giving rise to the $L\eta$ line could be excluded from the L_α line, whereas in previous measurement it has perforce been included. The reduction of this contribution reduces the value of ω_2 as compared with previous measurements when $L\eta$ could not be excluded.

5.2.4 Thallium L Yields from Hg^{203} Decay

The L yields of Z = 81 (Ta) were measured from the decay of Hg^{203} mainly to investigate the effect of the $L\eta$ subtraction on the results, as this isotope had been previously investigated (25). The TAC mode was used with fourfold routing and the total resolving time was less than 200 ms. The decay of Hg^{203} is given in Figure 13. The source was prepared as usual by droplet evaporation on thin mylar and was about 5 μ Ci strong.

5.2.5 Os and Pt L Yields from Ir^{192} Decay

Ir^{192} decays by β^- decay into Pt^{192} and by electron capture into Os^{192}. Hence, the investigation of the decay of Ir^{192} enables one to determine simultaneously the L subshell yields in two closely spaced Z, namely Os and Pt, i.e. Z = 76 and Z = 78, respectively.

Approximately 5 mg of natural iridium (38.5% Ir^{191} and 61.5% Ir^{193}) was irradiated in the reactor at 8×10^{12} nvt for 100 hrs. The source was then cooled for five months to let the short-lived activities die out and the source was prepared by droplet evaporation from the solution on thin mylar. Two sources of approximately 5 and 10 μ Ci were prepared.

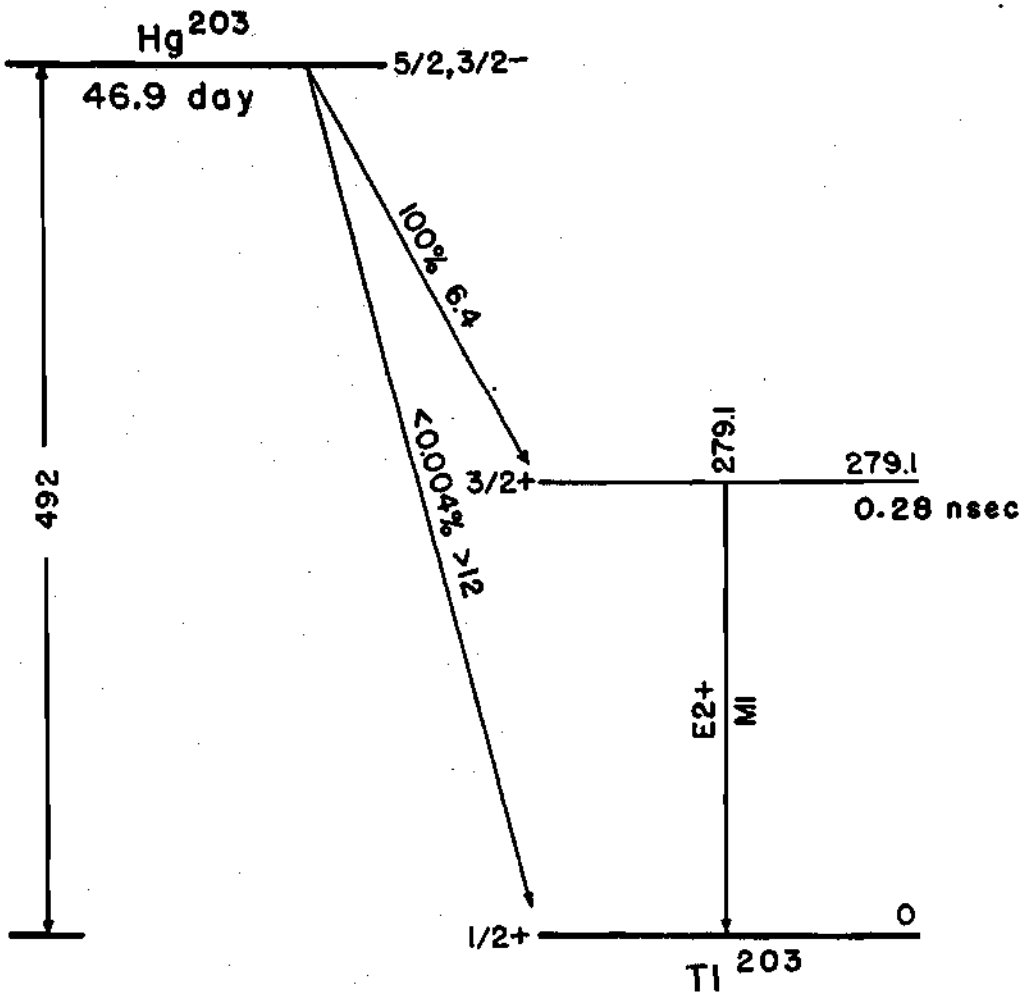

Figure 13. Decay Scheme of Hg^{203}.

Table 8. Gate Composition in Hg^{203} Measurements.

Fraction Falling Under Gated Peak of (%)	K_{α_1} Gate	K_{α_2} Gate
Continuum from Higher Energy	5.83%	10.34%
Overlap from K_{α_1}	-	2.59%
True Peak	94.17%	87.07%

Table 9. True and Chance Contributions in Hg^{203} Measurements. Composition of Coincidence Spectra.

	$L(K_{\alpha_1})$ Coincidences	$L(K_{\alpha_2})$ Coincidences
Chance and Nuclear Cascade Coincidences	11.35%	9.40%
Coincidences with Higher Energy Continuum	1.14%	2.02%
True Coincidences	87.51%	88.58%

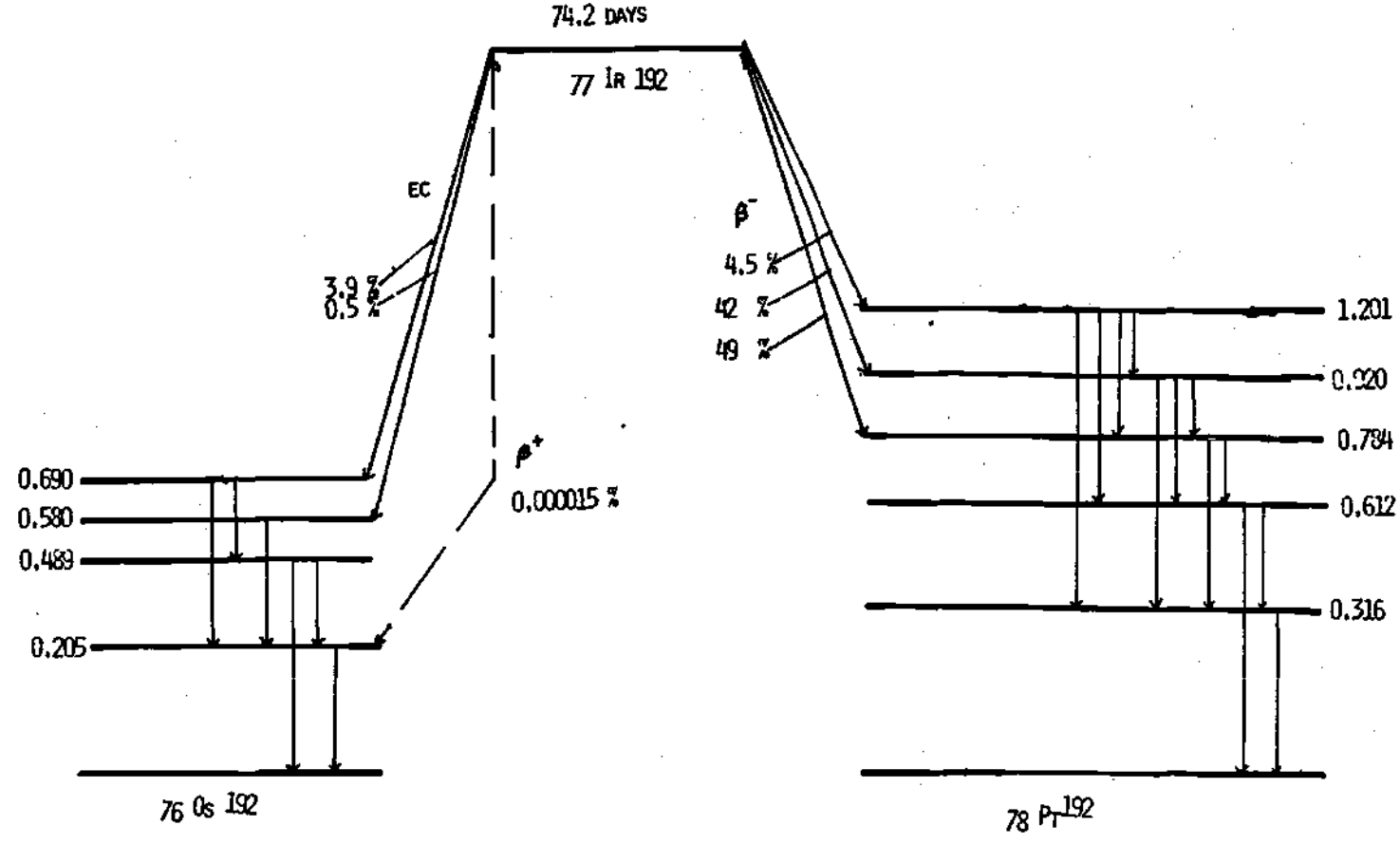

Figure 14. Decay Scheme of Ir^{192}.

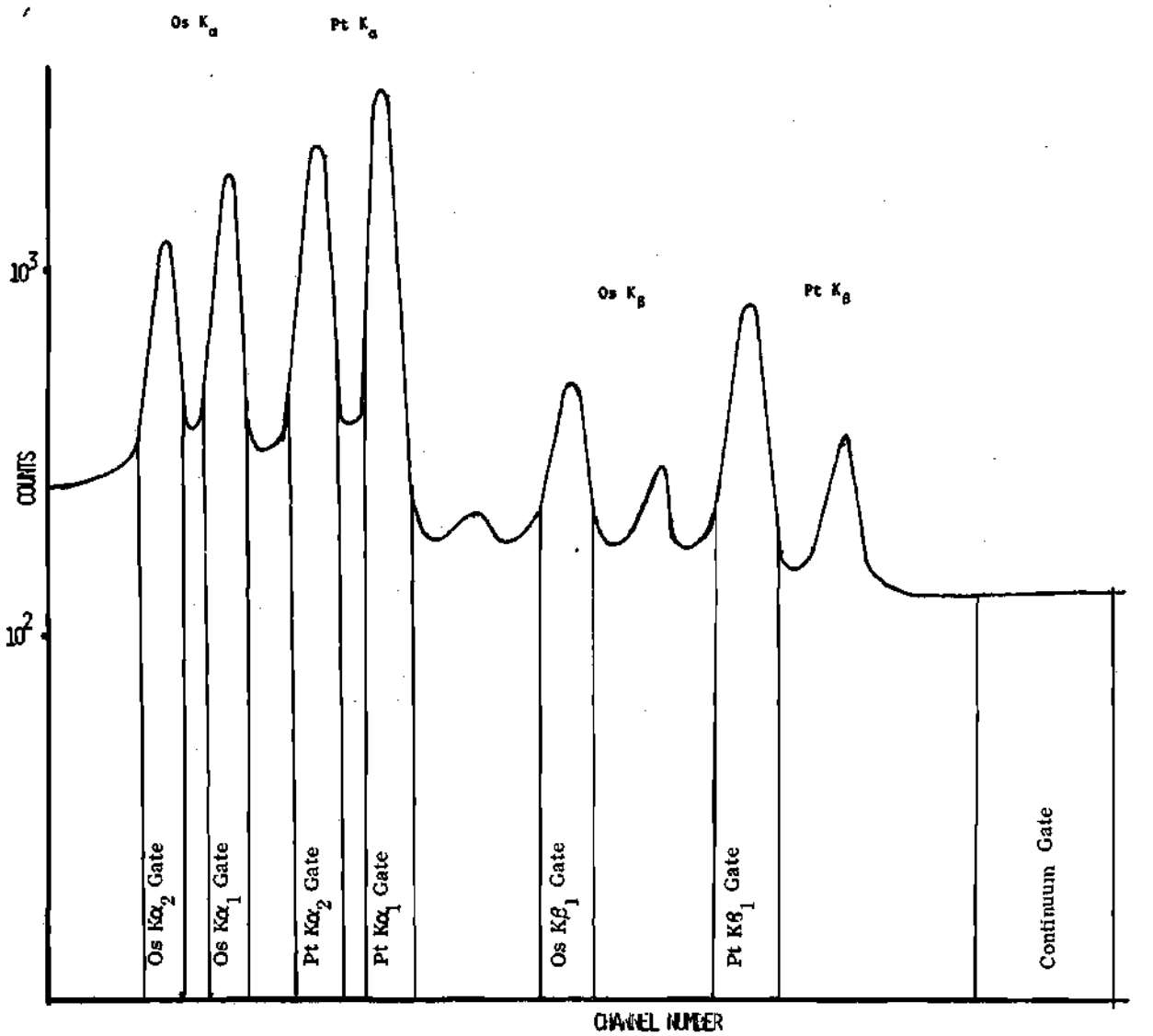

Figure 15. K X-ray Gates in Ir^{192} Measurements.

Table 10. Gate Composition in Ir^{192} Measurements.

Fraction falling under gated peak of (%)	Gated Peaks			
	$K_{\alpha 2}$ of Os	$K_{\alpha 1}$ of Os	$K_{\alpha 2}$ of Pt	$K_{\alpha 1}$ of Pt
$K_{\alpha 1}$ of Os	4.07			
$K_{\alpha 2}$ of Pt	2.90	3.81		
$K_{\alpha 1}$ of Pt	4.40	4.78	3.41	
$K_{\beta 1}$ of Os	0.92	0.70	0.61	0.25
$K_{\beta 2}$ of Os	0.17	0.28	0.22	0.13
$K_{\beta 1}$ of Pt	0.61	1.30	0.97	0.59
$K_{\beta 2}$ of Pt	0.25	0.19	0.14	0.13
Continuum	15.05	11.30	9.65	8.29
TRUE PEAK (%)	71.63	77.64	85.00	90.61

Table 11. True and Chance Contributions in Ir^{192} Measurements. Composition of Coincidence Spectra.

Coincidence	$L(K_{\alpha 2})$ of Os	$L(K_{\alpha 1})$ of Os	$L(K_{\alpha 2})$ of Pt	$L(K_{\alpha 1})$ of Pt
Contamination from other Z (%)	5.40	6.31	negligible	negligible
Nuclear Cascade and Chance Coincidence(%)	23.95	28.56	19.75	22.59
Coincidences with the Continuum (%)	5.33	3.98	1.66	0.99
True Coincidences (% of total)	65.32	61.15	78.59	76.42

The decay scheme is given in Figure 14. The branching ratios are 95.5% and 4.5% for the β^- and electron capture decays, respectively (59, 60). P_K/P_{total} for EC is $0.811 \pm .05$ (59) and hence an adequate number of K x-rays of Os are generated.

The coincidences were made on the standard TAC type with four-fold routing and the coincidence efficiency was very close to unity as shown from separate time-spectrum study.

In order to reduce unwanted events the L detector was covered by 94 mg/cm^2 of Be and the K-detector was covered by 380 mg/cm^2 of Al to stop the β particles. The gates were set up on the $K\alpha_2$, $K\alpha_1$ of Os and Pt, $K\beta$ of Os and Pt and the continuum above the K x-rays. The L coincident spectra have to be stripped of contamination by the peaks of the other Z, and the usual cascade and chance corrections have to be made.

CHAPTER VI

RESULTS AND DISCUSSION

6.1 Tm^{170} and Tm^{171} Decays

6.1.1 L_2 and L_3 Subshell Fluorescence Yields and Coster-Kronig Transition Probability f_{23} in Yb (Z = 70)

Figure 8 gives the singles and $L(K\alpha_{1,2})$ coincident spectra of Tm^{171} decay, with a detector resolution of 400 eV FWHM at 6.4 keV. The L-spectra from Tm^{170} decay are similar, except for somewhat higher background and bremsstrahlung continuum. Table 12 gives the results obtained from this experiment apart from ω_2, ω_3, and f_{23}, the quantities ν_2, i.e. the average number of L x-rays emitted per L_2 vacancy, and the relative intensity $S_3 = L\beta/L\alpha + \ell$ and $S_2 = Lr/L_{\beta+\eta}$ are also measured. The effects of angular correlation are taken into account in the $L(K\alpha_1)$ coincidences leading to the value of ω_3; this correction does not amount to more than 2%. There is general agreement with the work of Jopson, et al. (22), but the present values are lower, as might be expected, since his method involved foil excitation. Foil excitation methods lead to higher results than radioactive decay methods due to source self excitation. A value of $\omega_3 = 0.19 \pm 0.05$ was obtained by Z = 71 by Gizon, et al. (61), from a study of the L-auger spectrum in the decay of Hf^{175}, in good agreement with the present value. The present values $S_3 = 0.165 \pm 0.009$ and $S_2 = 0.192 \pm 0.010$ may be compared with Scofield's theoretical estimates (41) of 0.175 and 0.181, respectively.

Table 12. L_2 and L_3 Subshell Yields at Z = 70.

Coinc.	Quantity	Decay of Tm^{170}	Decay of Tm^{171}	Average	Jopson* (expt.)	Scofield** (theor.)
$L(K_{\alpha 1})$	ω_3	0.185±011	0.180±011	0.183±011	0.20±0.02	
	S_3	0.170±009	0.161±009	0.165±009		0.175
$L(K_{\alpha 2})$	ν_2	0.218±013	0.210±013	0.214±013	0.34±05	
	S_2	0.187±011	0.196±011	0.196±010	0.192±010	0.181
	ω_2	0.185±011	0.179±011	0.182±011		
	f_{23}	0.174±009	0.165±009	0.170±009		

* See Reference (22).

** See Reference (41).

6.1.2 K-Conversion Coefficient of 86.3 keV Transition

$Tm^{170} \rightarrow Yb^{170}$ Decay

The K-shell conversion coefficient α_k of the 84.3 keV E2 transition in Yb^{170} following β^- decay of Tm^{170} has been often investigated, because this transition was one of the first leading to the discovery of anomalies in the experimental E2 conversion coefficients in the deformed region. Accurate measurement of conversion coefficients is of importance in view of their use in the determination of multipolarities and mixing ratios. The main methods for measurement of α_k are (1) measurement of the intensity ratio of the k-x-ray to the γ-ray intensities (XPG method), (2) the internal-external conversion method, and (3) Coulomb excitation and lifetime measurements. In the present work, the XPG method was used (utilizing semiconductor detectors) to measure α_k of the 84.3 keV transition. Previous measurements (see Appendix A) of this transition by the XPG method employed NAI(Tl) spectro-meters, even the best of which could not clearly resolve the 84.3 keV γ-ray from the Yb K-x-rays. In addition, Er X x-rays from the EC decay of Tm^{170} (discussed below) and the iodine k-x-ray escape peak complicate the problem in the NAI(Tl) measurements. In the present case the resolution was adequate to clearly resolve the 84.3 keV Yb^{170} γ-ray, the 78.6 keV Er^{170} γ-ray, the Yb K x-rays and the Er K-x-rays. Hence, no correction was needed for the EC decay branch in estimating the α_k of the 84.3 keV Yb^{170} transition.

The value of α_k for the 84.3 keV transition is obtained from the relationship

$$\alpha_k = \frac{1}{\omega_k} \frac{I_{kx}}{I_\gamma} \tag{45}$$

and a value of 0.937 for ω_k is used (62). The ratio of the relative intensities of Yb K-x-rays and the 84.3 keV γ-ray (after corrections for the detection efficiency, alternation in the 3.2 mm plexiglas β absorber. Be window of detector, etc. was obtained as 1.304 ± 0.039. With the assumed value of ω_k, this gives a value for the K-conversion coefficient of the 84.3 keV E2 transition in Yb^{170} as $\alpha_k = 1.39 \pm 0.04$.

In tables I and II of Appendix A a survey of the existing measurements of α_k of the 84.3 keV transition are given. To facilitate comparison, the $I_{kx}/I_{k\gamma}$ intensity ratios given by the various authors have been corrected for the Er K x-rays arising from the EC decay of Tm^{170}, and $\omega_k = 0.937$ was used to recalculate the result. The spread in values is attributed to the low resolution of the NaI(Te) spectrometers used. Nelson and Hatch (63) used a curved crystal spectrometer and their value (1.43 ± 0.04) is in fair agreement with the present results for the most recent XPG results (including the present work) and the conversion electron method results. There is good agreement with theoretical estimates (Table II in Appendix A) for pure E2 multipolarity. The accuracy of the experiments was not adequate to distinguish among the various theoretical estimates.

6.1.3 K-Conversion Coefficient of the 66.7 keV Transition in Yb^{171}

The intensity ratio of the Yb K x-ray and the 66.7 keV γ-ray following Tm^{171} β decay was found to be (after corrections) 6.98 ± 0.34 (see Appendix A). With $\omega_k = 0.937$, this gives $\alpha_k = 7.45 \pm 0.36$. Two previous measurements of this transition give $\alpha_k = 7.4 \pm 1.0$ (64) and 6.9 ± 1.0 (65), which agree with the

present work. Using the theoretical estimates of Hager and Seltzer (71) for the mixing ratio, the 66.6 keV transition in $Tm^{171} \rightarrow Yb^{171}$ decay is estimated to be 74% M_1 and 26% E_2.

6.1.4 The Electron Capture Decay of Tm^{170}

A detailed investigation of the EC branching of Tm^{170} was attempted in the present investigation for the first time (see Appendix A). Graham et al. (66) let an upper limit of 0.3% for K-capture and 0.01% for β^+ emission from Tm^{170}. Day (67) used a bent crystal spectrometer to measure the relative intensity of Er K x-rays and the 86.3 keV Yb^{170} γ-ray and obtained a K-capture branching of 0.15%. Nelson and Hatch (63) estimated the EC branching to be 0.19 ± 0.04%.

All these estimates are based on the assumption that all the EC capture decays lead to the ground state of Er^{170}. However, from Coulomb excitation studies (68), the partial level structure of Er^{170} is known and a first excited state is expected at 79 keV. Since the decay energy is adequate ($Q_{EC} \simeq 460$ keV) (69) the feeding of both the fround state and the first excited state is possible. Hansen and Hellström (70) used a Si(Li) detector (1.5 keV FWHM at 86 keV) to study the singular spectrum from Tm^{170} decay, and by unfolding the unresolved K x-ray photo-peaks, estimated the EC including to be 0.25% and reported a γ transition in Er^{170} at 78.7 keV.

In the present work, a γ-ray was observed at 78.6 ± 0.4 keV, thus confirming that EC in Tm^{170} feeds both ground and excited states. From data in Table IV in Appendix A a value of $2.64 \pm 0.60 \times 10^{-2}$ is obtained for the ratio of Er K x-rays to Yb K x-rays. The Er K x-rays arise from internal conversion of

the 78.6 keV γ-ray and from k-captive to the ground and excited states in Er^{170}. Assuming a theoretical conversion coefficient $\alpha_k = 1.77$ (71) and $\omega_k = 0.933$ at Z = 68 (Er) (62), we can estimate the total number of k-conversion x-ray from the intensity of the 78.6 keV transition. The fraction of total Er K x-rays due to this K-conversion is 0.059. The EC branching can be calculated using theoretical EC ratios (21) to the ground and first excited states. Taking the value of Q_{EC} = 460 keV (69) P_k, the theoretical k-capture ratios to the ground and first excited states in Er^{170} are 0.800 and 0.837, respectively. Using the relative intensities presented in Table IV in Appendix A we get an EC branching ratio of 0.04% to the 78.6 keV level and 0.10% to the ground state in Er^{170}.

6.2 The L_2 and L_3 Subshell Yields in Tantalum

As pointed out in Chapter II and V, the decay of W^{181} gives a convenient source of L_1-subshell vacancies. Approximately 0.2% of the decays lead to the 136 and 159 keV levels (see Figure 10 and Appendix B). The transition energy available for the decay is 187 $\pm$ 10 keV (72), which permits no K-capture to the levels at 136 and 159 keV.

The L x-ray spectrum was gated by the 153 keV γ-ray and the coincidence rate is

$$C_L(\gamma) = C_\gamma \bar{\omega}_L P_L \qquad (46)$$

where C_γ is the number of 153 keV γ-rays gating the coincidence system, P_L is the probability of L electron capture feeding the 159 keV level and $\bar{\omega}_L$ is the mean

L fluorescence yield at Z = 73. The average number of L x-rays per L_1 vacancy, ν, is obtained from

$$\nu_1 = [N_2(\omega_2 + f_{23}\,\omega_3) - \bar{\omega}_L]/N_1 \qquad (47)$$

where N_1 and N_2 are the primary L_1 and L_2 subshell vacancies. In the present case, no L_3 vacancies are created, according to the present theory of electron capture decay. The distribution of L subshell primary vacancies are estimated to be $N_1:N_2:N_3 = 0.96:0.06:0$ from Zyrynova and Suslov (21). The L captive probability, $P_L = 0.76$ to the 159 keV level, is available from theoretical results as described by Wood et al. (73).

With the use of Equation (9a-d) in Chapter II, the L(153γ) coincidences yield $f_{13} + f_{12}f_{23} = 0.36 \pm 0.02$ at Z = 73 and $\omega_1 + f_{12}\,\omega_2 = 0.14 \pm 0.02$ at Z = 73. These set upper limits of $f_{13} < 0.36$ and $\omega_1 < 0.14$. The results are presented in Table 13 below.

6.3 Platinum Yields from Au^{195} Decay (75)

In the decay of $Au^{195} \rightarrow Pt^{195}$ decay most of the decays lead to the first two excited states at 98.8 and 129.6 keV (58% and 41% respectively)(Fig. 11). K x-rays are produced by k-conversion of these transitions and hence the nuclear cascade terms are considerable, as could be found from Table 7. The nuclear cascade terms are removed by gating on the k β x-rays, as explained in Chapter II.

The detector resolution in this case was adequate to separate the Lη term (L_2-M_1 transition) from the Lα term. The effect of this is to decrease the final value of f_{23} somewhat.

Table 13. L Yields in Ta from W^{181} Decay.

Expt.	Quantity Present Work	Previous Work (62,72,74)
$L(K_{\alpha 1})$ Coinc.	$\omega_3 = 0.228 \pm .013$	0.27 ± 0.01
		0.23 ± 0.02
		0.25 ± 0.03
		0.234 ± 0.024
	$S_3 = 0.205 \pm .010$	0.183 (Theory)(41)
$L(K_{\alpha 2})$ Coinc.	$\omega_2 = 0.250 \pm 013$*	0.25 ± 02
		0.23 ± 04
		0.37 ± 06
	$f_{23} = 0.180 \pm 007$*	0.20 ± 04
$L(K_{\alpha 2})$ Coinc.	$\nu_2 = 0291 \pm 013$	0.303 ± 030
	$S_2 = 0.215 \pm 013$	0.191 (Theory)(41)
L(x)ay - 153 KeV	$\nu_1 = 0.218 \pm 018$	0.22 ± 01
γ Coinc.	$f_{13} + f_{12} f_{23} = 0.36 \pm 02$	
	$\omega_1 + f_{12} \omega_2 = 0.14 \pm 02$	

* Not Corrected for the L_η Contribution.

The results of the experiments are given in Table 14, Z = 78.

6.4 L Yields in Tl from the Decay of Hg^{203}

From the decay of Hg^{203}, the L yields of Tl were measured mainly in order to exploit the superior resolution of the L x-ray detector in separating the $L\eta$ transition from the others. This decay has been investigated earlier by Rao et al. (25). The results of Rao et al. (25) are consistently lower than the present work and this could be possibly ascribed to an error in their detector efficiency calibration. Sujkowski and Melin (76) determined L yields in thallium from the decay of Pb^{293}, using a double focusing β spectrometer. Price et al. (23) used foil excitation methods to measure the L yields of Tl.

The high values of Price et al. are due to self-excitation in the Tl foil used. Suykowski assigned a value of 0.32 for ω_3 in order to calculate the other quantities.

6.5 L Yields in Os and Pt from Ir^{192} Decay

The simultaneous beta and electron capture decay of Ir^{192} was used to determine simultaneously the L yields of $_{76}Os$ and $_{78}Pt$. Fairly large nuclear cascade contributions exist and in the case of Os L x-rays, the partial overlap of Pt L x-rays contributes significant number of extra coincidences. Nonetheless, the results are consistent with other results in this region, and with previous measurements (23, 75). They are presented in Table 16.

6.6 Errors and Accuracy

The errors quoted are all 2σ errors, with statistical errors added quadratically and instrument errors linearly. The main contribution to the latter comes

Table 14. L_2 and L_3 Yields in Platinum (Z = 78) from Au^{195} Decay.

Coincidence	Present Work	Previous Work	Reference
$L(K_{\alpha 1})$	$\omega_3 = 0.291 \pm 018$	0.317 ± 029	23
		0.262	4
		0.31	22
	$L_\alpha / L_\ell = 20.0 \pm 2.8$	20.4	41
	$f_{23} = 0.114 \pm 020$		
$L(K_{\alpha 2})$	$\nu_2 = 0.367 \pm 021$	$0.382 \pm .028$	23
	$\omega_2 = 0.336 \pm 021$	$0.341 \pm .028$	23
	$S_2 = 0.232 \pm 029$	0.216	41
	$S_3 = 0.189 \pm 028$	0.206	41
	$L_\eta / L_\beta = 0.028 \pm 006$	0.027	41

Table 15. L Yields in Tℓ (Z = 81) from Hg^{203} Decay.

Experiment	Quantity	Present Work	Previous Work	Reference
$L(K_{\alpha 1})$ Coinc.	ω_3	0.330± 021	0.306±010	(25)
			0.32	(76)
			0.386±053	(23)
	S_3	0.225±025	0.228±012	(25)
	L_α/L_ℓ	22.2±3.7	19.2	(41)
$L(K_\alpha 2)$ Coinc.	ω_2	0.373±025	0.319±010	(25)
			0.32±025	(76)
			0.400±079	(23)
	f_{23}	0.130±007	0.169±010	(25)
			0.25±0.13	(76)
	ν_2	0.423±024	0.371±010	(25)
			0.450±061	(23)
	S_2	0.246±020	0.238±012	(25)
	L_η/L_β	0.032±006	0.027	(41)

Table 16. L Yields of Os and Pt from Ir^{192} Decay.

	Quantity	This Work	Previous Work	Reference
Z = 76	ω_3	0.301 ± 020	0.290 ± 030	23
	ω_2	0.300 ± 022	0.328 ± 054	23
	f_{23}	0.106 ± 023		
Z = 78	ω_3	0.309 ± 020	0.317 ± 029	23
			0.291 ± 018	75
	ω_2	0.318 ± 022	0.341 ± 058	23
			0.336 ± 021	75
	f_{23}	0.126 ± 021	0.114 ± 020	75

from the efficiency of the L detector, for which $\pm$ 4% has been added linearly in most cases.

Secondly, the efficiency curve is not strictly flat in all cases, and this affects the statistical error. The statistical error for the three quantities ω_2, ω_3 and f_{23} are obtained from the following equations:

$$\Delta\omega_2 = \left\{ \left[\left(\frac{C_{L_\beta}}{\epsilon_{L_\beta}} + \frac{C_{L_\gamma}}{\epsilon_{L_\gamma}} \right) \frac{1}{C_{K_{\alpha_2}}} \right]^2 \left(\frac{\Delta\epsilon}{\epsilon} \right)^2 \right.$$

$$+ \left(\frac{1}{C_{K_{\alpha_2}}} \right)^2 \left(\frac{\Delta C_{L_\beta}}{\epsilon_{L_\beta}} + \frac{\Delta C_{L_\gamma}}{\epsilon_{L_\gamma}} \right)^2$$

$$\left. + \left(\frac{C_{L_\beta}}{\epsilon_{L_\beta}} + \frac{C_{L_\gamma}}{\epsilon_{L_\gamma}} \right)^2 \left(\frac{1}{C_{K_{\alpha_2}}} 2 \right) \left(\Delta C_{K_{\alpha_2}} \right)^2 \right\}^{\frac{1}{2}} \qquad (48)$$

$$\Delta\omega_3 = \left\{\left[\left(\frac{C_{L_\ell}}{\epsilon_{L_\ell}} + \frac{C_{L_\alpha}}{\epsilon_{L_\alpha}} + \frac{C_{L_\beta}}{\epsilon_{L_\beta}}\right)\left(\frac{\Delta\epsilon}{\epsilon}\right)^2\right.\right.$$

$$+ \left(\frac{1}{C_{K_{\alpha_1}}}\right)^2\left(\frac{\Delta C_{L_\ell}}{\epsilon_{L_\ell}} + \frac{\Delta C_{L_\alpha}}{\epsilon_{L_\alpha}} + \frac{\Delta C_{L_\beta}}{\epsilon_{L_\beta}}\right)^2$$

$$\left.\left. + \left(\frac{C_{L_\ell}}{\epsilon_{L_\ell}} + \frac{C_{L_\alpha}}{\epsilon_{L_\alpha}} + \frac{C_{L_\beta}}{\epsilon_{L_\beta}}\right)^2\left(\frac{1}{C_{K_{\alpha_1}}}\right)^2\left(\Delta C_{K_{\alpha_1}}\right)^2\right\}^{\frac{1}{2}} \qquad (49)$$

and

$$\Delta f_{23} = \left[\left(\frac{C}{BD}\right)^2(\Delta A)^2 + \left(\frac{AC}{DB^2}\right)^2(\Delta B)^2\right.$$

$$\left. + \left(\frac{A}{BD}\right)^2(\Delta C)^2 + \left(\frac{AC}{BD^2}\right)(\Delta D)^2\right]^{\frac{1}{2}} \qquad (50)$$

where

$$A = C_{L_\alpha}(K_{\alpha_2}) \ , \quad B = C_{L_\alpha}(K_{\alpha_1}) \ , \quad C = C_{K_{\alpha_1}} \text{ and } D = C_{K_{\alpha_2}}$$

Here $C_{L_{\alpha_1}}$, $C_{K_{\alpha_1}}$ etc. stand for the total number of counts collected in L_{α_1}, K_{α_1} gate, etc. during the experiment. ϵ_{L_α} etc. are the absolute efficiencies of the detector at energies of L_α etc. An estimated error is added in linearly to account

for any errors associated with the corrections quoted in Chapter IV.

6.7 Comparison with Theory

Only two completed sets of theoretical L yields have been reported: these are due to Chen et al. (43, 49) and McGuire (40). Details of their respective theoretical approaches have been given in Chapter III.

In Figures 16, 17, 18, ω_2, ω_3 and f_{23} are plotted according to the theoretical results of Chen et al., and McGuire. The points collected in the course of this work are shown.

The data for ω_2 and ω_3 are in reasonable agreement with the curves of Chen et al. and McGuire. The data are also in agreement with the values derived from Scofield (41). The values of Price et al. (23) are less reliable.

The Coster-Kronig yield f_{23} deviates from theory somewhat. Table 18 gives the f_{23} values as calculated recently by Chen et al (49) with an independent particle model as also with the hydrogenic wavefunctions used in their previous calculations. This reduces the discrepancy.

As can be seen, there is reasonable agreement of f_{23} values with the revised theory.

The energetics of the C-K process are such that the $L_2 - L_3 M_5$ transition in the region $30 < Z < 90$ and the $L_2 - L_3M_4$ transition in the region $30 < Z < 92$ are not possible. The exact location of these discontinuities is somewhat uncertain, because of the difficulty of calculating the exact energies.

The Coster-Kronig yield f_{23} should increase significantly when the extra M ejection modes are available. The "jump" in the value of f_{23} at Z = 91-95 and the corresponding drop in ω_2 are both borne out experimentally.

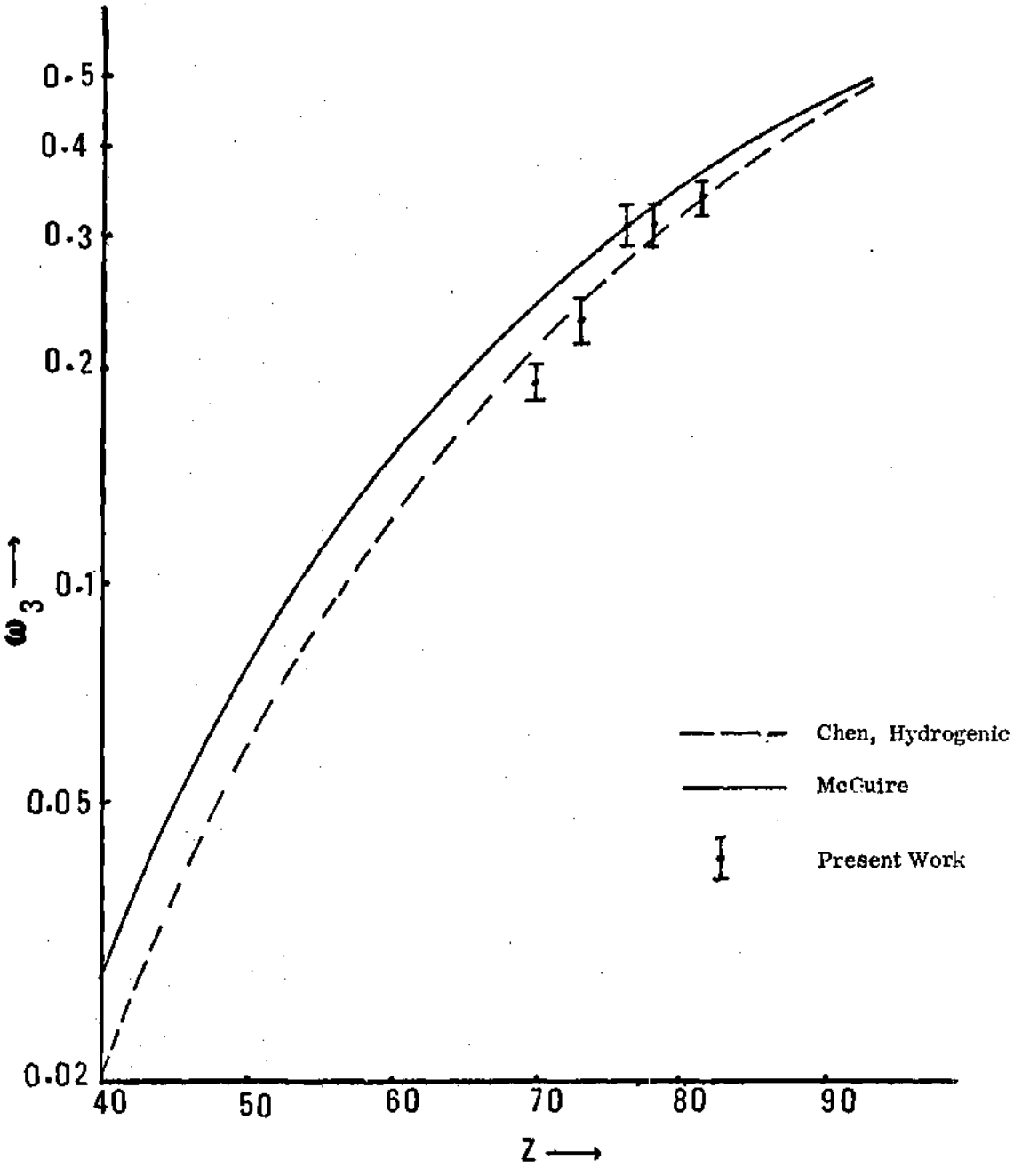

Figure 16. Plot of ω_3 vs. Z.

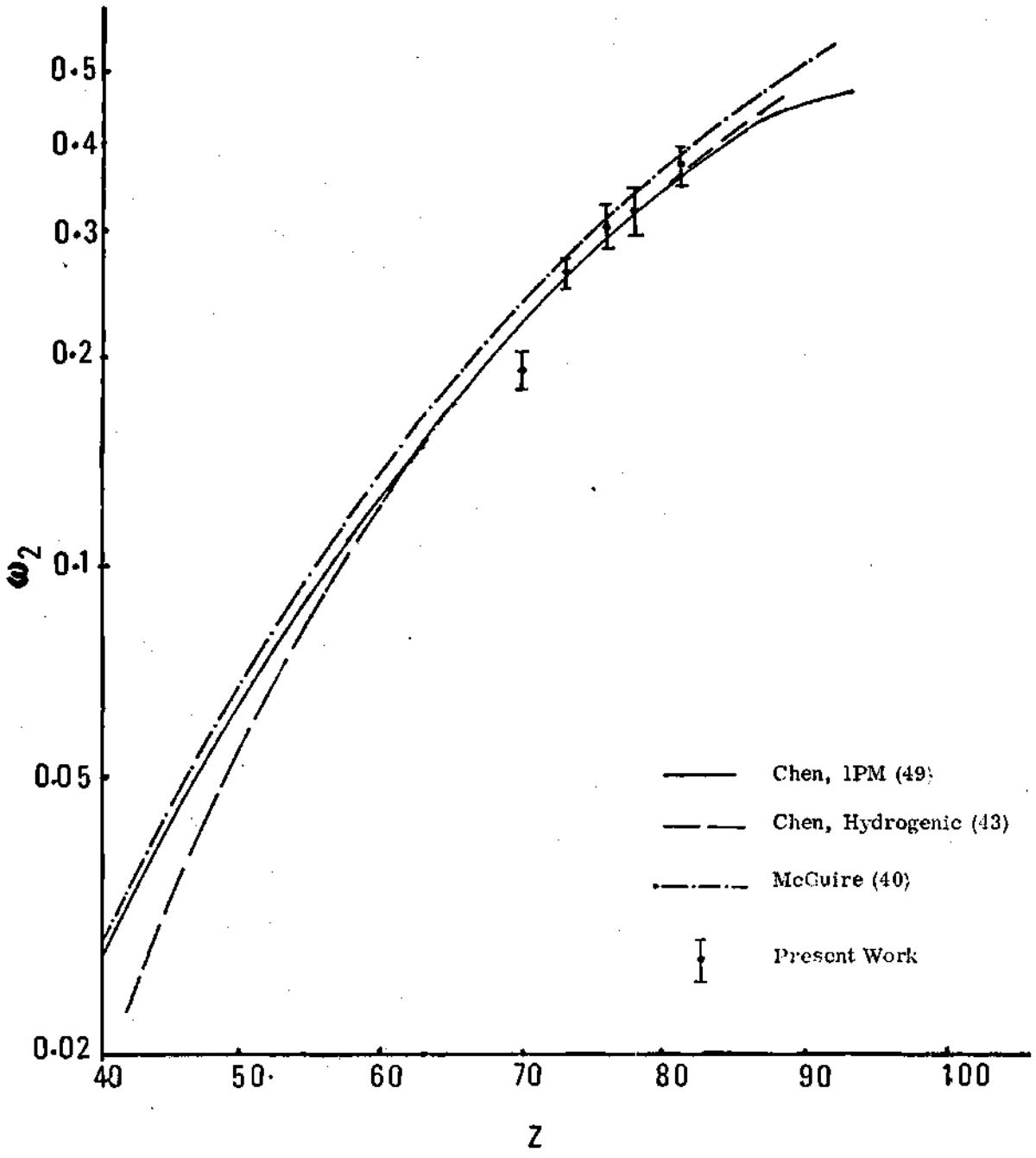

Figure 17. Plot of ω_2 vs. Z.

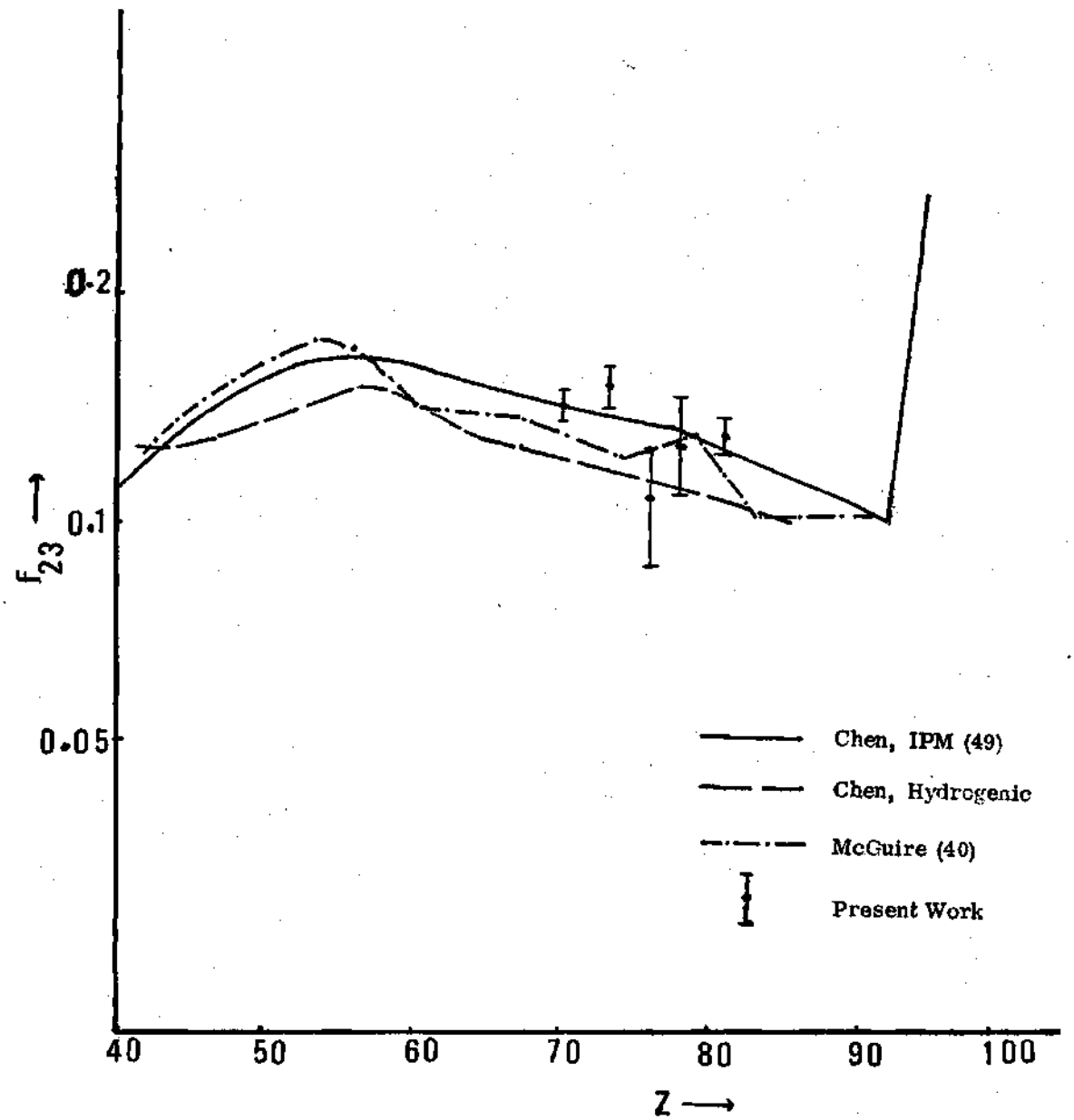

Figure 18. Plot of f_{23} vs. Z.

Table 17. Effect of L_η Correction on f_{23} and ω_2.

Z	Ref	ω_2		f_{23}	
		Original	Corrected for L_η	Original	Corrected for L_η
65	27	0.160±018	0.165± 018	0.090±014	0.066±014
70	77	0.187±011	0.188±011	0.170±009	0.142±0.009
73	28	0.250±013	0.257±013	0.180±007	0.150±007
80	26	0.316±010	0.319±010	0.190±010	0.188±010

Table 18. Experimental Values of f_{23} Compared with Theoretical Values.

Z	Exptl Results	Chen IPM (49)	Chen Hydrogenic (43)	McGuire (40)
60		0.161	0.142	0.141
61				
62				
63				
64				
65	0.066±014		0.131	
66				
67		0.147		0.138
68	0.106±023			
69				
70	0.142 ±009*	0.141		
71				
72				
73	0.150 ±010*			
74		0.138	0.117	0.123
75				
76	0.106±0.023			
77				
78	0.126±0.020			
79				0.132
80		0.130	0.108	
81	0.130±007			
82	0.129±013			
83				0.101
84				
85		0.115	0.100	

*Corrected for the presence of L_η x-rays. This correction makes a considerable difference (see Appendix C).

A somewhat surprising result is the influence of the $L\eta$ transition on the value of f_{23} (see Appendix C). In the previous measurements of f_{23}, the $L\eta$ line could not be resolved from the $L\alpha$ x-rays. Although the $L\eta\,[L_2 - M_1]$ x-ray is only $\simeq$ 3% of the L_3-M_4 line, its intensity relative to the $L\alpha$ x-ray intensity is given by

$$\frac{C_{L\eta}(K\alpha_2)}{C_{L\alpha}(K\alpha_2)} = \left[\left(\frac{L\eta}{L_2}\right)\omega_3\,\epsilon_{L\eta}\right] \Big/ \left[\left(\frac{L\alpha}{L_3}\right) f_{23}\,\omega_3\,\epsilon_{L\alpha}\right] \qquad (51)$$

where $L\eta/L_2$ is the intensity ratio of the $L\eta$ component to all L_2 x-ray transitions, and $L\alpha/L3$ is similarly the intensity ratio of the $L\alpha$ component to all L_3 x-ray transitions. It is apparent that in experiments where the $L\eta$ x-ray line is not resolved, a significant correction in the value of f_{23} will be required and will reduce its value. At the same time, the value of ω_2 goes up but only slightly.

6.8 Conclusions

The following conclusions can be drawn from the above experiments:

First, the experimental radiative yields ω_2 and ω_3 are in reasonable agreement with the available theory and other experiments. The accuracy of the available experiments is not adequate to choose conclusively between the two theories of Chen and McGuire. Despite the highly different approaches used by Chen and McGuire, the results approach closely.

Secondly, some discrepancy between the measured f_{23} values and the theoretical values persists. The experiments and theories both bear out the expected increase in the Coster-Kronig yield due to the availability of the

L_2-$L_3M_{4,5}$ transition above Z = 92. The sharp rise at this point, together with a similar jump at Z = 32 indicate the sensitive nature of the process.

The necessity for more high resolution experiments on f_{23} below Z = 80 is indicated by the sharp reduction in the values of f_{23} when the $L\eta$ x-rays are subtracted out. This reduction brings the f_{23} results in closer agreement with the values obtained from the assumption of the independent particle model (49).

The discrepancy between experiment and theory in the values of f_{23} must be attributed to the fact that the Coster-Kronig decay rates are extremely sensitive to the energy of the outgoing electron. The exact electron binding energies in atoms with an inner shell vacancy cannot be calculated very accurately. Further work on Auger-electron spectra can be expected to clarify this point.

6.9 Suggestions for Further Work

Apart from investigating additional nuclides to collect further data points, which are urgently needed in order to provide comparison with theory and to enable a choice between the various theoretical results to be made, two new directions for expanded research on fluorescence and Coster-Kronig yields appear to be promising.

A) Multiple vacancy effects: All of the preceding work has been concerned with the fate of a single vacancy. All of the f_{23} measurements rely on the assumption that $\omega_3 = \omega_3'$ where ω_3' is the L_3 subshell fluorescence yield in the presence of an outer shell vacancy. Very recent experiments (Veluri et al. (79)) have indicated that this assumption is justified, but that the mean L fluorescence yield in the presence of another vacancy increases dramatically

(~30%).

It is therefore incorrect to employ single vacancy yields in ion-atom collision. One means of measuring fluorescence yields with multiple vacancies is from a triple coincidence between K x-ray, L x-ray, and fission fragments in a time of flight arrangement.

B) Chemical effects: Because of the extremely low energy of the ejected C-K electrons, it is possible that the C-K processes may be affected by the matrix of the radioactive material. Tolea (78) has investigated this in the case of Hg^{203} and found essentially no difference ($\leq$ 5%) in the value of f_{23} when the Hg^{203} is in different chemical environments. If there is a chemical effect on f_{23}, this might be found at the rare earth region.

APPENDIX A

Reprinted from THE PHYSICAL REVIEW C, Vol. 1, No. 1, 254–259, January 1970
Printed in U. S. A.

Decays of Tm^{170} and Tm^{171}: L_1 and L_2 Subshell-Fluorescence Yields, Coster-Kronig Transition Probabilities, and K-Shell Conversion Coefficients in Yb†

S. MOHAN, H. U. FREUND, AND R. W. FINK
School of Chemistry, Georgia Institute of Technology, Atlanta, Georgia 30332
AND
P. VENUGOPALA RAO
Department of Physics, Emory University, Atlanta, Georgia

(Received 1 August 1969)

High-resolution Ge(Li) and Si(Li) x-ray detectors [404- and 290-eV full width at half-maximum (FWHM) at 6.4 keV, respectively] were employed to study the singles and coincidence spectra of x rays and γ rays from the decays of Tm^{170} and Tm^{171}. Measurements of the rates of L_α, L_β, and L_γ x-ray emission in coincidence with K_{α_1} and K_{α_2} x rays yielded the following values for L_2 and L_3 subshell-fluorescence yields (ω_2, ω_3), L_2-L_3X Coster-Kronig transition probability (f_{23}), and relative L x-ray intensity ratios (s_2, s_3): $\omega_2=0.182\pm0.011$, $\omega_3=0.153\pm0.011$, $f_{23}=0.170\pm0.009$, $s_2=0.192\pm0.010$, and $s_3=0.165\pm0.009$. The K-conversion coefficient of the 84.3-keV $E2$ transition in Yb^{170} is found to be 1.39 ± 0.04 by the measurement of the intensity ratio for the K-x-ray and γ transitions (XPG method). The K-conversion coefficient of the 66.7-keV transition in Yb^{171} is found to be 7.45 ± 0.36, which leads to a value of 0.34 for the mixing ratio of $E2/M1$. The orbital-electron-capture branchings of Tm^{170} to the first excited state (78.6 keV) and to the ground state in Er^{170} are determined to be 0.04 and 0.10%, respectively.

I. INTRODUCTION

THE present investigation was carried out particularly to exploit the new high-resolution techniques developed during recent years in low-energy photon spectrometry. Detectors of Si(Li) and Ge(Li) with sufficient resolution to separate clearly the full-energy peaks above $Z\approx65$ of the K_{α_1}, K_{α_2}, $K_{\beta_1'}$, and $K_{\beta_2'}$ components of K x rays and the L_α, L_β, L_β, and L_γ components of the L x rays of interest are available. Coincidence methods[1] are employed to measure the L_2 and L_3 subshell-fluorescence yields and the L_2-L_3X Coster-Kronig transition probability in Yb from decay of Tm^{170} and Tm^{171}. No prior measurements on Yb exist in which a radioactive source of L subshell vacancies is used. Jopson *et al.*[2] measured L_2 and L_3 subshell-fluorescence yields by coincidence methods with NaI(Tl) detection and Yb foil targets in which K and L ionization was produced by an incident beam of γ rays from a Co^{57} source.

The K-shell conversion coefficient of the 84.3-keV $E2$ transition in Yb^{170} following the β decay of Tm^{170} has been of considerable interest and has been the subject of many investigations since 1952. This transition was one of the first leading to a suspicion at one time that anomalies existed in experimental $E2$ conversion coefficients in the deformed region. Essentially three different techniques were employed to measure α_K: (1) Measurement of the intensity ratio of the K-x-ray

* Work supported in part by the U.S. Atomic Energy Commission at Georgia Tech.

[1] P. Venugopala Rao, R. E. Wood, J. M. Palms, and R. W. Fink, Phys. Rev. 178, 1997 (1969).

[2] R. C. Jopson, J. M. Khan, Hans Mark, C. D. Swift, and M. A. Williamson, Phys. Rev. 133, A381 (1964).

TABLE I. K-shell conversion coefficient for the 84.3-keV $E2$ transition in Yb^{170} as measured by the XPG method.

Author	Ref.	Year	I_{K_α}/I_γ	ω_K assumed	α_K	Correction for EC applied	I_{K_α}/I_γ (recalc)[a]	α_K (recalc)[a]
Graham *et al.*	3	1952	1.47	0.92	1.60±0.02	no	1.433	1.53
McGowan	4	1952			1.5±0.2			
Liden and Starfelt	5	1954			1.56±0.15			
McGowan and Stelson	6	1957	1.535	0.930	1.65±0.12	no	1.497	1.60
Houtermanns	7	1957	1.246	0.930	1.34±0.07	no	1.215	1.30
Bisi *et al.*	8	1956	1.571	0.93	1.69±0.02	no	1.532	1.64
			1.497	0.93	1.61	not necessary	1.499	1.60
Hooten	9	1964	1.357	0.93	1.46±0.05	no	1.322	1.41
Thosar	10	1964	1.212	0.93	1.31	not necessary	1.213	1.29
Croft *et al.*	11	1965	1.555	0.937	1.66±0.11	yes, 6%	1.614	1.72
			1.424	0.937	1.52±0.007	yes, 6%	1.478	1.58
Dingus *et al.*	12	1966	1.377	0.937	1.47±0.05	yes, 3.3%	1.389	1.48
Jansen *et al.*	13	1966	1.237	0.937	1.32±0.005	yes, 3.4%	1.247	1.33
Nelson and Hatch	14	1969	1.340	0.937	1.43±0.04	not necessary	1.340	1.43
Present work		1969		0.937		not necessary	1.304±0.039	1.39±0.04

[a] The values are corrected by using the correction for Er K x rays from the present work and a value of 0.937 for ω_K.

transition to the γ transition (XPG),[1-14] (2) internal-conversion–external-conversion method (IEC),[15-17] and (3) Coulomb-excitation and lifetime measurements.[18,19] Almost all measurements of method 1 employed NaI(Tl) spectrometers, even the best of which have not clearly resolved the 84.3-keV γ from the Yb K x rays. In addition, the Er K x rays from the EC decay of Tm^{170} and the unresolved iodine K-x-ray escape peaks complicated the analysis. Tables I and II present a survey of the existing measurements of the α_K of the 84.3-keV transition in Yb^{170}. The theoretical estimates[20-22] of α_K show a spread of 10%, thus making it difficult to discuss meaningfully the deviations from theory of existing experimental values.

In the case of the 66.7-keV transition in Yb^{171} fed from Tm^{171}, very little effort has been made to obtain accurate information on α_K. The transition is of mixed $E2$-$M1$ type ($\frac{5}{2}^- \rightarrow \frac{1}{2}^-$) and an accurate measurement of α_K is of value in estimating the $E2/M1$ mixing ratio. Hansen[24] measured a value of 7.4±1.0 for α_K from the relative intensities of Yb K x rays and 66.7-keV γ. Dingus *et al.*[12] measured a value of 6.9±1.0.

A detailed investigation of the EC branching of Tm^{170} has not been made. Graham *et al.*[3] set an upper limit of 0.3% for K capture and 0.01% for β^+ emission. Day[25] used a bent-crystal spectrometer to measure the relative intensities of Er K x rays and 84.3-keV γ rays and obtained an estimate of K-capture branching of 0.15%. Recently, Nelson and Hatch[14] estimated the K-capture branching to be 0.19±0.04%. These estimates were based on the assumption that all the EC leads to the ground state of Er^{170}. The level structure of the even-even nucleus Er^{170} is partially known from Coulomb excitation,[26] and the first excited state is at about 79 keV. Since $Q_{EC} \approx 500$ keV [27] feeding of both

[1] R. L. Graham, J. L. Wolfson, and R. E. Bell, Can. J. Phys. 30, 459 (1952).
[2] F. K. McGowan, Phys. Rev. 85, 142 (1952).
[3] K. Liden and N. Starfelt, Arkiv Fysik 7, 109 (1954).
[4] F. K. McGowan and P. H. Stelson, Phys. Rev. 107, 1674 (1957).
[5] H. Houtermans, Z. Physik 149, 215 (1957).
[6] A. Bisi, E. Germagnoli, and L. Zappa, Nuovo Cimento 3, 1007 (1956).
[7] B. W. Hooten, Nucl. Phys. 59, 341 (1964).
[8] B. V. Thosar, M. C. Joshi, R. P. Sharma, and K. G. Prasad, Nucl. Phys. 50, 305 (1964).
[9] W. L. Croft, B. G. Petterson, and J. H. Hamilton, Nucl. Phys. 70, 273 (1965).
[10] R. S. Dingus, W. L. Talbert, Jr., and M. G. Stewart, Nucl. Phys. 83, 345 (1966).
[11] J. F. W. Jansen and A. H. Wapstra, in *Internal Conversion Processes*, edited by J. H. Hamilton (Academic Press Inc., New York, 1966), p. 237.
[12] G. C. Nelson and E. N. Hatch, Nucl. Phys. A127, 560 (1969).
[13] J. F. W. Jansen, S. Hultberg, P. F. A. Goudsmit, and A. H. Wapstra, Nucl. Phys. 38, 121 (1962).
[14] P. Erman and S. Hultberg, in *Internal Conversion Processes*, edited by J. M. Hamilton (Academic Press Inc., New York, 1966), p. 249.
[15] E. N. Hatch, G. W. Eakins, G. C. Nelson, and R. E. McAdams, in *Internal Conversion Processes*, edited by J. M. Hamilton (Academic Press Inc., New York, 1966), p. 183.
[16] E. M. Bernstein, Phys. Rev. Letters 8, 100 (1962).
[17] D. B. Fossan and B. Herskind, Phys. Letters 2, 155 (1962).
[18] R. S. Hager and E. C. Seltzer, Nucl. Data A4, 1 (1968).
[19] C. P. Bhalla, Phys. Rev. 157, 1136 (1967).
[20] L. A. Sliv and I. M. Band, in *Alpha-, Beta-, and Gamma-Ray Spectroscopy*, edited by K. Seigbahn (North-Holland Publishing Co., Amsterdam, 1965).
[21] M. E. Rose, *Internal Conversion Coefficients* (North-Holland Publishing Co., Amsterdam, 1958).
[22] P. G. Hansen, Danish Atomic Energy Commission Risö Report No. 92, 1964 (unpublished).
[23] P. F. Day, Phys. Rev. 102, 1572 (1956).
[24] Nuclear Data Sheets, Nuclear Data Group, Oak Ridge National Laboratory, Oak Ridge, Tenn. (unpublished).
[25] J. H. E. Mattauch, W. Thiele, and A. H. Wapstra, Nucl. Phys. 67, 1 (1965).

TABLE II. K-conversion coefficient of the 84.3-keV transition in Yb^{169} from methods other than XPG and from theory.

Authors	Ref.	Year	Method	α_K
Bernstein	18	1962	Coulomb excitation	1.32±0.12
Fossan and Herskind	19	1962	Coulomb excitation	1.41±0.11
Jansen *et al.*	15	1966	IEC	1.36±0.10
Erman and Hultberg	16	1966	IEC	1.37±0.07
Hatch	17	1966	Magnetic and bent-crystal spectrometers	1.47±0.10
Hager and Seltzer	20		Theory (pure $E2$)	1.42
Bhalla	21		Theory (pure $E2$)	1.36
Sliv and Band	22		Theory (pure $E2$)	1.36
Rose	23		Theory (pure $E2$)	1.33

the ground and first excited states by EC is possible. Hansen and Hellström[28] used a Si(Li) detector with a resolution of only 1.5-keV FWHM at 84 keV to study the singles photon spectrum from the decay of Tm^{170}. By unfolding the unresolved photopeaks of K_α and K_β x rays, they measured the intensity of Er K x rays and estimated the total EC branching to be 0.25%. They observed the γ transition in Er^{170} at 78.7 keV.

II. EXPERIMENTAL

A. Source Preparation

Thin, uniform sources of radioactive Tm^{170} and Tm^{171} were obtained by evaporating from dilute HCl solution the activity on a Plexiglas holder. The Tm^{170} source was of high specific activity and of approximately 10 $\mu g/cm^2$ thickness; the Tm^{171} source was carrier free.

B. Singles-Spectrum Studies

A Si(Li) x-ray detector having a resolution of 290-eV FWHM at 6.4 keV was employed to study the singles K-x-ray and γ spectra of Tm^{170}. A typical spectrum is shown in Fig. 1. A detailed description of the detector and the determination of its photopeak efficiency are given elsewhere.[28] K x rays of Er from the EC decay of Tm^{170} are clearly separated from Yb K x rays. γ spectra from Tm^{170} taken with a 16-cm^3 coaxial Ge(Li) detector indicated the presence of γ rays with energies of 66.7 and 443 keV. These are attributed to the presence of Tm^{171} and Tm^{169} in trace amounts in the Tm^{170} source. The latter contributes Er K x rays from its EC decay, and the former contributes Yb K x rays from conversion of the 66.7-keV transition in Yb^{171}. These contributions were calculated from the known values of the ratio of the intensities of Er K x rays to 443-keV γ rays in Tm^{169} decays,[29–31] and from the ratio of intensities of Yb K x rays to the 66.7-keV γ in Tm^{171} decay measured in the present work. A trace of Bi^{207} also was identified but had no complicating influence on the present studies. No Tm K x rays were observed (Fig. 1), indicating that source thickness was sufficiently small that self-excitation of K x rays was negligible. The Ge(Li)–Ge(Li) coincidence system described below was used in a β-γ coincidence arrangement at close geometry to search for β-excited K x rays, which were negligible.

In Fig. 2 is shown the spectrum of Yb K x rays and the 66.7-keV γ from Tm^{171} decay. No disturbing im-

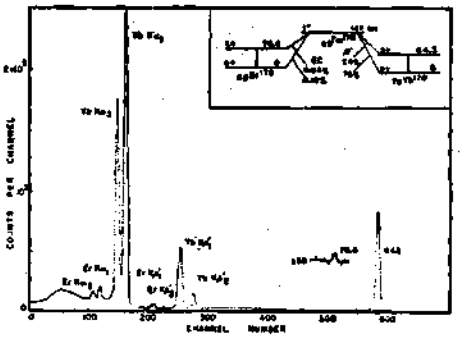

FIG. 1. The photon spectrum from Tm^{170} decay taken with the Si(Li) detector in the region 50–85 keV (resolution 290-eV FWHM at 6.4 keV). A Plexiglas absorber of 3.2 mm thickness was used to stop β rays. The inset shows the revised decay scheme of Tm^{170}, based on the present work. Energies are in keV.

[28] H. H. Hansen and S. Hellström, Z. Physik 223, 139 (1969).
[29] J. M. Palms, R. E. Wood, and P. Venugopala Rao (to be published).
[30] J. J. Reidy, E. G. Funk, and J. W. Mihelich, Phys. Rev. 133, B556 (1964).
[31] P. F. Kenealy, E. G. Funk, and J. W. Mihelich, Nucl. Phys. A110, 561 (1968).
[32] G. E. Keller, E. F. Zganjar, and J. J. Pinajian, Nucl. Phys. 129, 481 (1969).

purities were found, and contamination from Tm^{169} contributed less than 0.3% to the total intensity of Yb K x rays.

C. Coincidence Measurements

Two Ge(Li) x-ray spectrometers (8 mm diam × 5 mm depth with 0.005-in.-thick Be window) were used at 180° to observe L_α, L_β, and L_γ x rays in coincidence with $K_{\alpha 1}$ or $K_{\alpha 2}$ x rays. The energy resolution was of the order of 404-eV FWHM at 6.4 keV. A complete description of the coincidence arrangement has been given previously.[33] The determination of the efficiency of these detectors was discussed by Freund, Hansen, Karttunen, and Fink.[34] Yb L x rays in coincidence with $K_{\alpha 1}$ or $K_{\alpha 2}$ x rays were observed with Tm^{170} and with Tm^{171} sources. Typical singles and coincidence L x-ray spectra are presented in Fig. 3. The L x-ray coincidence rates, corrected for the efficiency and solid angle of the detector and the attenuation due to materials between source and detector, are related to ω_2, the L_2 subshell-fluorescence yield; ω_3, the L_3 subshell-fluorescence yield; f_{23}, the L_2-L_3X Coster-Kronig transition probability; s_2, the ratio of L_γ to $L_{\beta+\gamma}$ x rays from the L_2 subshell; and s_3, the ratio of L_β to $L_{\alpha+\beta}$ x rays from the L_3 subshell. The derivation of the necessary relationships and a detailed account of the basis of the coincidence method was given in Ref. 1.

Two complete sets of coincidence runs were made with each source and coincidence resolving times of 600 and 1200 nsec, respectively. The multichannel analyzer stored $K_{\alpha 1}$-L and $K_{\alpha 2}$-L coincidence spectra simultaneously, one in each half of the memory, the two coincidence units being run with equal resolving times. The coincidence efficiency was found to be unity, as verified by the independence of the results on the resolving time and further confirmed by a time–to–pulse-height-converter spectral analysis. The minimum resolving time for 100% coincidence efficiency was only 290 nsec. Chance coincidences were observed separately by introducing 3-μsec delay in the gating channel. Bremsstrahlung due to the β continuum in the coincidence spectra is negligible, as seen in Fig. 3.

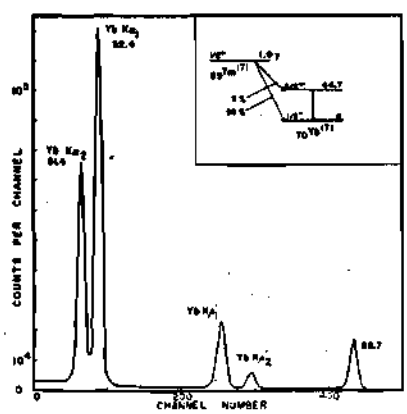

FIG. 2. The photon spectrum from Tm^{171} decay taken with the Si(Li) detector in the region of 50–70 keV. The inset shows the decay scheme of Tm^{171} from the literature. Energies are in keV.

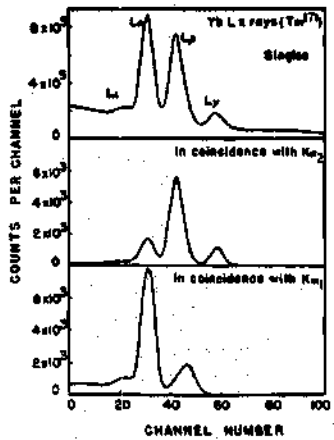

FIG. 3. L x-ray spectra from Tm^{171} decay taken with a Ge(Li) detector having resolution of 404-eV FWHM at 6.4 keV. Top: the singles spectrum, middle: L x rays in coincidence with $K_{\alpha 2}$ x rays, bottom: L x rays in coincidence with $K_{\alpha 1}$ x rays.

III. RESULTS AND DISCUSSION

Results of the present work are summarized in Tables III and IV, and are discussed below. The errors quoted are standard errors and include contributions from all experimental origins. No attempt has been made to include errors in quantities obtained from theory.

A. L_2 and L_3 Subshell-Fluorescence Yields and L_2-L_3X Coster-Kronig Transition Probability in Yb

Table III presents the values of ω_2, ω_3, and f_{23} obtained from $L_{\alpha,\beta,\gamma}$-$K_{\alpha 1,\alpha 2}$ coincidence measurements using both Tm^{170} and Tm^{171} decays as sources of K and L vacancies. The average number of L x rays emitted per L_2 vacancy, r_2, is also included in Table III. The effects of angular correlation in the L_γ x-ray–$K_{\alpha 1}$ x-ray

[33] E. Karttunen, H. U. Freund, and R. W. Fink, Nucl. Phys. A131, 343 (1969).

[34] H. U. Freund, J. S. Hansen, E. Karttunen, and R. W. Fink, in *Proceedings of the Conference on Radioactivity in Nuclear Spectroscopy, Nashville, Tennessee, 1969* (Gordon and Breach Science Publishers, New York, to be published).

TABLE III. Results on the L_2 and L_3 subshells in Yb.

Coincidence method	Quantity measured	Present work Tm^{170} decay	Present work Tm^{171} decay	Average	Jopson *et al.*[a]	Scofield[b] (theory)
$L_{\alpha,\beta,\gamma}$-K_{α}	ω_3	0.185±0.011	0.180±0.011	0.183±0.011	0.20±0.02	
	s_3	0.170±0.009	0.161±0.009	0.165±0.009		0.175
$L_{\alpha,\beta,\gamma}$-K_{α}	ν_2	0.218±0.013	0.210±0.013	0.214±0.013	0.34±0.05	
	ω_2	0.185±0.011	0.179±0.011	0.182±0.011		
	f_{23}	0.174±0.009	0.165±0.009	0.170±0.009		
	s_2	0.187±0.011	0.196±0.010	0.192±0.010		0.181

[a] Reference 2. [b] Reference 41.

coincidence measurement are taken into account[35–38] in obtaining the value of ω_2. This correction amounts to 2%. There is agreement with the previous work of Jopson *et al.*[2] in the case of ω_3, but the present value of ν_2 seems to be considerably lower, as is generally found in comparisons of radioactive source methods with methods based on fluorescent excitation of foils. A recent study[39] of the L Auger-electron spectrum in the EC decay of Hf^{175} gave a value of $\omega_1=0.19\pm0.05$ for $Z=71$, in good agreement with the present result for $Z=70$. The present work also confirms the earlier results[1,37,40] that a considerable number of L_2 vacancies are filled by nonradiative Coster-Kronig transitions of the L_2-L_3X type ($f_{23}\neq 0$).

The relative intensities of the resolved groups of L x rays from the L_2 and L_3 subshells also are obtained from the present coincidence experiment and are compared with theoretical values derived from the recent work of Scofield.[41] The ratio of L_3 x rays to $L_{\alpha,1}$ x rays, s_3, is determined to be 0.165±0.009 (Table III) and compares well with Scofield's estimate[41] of 0.175. Similarly, the ratio of L_γ to $L_{\beta_{2,6}}$ x rays from the L_2 subshell s_2 is determined to be 0.192±0.010 (Table III) and compares well with Scofield's estimate[41] of 0.181.

B. K-Conversion Coefficient of 84.3-keV Transition in Yb^{170}

Table IV contains the relative intensities of the Yb K x rays and the γ rays observed from the decay of Tm^{170}, after correction for detector efficiency and attenuation of the 3.2-mm Plexiglas β absorber. The ratio of intensities of Yb K x rays and 84.3-keV γ rays (I_{K_α}/I_γ) is calculated to be 1.301±0.039. The value is compared with the results of earlier work in Table I, which contains the intensity ratios and the values of ω_K, the K-shell-fluorescence yield of Yb, used to obtain the reported values of α_K. To facilitate comparison with the present value of I_{K_α}/I_γ, the intensity ratio from the various authors has been recalculated by using the correction for Er K x rays arising from orbital electron capture as found in the present work (Sec. III D). The spread in the recalculated values apparently is due to the low resolution of the NaI(Tl) spectrometers used. The most recent measurement by Nelson and Hatch,[14] in which a bent-crystal spectrometer was employed to obtain the monoenergetic response function of an NaI(Tl) spectrometer, is in fair agreement with the present result.

The present value of α_K of the 84.3-keV transition was obtained from the relationship

$$\alpha_K=(1/\omega_K)(I_{K_\alpha}/I_\gamma), \qquad (1)$$

where a value of 0.937 for ω_K is used.[42] For comparison we have listed the literature values of α_K, determined by the XPG method, which are recalculated using $\omega_K=0.937$ and recalculated values of the intensity ratio. Taking into account only the recent XPG results (Ref. 13, 14, and the present work) and the other conversion-electron methods, the agreement with theoretical estimates (Table II) for pure $E2$ multipolarity is good. On the other hand, the accuracy of any of the experimental methods is insufficient to distinguish among the various theoretical estimates.

C. K-Conversion Coefficient of the 66.7-keV Transition in Yb^{171}

The ratio of intensities of Yb K x rays and 66.7-keV γ rays following β decay of Tm^{171} was measured to be 6.98±0.34. With $\omega_K=0.937$, a value of $\alpha_K=7.45\pm0.36$ is obtained. The two previous measurements of this value are $\alpha_K=7.4\pm1.0$ [31] and 6.9 ± 1.0 [12] and these are in agreement with the present work. The mixing ratio is calculated to be 0.34 using the theoretical estimates of Hager and Seltzer,[20] so that the transition is a mixture of 74% $M1$ and 26% $E2$ multipolarity.

[35] H. W. Beste, Z. Physik **213**, 333 (1968).
[36] R. E. Price, Hans Mark, and C. D. Swift, Phys. Rev. **176**, 3 (1968).
[37] R. E. Wood, J. M. Palms, and P. Venugopala Rao, Phys. Rev. **187**, 1497 (1969).
[38] A. L. Catz and C. D. Coryell, Bull. Am. Phys. Soc. **14**, 83 (1969).
[39] J. Gizon, A. Gizon, and J. Valentin, Nucl. Phys. **A120**, 321 (1968).
[40] P. Venugopala Rao and B. Crasemann, Phys. Rev. **139**, 1926 (1965).
[41] J. H. Scofield, Phys. Rev. **179**, 9 (1969).
[42] R. W. Fink, R. C. Jopson, Hans Mark, and C. D. Swift, Rev. Mod. Phys. **38**, 513 (1966); W. Bambynek, B. Crasemann, R. W. Fink, H.-U. Freund, Hans Mark, R. E. Price, P. Venugopala Rao, and C. D. Swift, *ibid.* (to be published).

D. Electron-Capture Decay of Tm^{170}

In Table IV are presented the intensities of Er K x rays and 78.6-keV γ rays from the EC decay of Tm^{170}. The 78.6-keV γ is attributed to the first excited state in Er^{170}. This energy state has not been previously established conclusively, although a value of 79.3 keV has been quoted.[28] Chupp *et al.*,[43] who investigated the first excited states by Coulomb excitation of natural Er targets, identified two γ rays at 78.59 and 79.31 keV, and assigned them to Er^{167} or Er^{170}. They were unable to determine which γ is associated with each Er isotope. In the present work, the 79.3-keV γ was not found, but γ rays at 78.6±0.4 keV were observed, leading to the conclusion that EC in Tm^{170} decay leads to both the ground and the first excited states in Er^{170}.

From data in Table IV, a value of $2.64\pm0.40\times10^{-2}$ is obtained for the ratio of intensities of Er K x rays to Yb K x rays in Tm^{170} decay. The former arise from internal conversion of the 78.6-keV transition and from K capture to the ground and first excited states in Er^{170}. Taking the theoretical conversion coefficient $\alpha_K=1.77$ from Hager and Seltzer[20] and a value of $\omega_K=0.933$ for $Z=68$,[42] the total number of K x rays arising from the K conversion of the 78.6-keV transition can be estimated. The fraction of total Er K x rays due to K conversion of this transition is 0.059. The EC branching can be calculated using theoretical EC ratios[44–46] to the ground and first excited states. Taking the value of $Q_{EC}=460$ keV,[27] the theoretical values of the probability of K capture, P_K, to the ground and first excited states in Er^{170} are 0.800 and 0.837, respectively. These values, together with the relative intensities presented in Table IV, yield 0.04% EC decay to the 78.6-keV level and 0.10% to the ground state in Er^{170}, if one assumes that 76% of the Tm^{170} β emission leads to the ground state of Yb^{170}.

TABLE IV. Relative intensities of K x rays and γ rays from the decay of Tm^{170} and Tm^{171} from the present work.

Source	Photon emission	Relative intensity
Tm^{170}	Er K x rays	3.44±0.14
	Yb K x rays	130.4±3.9
	78.6-keV γ	0.122±0.024
	84.3-keV γ	100
Tm^{171}	Yb K x rays	698±34
	66.7-keV γ	100

[43] E. L. Chupp, J. W. DuMond, F. J. Gordon, R. C. Jopson, and Hans Mark, Phys. Rev. 112, 518 (1958).

[44] L. N. Zyryanova and Yu. P. Suslov, in *Proceedings of the International Conference on Electron Capture and Higher-Order Processes in Nuclear Decay, Debrecen, Hungary, 1968* (Eötvös Lorand Physical Society, Budapest, Hungary, 1968), p. 45.

[45] H. Behrens and W. Bühring, Ref. 44, p. 61.

[46] B. L. Robinson, Nucl. Phys. 64, 197 (1965).

APPENDIX B

Z. Physik 239, 423—428 (1970)

Electron Capture Decay of ^{181}W: L Subshell Fluorescence and Coster-Kronig Yields in Ta

S. Mohan and R. W. Fink
School of Chemistry, Georgia Institute of Technology, Atlanta, Georgia, USA*

R. E. Wood, J. M. Palms, and P. Venugopala Rao
Department of Physics, Emory University, Atlanta, Georgia, USA**

Received August 4, 1970

The Ta L x-ray spectrum from the 140 d electron capture decay of ^{181}W was studied with high resolution semiconductor detectors and fast coincidence techniques. Measurement of L x-ray−K x-ray and L x-ray−γ-ray coincidence rates yielded the following L shell fluorescence and Coster-Kronig yields and radiative decay branching ratios: $\omega_2=0.250\pm0.013$, $\omega_3=0.228\pm0.013$ (corrected for angular correlation effects), $f_{23}=0.180\pm0.007$, $\nu_1=0.218\pm0.016$, $s_3=0.205\pm0.010$, $s_2=0.215\pm0.010$, $f_{13}+f_{12}f_{23}=0.36\pm0.02$, and $\omega_1+f_{12}\omega_2=0.14\pm0.02$, from which upper limits were obtained of $f_{13}<0.36$ and $\omega_1<0.14$.

1. Introduction

The electron capture decay of ^{181}W was investigated earlier by many authors[1–10], and a detailed knowledge of the decay scheme is available. Almost all of the decay leads to the ground state and the first excited state at 6.25 keV, while only 0.2% of the decay leads to the pair of levels at 136 and 159 keV (see Fig. 1). The transition energy available for the decay is 187 ± 10 keV, which permits no K capture to the levels at 136 and 159 keV[10]. These features have interesting consequences which are

* Supported in part by the U.S. Atomic Energy Commission.
** Supported in part by a USAROD basic research grant.

1 Bisi, A., Terrani, S., Zappa, L.: Nuovo Cimento 4, 651 (1955).
2 Muir, A. H., Jr., Bochm, F.: Phys. Rev. 122, 1564 (1961).
3 Jopson, R. C., Mark, H., Swift, C. D., Zenger, J. H.: Phys. Rev. 124, 157 (1961).
4 Venugopala Rao, P., Crasemann, B.: Phys. Rev. 139, A 1936 (1965).
5 Debrunner, P., Heer, E., Kündig, W., Rüetschi, R.: Helv. Phys. Acta 29, 235 (1956).
6 Clark, M. A.: Can. J. Phys. 39, 1090 (1961).
7 Hauser, U.: Nucl. Phys. 24, 488 (1961).
8 Muir, A. H., Jr.: Nucl. Phys. 68, 305 (1965).
9 Blumberg, H., Hager, R. S., Seltzer, E. C.: Nucl. Phys. A 136, 624 (1969).
10 Venugopala Rao, P., Crasemann, B.: Phys. Rev. 142, 768 (1966).

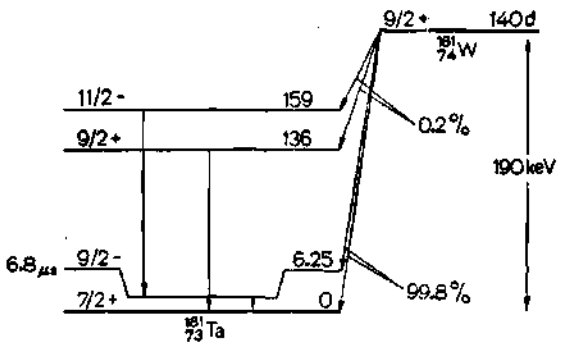

Fig. 1. The decay scheme of 140 d ^{181}W

exploited in the present work to measure the L subshell yields for tantalum ($Z=73$). The L x-rays observed in coincidence with 153 keV gammas deexciting the 159 keV level arise mainly from the filling of L_1 subshell vacancies, while those in coincidence with K_{α_2} and K_{α_1} x-rays come only from the filling of L_2 and L_3 subshell vacancies, respectively, with no complications due to cascading nuclear transitions. In effect the decay of ^{181}W is an ideal source of L_1, L_2, and L_3 subshell vacancies which can be studied individually.

Earlier work on L shell fluorescence yields of Ta was performed with the use of scintillation and proportional counters[11]. The present work is an attempt to obtain accurate information on the decay of L subshell vacancies in Ta by using high resolution semiconductor x-ray detectors. The basic principles of the methods have been given previously[12].

2. Experimental

2.1. Radioactive Source

The source was prepared from a high specific activity solution (2.62 C/g of W in 0.1 N HF) by droplet evaporation onto a 1.5 mg/cm^2 mylar foil. Two sources of approximately 5 and 10 μC were prepared.

2.2. Detectors

The L x-ray spectra were observed with a Si(Li) detector of 2.5 mm depth, fitted with a 2 mil (0.051 mm) Be window and having a resolution

11 Fink, R. W., Jopson, R. C., Mark, H., Swift, C. D.: Rev. Mod. Phys. **38**, 513 (1966). — Bambynek, W., Crasemann, B., Fink, R. W., Freund, H. U., Mark, H., Price, R. E., Venugopala Rao, P., Swift, C. D.: To be published.

12 Venugopala Rao, P., Wood, R. E., Palms, J. M., Fink, R. W.: Phys. Rev. **178**, 1997 (1969).

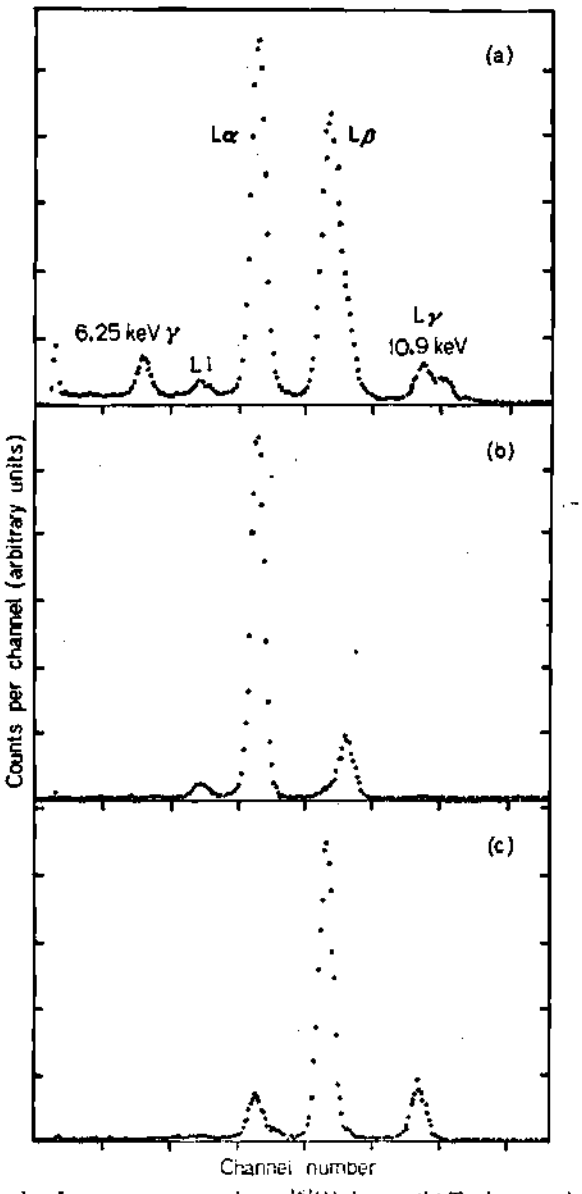

Fig. 2. (a) Singles L x-ray spectrum from ^{181}W decay. (b) Ta L x-rays in coincidence with K_{α_1} x-rays. (c) Ta L x-rays in coincidence with K_{α_2} x-rays

of 260 eV FWHM at 6.4 keV. The photopeak efficiency of the detector was measured using calibrated IAEA sources of low energy x-rays and gamma rays. The calibration procedure is described elsewhere[13].

13 Palms, J. M., Wood, R. E., Venugopala Rao, P.: To be published.

The Ta K x-rays were detected by a Ge(Li) x-ray spectrometer having a resolution of 470 eV FWHM at 6.4 keV, and the 153 keV gammas were observed with a 4 cm^3 Ge(Li) detector.

The fast coincidence arrangement used for measuring the coincidence rates was described previously[12], and the present measurements were made with a coincidence resolving time of $2t \approx 80$ nsec with a coincidence efficiency $\varepsilon_c = 0.96$. The coincidence system is provided with a single-channel analyser to set windows on K_{α_1}, K_{α_2} x-rays, or 153 keV γ-rays, respectively. Careful analysis of the gates admitted through these windows was performed according to procedures outlined earlier[12]. In a typical K_{α_2} x-ray window, 93% of the admitted events are due to K_{α_2} x-rays; 5%, to the low energy continuum following the photopeak of the K_{α_1} x-rays; and 2%, to higher energy components. In the determination of the true coincidence rates, account was taken of the contributions to the gate counting rate from each of the above categories. Chance coincidences were measured separately and corrected for. Typical coincident L x-ray spectra are shown in Fig. 2.

The measured L x-ray coincidence rates $C'_{L_i(x)}$ in each resolved peak were corrected for attenuation due to air and mylar covering on the source (f), photopeak efficiency (ε), fractional solid angle (Ω), and coincidence efficiency ε_c, to obtain the number of coincidences $C_{L_i(x)}$ in coincidence with the gates C_x by means of the relationship

$$C_{L_i(x)} = C'_{L_i(x)}/\varepsilon \Omega f \varepsilon_c . \tag{1}$$

Data taken with two different geometries were averaged.

3. Results and Discussion

The L x-ray–K x-ray coincidence rates are related to L_2 and L_3 subshell yields ω_2, ω_3, and f_{23} through the relationships summarized previously[12,14]. The results are presented in the Table, which also includes the radiative decay branching ratios s_2 and s_3, as defined in Ref.[12]. The present experimental values of s_2 (0.215 ± 0.010) and s_3 (0.205 ± 0.010) should be compared with the theoretical calculations of Scofield, 0.191 and 0.183, respectively[16]. The transfer of L_2 subshell vacancies to the L_3 subshell is apparent from the value of 0.180 ± 0.007 for f_{23} and is in agreement with recent work in this Z region. The angular correlation effects in L x-ray–K_{α_1} x-ray coincidences were taken into account in evaluating ω_3, as described previously[14,15].

14 Wood, R. E., Palms, J. M., Venugopala Rao, P.: Phys. Rev. 187, 1497 (1969).
15 McGeorge, J. C., Freund, H. U., Fink, R. W.: Nucl. Phys. (in press).
16 Scofield, J. H.: Phys. Rev. 179, 9 (1969).

Table. *L Subshell Fluorescence and Coster-Kronig Yields for Z=73*

Experiment	Quantities measured Present work	Previous work (Refs.[10, 11, 17])
L x-ray–K_{α_1} coincidences	$\omega_3=0.228\pm0.013$	$0.27\ \pm0.01$ $0.23\ \pm0.02$ $0.25\ \pm0.03$ 0.234 ± 0.025
	$s_3=0.205\pm0.010$	
L x-ray–K_{α_2} coincidences	$\omega_2=0.250\pm0.013$	$0.25\ \pm0.02$ $0.23\ \pm0.04$ $0.37\ \pm0.06$
	$f_{23}=0.180\pm0.007$	$0.20\ \pm0.04$
	$\nu_2=0.291\pm0.013$	0.303 ± 0.030
	$s_2=0.215\pm0.010$	
L x-ray–153 keV γ coincidences	$\nu_1=0.218\pm0.018$	$0.22\ \pm0.01$
	$f_{13}+f_{12}f_{23}=0.36\pm0.02$	
	$\omega_1+f_{12}\,\omega_2=0.14\pm0.02$	

The coincidence rate $C_{L(\gamma)}$ is related to L_1 subshell yields through the relationship

$$C_{L(\gamma)}=C_\gamma\,\bar{\omega}_L P_L \tag{2}$$

where C_γ is the number of 153 keV gammas gating the coincidence system. P_L is the probability of L electron capture feeding the 159 keV level ($\Sigma P_i=1$), and $\bar{\omega}_L$ is the mean L shell fluorescence yield[11]. The average number of L x-rays per L_1 subshell vacancy ν_1 is obtained from the relationship[11]

$$\bar{\omega}_L=N_1\,\nu_1+N_2(\omega_2+f_{23}\,\omega_3) \tag{3}$$

where N_1 and N_2 are the relative number of primary L_1 and L_2 subshell vacancies, respectively. No L_3 vacancies are created in the allowed and first-forbidden EC transitions of present interest, according to present theory of orbital electron capture decay. The distribution of L subshell primary vacancies are estimated to be $N_1:N_2=0.94:0.06$ from the tables of Zyryanova and Suslov[18]. The L capture probability P_L is cal-

17 Venkatesopala Rao, P.: in: Proc. Int. Conf. on Electron Capture and Higher Order Processes in Nuclear Decay, Debrecen, Hungary, 1968 (Eötvös Lorand Phys. Soc., Budapest); p. 222.

18 Zyryanova, L. N., Suslov, Yu. P.: in: Proc. Int. Conf. on Electron Capture and Higher Order Processes in Nuclear Decay, Debrecen, Hungary, 1968 (Eötvös Lorand Phys. Soc., Budapest); p. 45.

culated to be 0.76 to the 159 keV level from available theoretical data, as described in Ref.[19].

The high resolution of the L x-ray detector permits the L x-ray components to be resolved, and this is further exploited by measuring the coincidence rates of L_α and $L_{\beta,\gamma}$ x-rays separately. Employing the relationships developed earlier[12], it is found that $f_{13}+f_{12}f_{23}=0.36\pm0.02$ and $\omega_1+f_{12}\,\omega_2=0.14\pm0.02$. These results set upper limits of $f_{13}<0.36$ and $\omega_1<0.14$, but it is significant to note that a large number of vacancies are transferred from the L_1 subshell to the L_2 and L_3 subshells by Coster-Kronig transitions, in spite of the fact that L_1-L_3M transitions are energetically forbidden.

19 Wood, R. E., Palms, J. M., Venugopala Rao, P.: in: Proc. Int. Conf. on Radioactivity in Nuclear Spectroscopy, Nashville, Tennessee, 1969. New York: Gordon and Breach, Publishers 1970 (in press).

Dr. Richard W. Fink
School of Chemistry
Ga. Institute of Technology
Atlanta, Georgia USA 30318

APPENDIX C

PHYSICAL REVIEW A VOLUME 4, NUMBER 3 SEPTEMBER 1971

Reevaluation of L_2-Subshell Coster-Kronig Transition Probability and Fluorescence Yield below $Z = 81$*

J. C. McGeorge, S. Mohan, and R. W. Fink
School of Chemistry, Georgia Institute of Technology, Atlanta, Georgia 30332
(Received 8 March 1971)

Recently published experimental values of the L_2-L_3 total Coster-Kronig and L_2-subshell fluorescence yields for $Z = 65$, 70, 73, and 80 have been corrected for the presence of the unresolved L_η [L_2-M_1] x-ray line in the L_α [L_3-$M_{4,5}$] x-ray group. It is shown that this appreciable correction does not explain the discrepancy between experiment and theory.

As pointed out in a recent paper by Chen *et al.*,[1] the value of the L_2-L_3 total Coster-Kronig yield f_{23} calculated theoretically disagrees with experimental values by about 35%. Although the theoretical calculations by McGuire[2] and Chen *et al.*[1] are based on quite different wave functions, their results are in rather close agreement with each other. This, together with the fact that six of the seven published experimental values of f_{23} are greater than theory predicts, and that all were measured by the same coincidence method suggests that there may be a systematic error in the experiments.

The experimental technique used[3-8] has been outlined by Rao *et al.*[3] and by Wood *et al.*[4] and consists of taking L x-ray spectra in coincidence with $K\alpha_1$ and $K\alpha_2$ x rays individually. The L x rays were observed in Si(Li) detectors which enable only the L_l, $L\alpha$, $L\beta$, and $L\gamma$ x-ray groups to be resolved in the middle-Z region, while above $Z = 80$, the L_η [L_2-M_1] component also can be resolved.

Table I lists the energies of the L_η, $L\alpha$, and $L\beta$ x-ray groups taken from the tables of Bearden[9] for $Z = 65$, 70, 73, and 80. It is clear that L_η cannot be resolved from $L\alpha$ x rays at $Z = 65$, 70, and 73 with the detectors used in the reported experiments (Table II), since the resolution was not better than 260 eV full width at half-maximum (FWHM) (at 6.4 keV), and L_η may be only partially resolved at $Z = 80$. In none of the published coincidence spectra is the L_η x-ray line clearly visible. A small "bulge" on the high-energy side of the $L\alpha$ peak can just be discerned in the L x-ray spectrum given[7] for $Z = 73$.

In the notation of Rao *et al.*[3] and Wood *et al.*,[4] the values of f_{23} were derived from the expression

$$f_{23} = \frac{C_{L\alpha(K\alpha_2)}/C_{K\alpha_2}}{C_{L\alpha(K\alpha_1)}/C_{K\alpha_1}} , \tag{1}$$

which is based on the assumption that the $L\alpha$ x-ray group contains only L x rays emitted in transitions to the L_3 subshell.

Although the L_η [L_2-M_1] x-ray line is only ≈3% of the intensity of the L_2-M_4 line, its intensity relative to the $L\alpha$ x-ray intensity in spectra taken in coincidence with $K\alpha_2$ x rays is given by

$$\frac{C_{L_\eta(K\alpha_2)}}{C_{L\alpha(K\alpha_2)}} = \left[\left(\frac{L_\eta}{L_2}\right)\omega_2\,\epsilon_{L_\eta}\right] \Big/ \left[\left(\frac{L\alpha}{L_3}\right) f_{23}\,\omega_3\,\epsilon_{L\alpha}\right] , \tag{2}$$

where L_η/L_2 is the intensity ratio of the L_η component to all x rays emitted in transitions to the L_2

TABLE I. L x-ray energies in keV at $Z = 65$, 70, 73, and 80 (from Ref. 9).

Z	$L\alpha_1$[L_3-M_5]	L_η[L_2-M_1]	$L\beta_1$[L_2-M_4]
65	6.273	6.284	6.978
70	7.416	7.580	8.402
73	8.146	8.426	9.343
80	9.989	10.651	11.823

TABLE II. Revision of f_{23} and ω_2 values and comparison of f_{23} with theory.

Original values Z	ω_2	f_{23}	Reference	Theoretical x-ray intensity ratios (from Ref. 10) L_η/L_2	$L\alpha/L_3$
65	0.160±0.018	0.090±0.014	5	0.0223	0.818
70	0.162±0.011	0.170±0.009	6	0.0221	0.815
73	0.250±0.013	0.180±0.007	7	0.0220	0.807
80	0.316±0.010	0.190±0.010	8	0.0215	0.785
81	0.319±0.010	0.169±0.010	4		
82	0.363±0.015	0.164±0.016	3		

Revised values Z	ω_2	f_{23}	k (Eq. 3)	Theoretical values of f_{23} Ref. 1	Ref. 2[a]
65	0.165±0.015	0.068±0.014	1.000	0.131	0.138
70	0.138±0.011	0.142±0.009	0.984	0.124[b]	0.130
73	0.257±0.013	0.150±0.007	0.979	0.120[b]	0.126
80	0.318±0.010	0.188±0.010	0.965[c]	0.108	0.124
81	0.319±0.010	0.169±0.010	0.000	0.106[b]	0.116
82	0.363±0.015	0.164±0.016	0.000	0.104[b]	0.110

[a]Linear interpolation between values given for $Z=65$, 74, 79, and 85.

[b]Linear interpolation between values given for $Z=60$, 67, 74, 79, and 83.

[c]Reference 12.

subshell, and $L\alpha/L_3$ is the intensity ratio of the $L\alpha$ component to all x rays emitted in transitions to the L_3 subshell. From Eq. (2) it is apparent that in experiments where the L_η x-ray line is not resolved, a significant correction in f_{23} will be required and will reduce its value.

Assuming that the x-ray efficiencies $\epsilon_{L\alpha}=\epsilon_{L_\eta}$, the correct value of f_{23} may be calculated from the formula

$$f_{23}=f'_{23}-\left(\frac{(L_\eta/L_2)(\omega_2/\omega_3)}{(L\alpha/L_3)}\right)k\,, \tag{3}$$

where f'_{23} is the uncorrected published value and k is the fraction of L x rays included in the $L\alpha$ x-ray peak.

Since the reported values of the L_2-subshell fluorescence yield ω_2 were determined essentially from the relationship

$$\omega_2=\nu_2-f_{23}\,\omega_3\,, \tag{4}$$

they depend slightly on f_{23}. An iterative procedure starting with the published values of ω_2 was therefore used on Eqs. (3) and (4) to reevaluate f_{23} and ω_2 (see Table II). Theoretical values of the ratios L_η/L_2 and $L\alpha/L_3$ were taken from Scofield,[10] as recent experimental work on relative L x-ray intensities shows reasonably good agreement[11] with the theory in this region of Z.

The value of k in Eq. (3) depends on the detector resolution, the energy separation between the L_η and the $L\alpha$ x-ray peaks (increasing with Z), and the method used to evaluate the $L\alpha$ x-ray intensity. Except for $Z=80$,[12] $k=1$ (see Table II).

It is apparent that while these corrections bring the experimental value of f_{23} at $Z=70$ and 73 into closer agreement with theory, some discrepancy still exists. At $Z=80$, the small correction does not significantly improve the agreement with the results at $Z=81$ and 82 (which probably do not require revision, since L_η was apparently resolved from $L\alpha$), and all three values still lie about 30% higher than theory. The result at $Z=65$ is pushed even further from theory by this correction.

The small corrections to the L_2-subshell fluorescence yield ω_2 are barely significant, and agreement with theory[1] remains satisfactory.

*Work supported in part by the U. S. Atomic Energy Commission.

[1]M. H. Chen, B. Crasemann, and V. O. Kostroun, Phys. Rev. A (to be published).

[2]E. J. McGuire, Phys. Rev. A 3, 587 (1971).

[3]P. V. Rao, R. E. Wood, J. M. Palms, and R. W. Fink, Phys. Rev. 178, 1997 (1969).

[4]R. E. Wood, J. M. Palms, and P. V. Rao, Phys. Rev. 187, 1497 (1969).

[5]J. C. McGeorge, H. U. Freund, and R. W. Fink, Nucl. Phys. A151, 536 (1970).

[6]S. Mohan, H. U. Freund, R. W. Fink, and P. V. Rao, Phys. Rev. C 1, 254 (1970).

[7]S. Mohan, R. W. Fink, R. E. Wood, J. M. Palms, and P. V. Rao, Z. Physik 239, 423 (1970).

[8]J. M. Palms, R. E. Wood, P. V. Rao, and V. O. Kostroun, Phys. Rev. C 2, 592 (1970).

[9]J. A. Bearden, Rev. Mod. Phys. 39, 78 (1967).

[10]J. H. Scofield, Phys. Rev. 179, 9 (1969).

[11]P. V. Rao, J. M. Palms, R. E. Wood, Phys. Rev. A (to be published).

[12]P. V. Rao, J. M. Palms, and R. E. Wood (private communication).

LITERATURE CITED

1. P. Auger, J. Phys. Rad. 6, 205 (1925).

2. D. Coster and R. Kronig, Physica 2, 15 (1935).

3. H. Lay, Z. Phys. 91, 533 (1934).

4. H. Kūstner and E. Arends, Ann. Phys. 22, 443 (1935).

5. R. J. Stephenson, Phys. Rev. 51, 637 (1937).

6. E. Stahel, Helv. Phys. Acta 8, 651 (1935).

7. B. B. Kinsey, Can. J. Res. 26A, 404, 421 (1948).

8. K. Hohmuth, Nucl. Phys. 48, 209 (1963).

9. K. Hohmuth and G. Winter, Phys. Lett. 10, 58 (1964).

10. R. C. Jopson, H. Mark, C. D. Swift and M. A. Williamson, Phys. Rev. 131, 1165 (1963).

11. M. Goldberg, Ann. Phys. 7, 329 (1962).

12. A. H. Compton and S. K. Allison, X-rays in Theory and Experiment, D. Van Nostrand Co. (1935).

13. E. V. Condon and C. H. Shortley, Theory of Atomic Spectra, Cambridge University Press (1959).

14. E. H. S. Burhop, The Auger Effect and Other Radiationless Transitions, Cambridge University Press (1952).

15. I. Bergstrōm and C. Nordling, α, β, γ Ray Spectroscopy, Ed: K. Siegbahn), Vol. 2, 1523 ff: North Holland Publishing Co. (1965).

16. W. Mehlhorn, Lectures on the Auger Effect, Behlen Laboratory of Physics, University of Nebraska (1970).

17. J. A. Bearden, J. Appl. Phys. 37, 1681 (1966).

18. A. J. Guttman and W. Wagenfeld, Acta Crystallographica 22, 334 (1967).

19. R. D. Deslattes, Ph.D. Thesis, John Hopkins University, (Unpublished) (1959).

20. I. M. Band, L. N. Zyrynova, T. Chen-Zhui, Bull. Akad Sci. USSR Phys. 20, 1269 (1956).

21. L. N. Zyrynova and Y. P. Suslov, Proc. Conf. Electron Capture and Higher Order, Processes in Nuclear Decay, Ed. D. Berenyi (Eotvõs Lorand Physical Society, Budapest, 45 (1968).

22. R. C. Jopson, J. M. Khan, H. Mark and M. A. Williamson, Phys. Rev. 133, A381 (1964).

23. R. E. Price, H. Mark, and C. D. Swift, Phys. Rev. 176, 3 (1968).

24. P. V. Rao, R. E. Wood and J. M. Palms, Phys. Rev. 178, 1997 (1969).

25. R. E. Wood, J. M. Palms and P. V. Rao, Phys. Rev. 187, 1497 (1969).

26. J. M. Palms, R. E. Wood and P. V. Rao, Phys. Rev. C2, 592 (1970).

27. J. C. McGeorge, H. U. Freund, and R. W. Fink, Nucl. Phys. A154, 526 (1970).

28. S. Mohan, R. W. Fink, R. E. Wood and P. V. Rao, Z. Phys. 239, 423 (1970).

29. J. Byrne, W. Gelletely, M. A. Ross and F. Shaikh, Phys. Rev. 170, 80 (1968).

30. J. W. Halley and D. Engelkemeir, Phys. Rev. 134, A24 (1964).

31. J. G. Ferreira, J. C. Soares, A. Barraso and F. B. Gill, J. Phys. A4, 679 (1971).

32. D. R. Hartree, Proc. Cambridge Phil. Soc., 26, 89 (1928).

33. V. Fock, Z. Phys. 64, 126 (1930; Z. Physik 62, 795 (1930).

34. J. C. Slater, Phys. Rev. 81, 385 (1951).

35. F. K. Richtmeyer et al., Phys. Rev. 46, 843 (1934).

36. J. A. Bearden and T. M. Snyder, Phys. Rev. 59, 162 (1941).

37. D. Coster and H. DeLang, Physica 13, 385 (1947).

38. E. G. Ramberg and F. K. Richtmeyer, Phys. Rev. 51, 913 (1937).

39. H. W. S. Massey and E. H. S. Burhop, Proc. Cambridge Phil. Soc. 32, 451 (1936).

40. E. J. McGuire, Phys. Rev. A3, 587 (1971).

41. J. H. Scofield, Phys. Rev. 179, 9 (1969).

42. H. R. Rosner and C. P. Bhalla, Z. Physik 231, 1367 (1970).

43. M. H. Chen, B. Crasemann and V. O. Kostroun, Phys. Rev. A4, 1 (1971).

44. W. Gordan, Z. Phys., 48, 180 (1928).

45. E. J. Callan, Rev. Mod. Phys. 35, 524 (1963).

46. P. O. Lowdin and K. Appel, Phys. Rev. 103, 1746 (1956).

47. B. Talukdar and D. Chatterji, Phys. Rev. A1, 33 (1970).

48. J. C. Nelson, S. I. Salem and B. G. Saunders, Atomic Data 1, 377 (1970).

49. M. H. Chen and B. Crasemann, Inner Shell Ionisation Phenomena and Future Applications, R. W. Fink, S. T. Manson, J. M. Palms and P. V. Rao (Eds.), North Holland Publishing Co., Amsterdam, 43 (1973).

50. A. E. S. Green, D. L. Sellin and A. S. Zachor, Phys. Rev. 184, 1 (1969).

51. J. S. Hansen, H. U. Freund, E. Karttunnen and R. W. Fink: Proc. Int. Conf. on Radioactivity in Nuclear Spectroscopy, Nashville, Tennessee (1969) (Gordon and Breach Publishers, New York, 1972).

52. J. C. McGeorge, J. S. Hansen, D. W. Nix, W. D. Schmidt-ott, I. Q. Unus, and R. W. Fink, Nucl. Instr. and Methods, (To be published).

53. W. Moellering and J. H. D. Jensen, Z. Phys. 144, 252 (1956).

54. H. W. Beste, Z. Phys. 213, 333 (1968).

55. H. Frauenfelder and R. M. Steffen, Alpha, Beta and Gamma Ray Spectroscopy: K. Siegbahn (Ed), North-Holland Publishing Co., Amsterdam 997ff (1964).

56. A. L. Catz, C. D. Coryell, Bull. Am. Phys. Soc. 14, 85 (1969).

57. A. L. Catz and E. S. Macias, Phys. Rev. A3, 849 (1971).

58. G. E. Keller, E. F. Zganjar and J. J. Pinajian, Nucl. Phys. 129, 481 (1969).

59. J. Legrand, J. Morel and C. Clement, Nucl. Phys. A142, 63 (1970).

60. B. Lindström and I. Marklund, Nucl. Phys. 49, 609 (1963).

61. J. Gizon, A. Gizon and J. Valentin, Nucl. Phys. A120, 321 (1968).

62. R. W. Fink, R. C. Jopson, H. Mark and C. D. Swift, Rev. Mod. Phys. 38, 513 (1966).

63. G. C. Nelson and E. N. Hatch, Nucl. Phys. A 127, 560 (1969).

64. P. G. Hansen, Danish Atomic Energy Commission Risö Report No. 92, (1964) (unpublished)

65. R. S. Dingus, W. L. Talbert, and M. G. Stewart, Nucl. Phys. 83, 545 (1966).

66. R. L. Graham, J. L. Wolfson and R. E. Bell, Can. J. Phys. 30, 459 (1952).

67. P. P. Day, Phys. Rev. 102, 1572 (1956).

68. Nuclear Data Sheets, Nuclear Data Group, Oak Ridge National Laboratories, Oak Ridge, Tenn. (unpublished).

69. J. H. E. Mattauch, W. Thiele and A. H. Wapstra, Nucl. Phys. 67, 1 (1965).

70. H. H. Hansen and S. Hellström, Z. Phys. 223, 139 (1969).

71. R. S. Hager, and E. C. Seltzer, Nucl. Data A4, 1 (1968).

72. P. V. Rao and B. Crasemann, Phys. Rev. 142, 768 (1966).

73. R. E. Wood, J. M. Palms and P. V. Rao, Proc. Int. Conf. on Radioactivity in Nuclear Spectroscopy, Nashville, Tenn. (1969): Gordon and Breach Publishers, New York (1970).

74. P. V. Rao, Proc. Int. Conf. on Electron Capture and Higher Order Processes in Nuclear Decay, Debecen, Hungary (Eötvös Lorand Phys. Soc. Budapest), 222 (1968).

75. S. Mohan, J. C. McGeorge and R. W. Fink, Bull. Am. Phys. Soc. Ser. II, 16 (4), 579 (1971).

76. Z. Sujkowski and O. Melin, Arkiv Fysik 20, 193 (1961).

77. S. Mohan, H. U. Freund, R. W. Fink and P. V. Rao, Phys. Rev. C1, 259 (1970).

78. F. Tolea, J. C. McGeorge (Private Communication).

79. V. R. Veluri (Private Communication)

80. F. Hermann and S. I. Skillmann, Atomic Structure Calculations, Prentice Hall (1963).

81. J. S. Hansen, Ph.D. Thesis, Georgia Institute of Technology (Unpublished), (1971).

82. E. I. Karttunnen, Ph.D. Thesis, Georgia Institute of Technology (Unpublished) (1971).

VITA

S. Mohan was born in Kerala, India on 18 May 1943. He graduated from Banaras Hindu University with an M.S. in Physics in 1965 and afterward worked at the Tata Institute of Fundamental Research (Bombay, India) in 1966 and 1967. He joined Georgia Tech in 1968.